PHOTOCONTROL OF PROTEIN-PROTEIN AND PROTEIN-NUCLEIC ACID INTERACTIONS

by

Sabine Kneissl

A thesis submitted to
Cardiff University
for the degree of
DOCTOR OF PHILOSOPHY

School of Chemistry
Cardiff University
July 2009

ProQuest LLC
789 East Eisenhower Parkway
P.O. Box 1346
Ann Arbor, MI 48106-1346

Acknowledgements

I would like to thank my supervisor, Prof. Rudolf Allemann for giving me the opportunity to join his research group and work on this very interesting project for three years. I wish to express my gratitude to Dr. James Redman, Dr. Joel Loveridge and Ruedi Blankart for proof reading of this thesis. I would like to thank Dr. Christopher Williams, Dr. Matt Crump, Dr. Joel Loveridge and Piotr Wysoczanski for their help with the NMR experiments and Dr. Andrea Brancale for demonstrating the use of MOE. I would also like to thank Thomas Fricke for the purification of the HDM2 protein.

I would like to extend special thanks to my friends and family for their moral support throughout the project.

Abstract

Proteins often depend on α-helices for binding to other biomacromolecules. Reversible control of α-helix stability was accomplished in previous studies by incorporating a photoisomerisable azobenzene cross-linker into peptides, subsequently enabling the optical control of DNA-protein interactions. This approach was extended in this study to include protein-protein and protein-RNA interactions.

One of the primary regulatory components in apoptosis signalling is the antiapoptotic protein Bcl-x_L which interacts with the α-helical BH3 domain of the Bak protein. The Rev/RRE interaction is crucially involved in the life cycle of Human Immunodeficiency Virus. These interactions were targeted by designing peptides based on the BH3 domain of Bak and on the RNA-binding domain of Rev; these peptides are activated by external light pulses after the incorporation of the cross-linker. The ability to control cross-linker conformation and hence peptide secondary structure was demonstrated by CD and UV/Vis spectroscopy. The binding to the target structure and complex disruption was determined in the dark-adapted and irradiated states using fluorescence based assays. Structural studies using NMR spectroscopy demonstrated that the alkylated peptides bind to the same part of the target molecule as the wild-type peptide, regardless of their structure. Moreover, one of the BH3 domain-based peptides and the light-controllable transcription factor PhotoMyoD were modified with protein transduction domains to enable future *in vivo* studies. Overall, this work opens the possibility to interfere reversibly and specifically with protein-protein and protein-RNA interactions and to study and modulate cellular function by optical control.

Table of contents

List of figures

List of schemes

List of tables

List of abbreviations

General

AIDS	Acquired immunodeficiency syndrome
BH	Bcl-2 homology
bHLH	Basic helix-loop-helix
BPN	Biophotonic nanoswitch
bZIP	Basic leucine zipper
CARD	Caspase recruitment domain
CD4	Cluster of differentiation 4
dad	Dark-adapted
DISC	Death inducing signalling complex
DD	Death domain
DED	Death effector domain
ER	Endoplasmic reticulum
HIV	Human immunodeficiency virus
IAP	Inhibitor of apoptosis
IC_{50}	The antagonist concentration that displaces 50% of the specific binding of the ligand from the target molecule
K_D	Dissociation constant
K_i	Inhibition constant
LB	Luria-Bertani
lid	Light-induced
LTR	Long terminal repeat
MMFF94	Merck molecular forcefield 94

MOMP	Mitochondrial outer membrane permeabilisation
MWCO	Molecular weight cut off
NES	Nuclear export sequence
NLS	Nuclear localisation sequence
OD	Optical density
PBS	Phosphate buffered saline
PT	Permeability transition
ROS	Reactive oxygen species
RT	Room temperature
Sn2	Bimolecular nucleophilic substitution reaction
SOB	Super optimal broth
TB	Transformation buffer
TM	Transmembrane
wt	Wild-type
YT	Yeast extract tryptone

Chemicals

APS	Ammonium persulfate
ATP	Adenosine triphosphate
BSBCA	3,3'-bis(sulfonato)-4,4'-bis(chloroacetamido)azobenzene
Boc	*t*-Butoxycarbonyl
CM	Carboxy methyl
dATP	Deoxyadenosine triphosphate
DCM	Dichloromethane
DEPC	Diethylpyrocarbonate

dCTP	Deoxycytidine triphosphate
dGTP	Deoxyguanosine triphosphate
DIEA	Diisopropylethylamine
DIPCDI	*N,N*-Diisopropylcarbodiimide
DMF	*N,N*-Dimethylformamide
DMSO	Dimethylsulfoxide
DTT	Dithiothreitol
dTTP	Deoxythymidine triphosphate
EDTA	Ethylenediaminetetraacetic acid
FAM	Carboxyfluorescein
Fmoc	9-Fluorenylmethoxycarbonyl
HBTU	2-(1H-benzotriazole-1-yl)-1,1,3,3-tetramethyluronium hexafluorophosphate
HEPES	4-(2-Hydroxyethyl)-1-piperazineethanesulfonic acid
HoBt	*N*-Hydroxybenzotriazole
IPTG	Isopropyl-β-D-thiogalactopyranoside
MBHA	4-Methylbenzhydrylamine
MTS	Methylalkanethiosulfonate
Pbf	2,2,4,6,7-Pentamethyldihydrobenzofuran-5-sulfonyl
PIPES	Piperazine-1,4-bis(2-ethanesulphonic acid)
PMSF	Phenylmethylsulphonyl fluoride
SDS	Sodium dodecyl sulfate
tBu	*t*-Butyl
TCEP	Tris(2-chloroethyl)phosphate
TEMED	*N,N,N',N'*-Tetramethylethane-1,2-diamine

TFA	Trifluoroacetic acid
TFE	2,2,2-Trifluoroethanol
TIPS	Triisopropylsilane
TMR	Carboxytetramethylrhodamine
Tris	Tris(hydroxymethyl)aminomethane
Trt	Trityl

The amino acids are abbreviated using standard one and three letter codes, except for homoserine which is abbreviated as Z.

Macromolecules

AIF	Apoptosis inducing factor
Apaf1	Apoptosis protease activating factor
aPP	Avian pancreatic polypeptide
Bak	Bcl-2 homologous antagonist/killer
Bcl-2	B-cell lymphoma-2
Bcl-x_L	B-cell lymphoma extra large
Bid	BH3-interacting domain death agonist
BSA	Bovine serum albumin
CAP	Calf alkaline phosphatase
CED	*C. elegans* death gene
CHOP	C/EBP homologous protein
CBP	CREB binding protein
CREB	cAMP response element binding protein
DIABLO	Direct IAP binding protein of low pI

DISC	Death inducing signalling complex
DNase	Deoxyribonuclease
DNA	Deoxyribonucleic acid
FasL	Fas ligand
GABP	GA binding protein
GCN4	General control nondepressible 4
EGL-1	Egg-laying defective 1
FOXO3A	Forkhead box O3A
gp41	Glycoprotein 41
gp120	Glycoprotein 120
HDH-3	Homeodomain helix-3
HDM2	Human double minute 2 protein
IAP	Inhibitor of apoptosis protein
IHF	Integration host factor
JAK	Janus kinase
KSI	Ketosteroid isomerase
mRNA	Messenger ribonucleic acid
MscL	Mechanosensitive channel of large conductance
TBP	TATA box binding protein
TNF	Tumour necrosis factor
p17	HIV matrix protein p17
p24	HIV matrix protein p24
p53	Tumour suppressor protein p53
RNA	Ribonucleic acid
RNase	Ribonuclease

RRE	Rev recognition element
SRY	Male sex determining factor
STAT	Signal transducer and activator of transcription
TAT	Transactivator of transcription
TNF	Tumour necrosis factor
tRNA	Transfer ribonucleic acid

Techniques

CD	Circular dichroism
ESI-MS	Electrospray ionisation mass spectroscopy
FPLC	Fast protein liquid chromatography
FRET	Fluorescence resonance energy transfer
HPLC	High pressure liquid chromatography
HSQC	Heteronuclear single quantum correlation
IR	Infrared
ITC	Isothermal titration calorimetry
MALDI-TOF	Matrix assisted laser desorption/ionisation time of flight
NMR	Nuclear magnetic resonance
PAGE	Polyacrylamide gel electrophoresis
PCR	Polymerase chain reaction
SPPS	Solid phase peptide synthesis
TOCSY	Total correlation spectroscopy
UV	Ultraviolet
Vis	Visual

CHAPTER 1:

Introduction

1.1 Preface

The modulation of biomolecular interactions using light has significant advantages over chemical methods, photons can be applied with excellent spatiotemporal resolution by using modern lasers (Renner *et al.* 2005). The incorporation of photochromic compounds into molecular assemblies provides an attractive strategy for the rapid and reversible interference with biochemical pathways such as signal transduction or transcription. This technology may be utilised to probe and reengineer macromolecular function in biological systems, enabling the potential development of novel medical technologies such as new light-activatable therapeutics or artificial photoreceptors (Gorostiza *et al.* 2008).

1.2 Biomacromolecular interactions

A variety of specific macromolecular interactions such as protein-DNA, protein-RNA, protein-protein, protein-lipid and protein-carbohydrate interactions are important in biological systems. Since the specific interactions between the cellular macromolecules form the basis for all biological processes, the ability to manipulate the formation of these complexes will open up possibilities to selectively interfere with these processes. Understanding the physical basis for specificity in the different systems and mapping the various networks of interactions is central to the subsequent reengineering of the processes (Cusick *et al.* 2005).

1.2.1 Protein-protein interactions

The formation of specific protein complexes is fundamental to most biological processes such as cell proliferation, viral self-assembly, differentiation, apoptosis and signal transduction (Toogood 2002). Many proteins are able to interact with multiple partners depending on availability and environment, this forms the basis of network complexity. The human interactome is large and has been estimated recently to contain around 650,000 interactions (Stumpf *et al.* 2008). This was established based on partial interaction data obtained through various methods, such as tandem affinity purification and yeast-two-hybrid analysis (Fields *et al.* 1989).

Proteins interact with each other with varying affinities, ranging from millimolar down to femtomolar. Despite this very large range, most protein-protein interactions maintain a high degree of specificity for their partners. The contact areas involved in these interactions are usually relatively large (700-1,500 $Å^2$ per protein) with a flat binding groove. This makes protein-protein interactions difficult to target with small molecules since a large number of small energetic contributions are involved in the interaction (Nooren *et al.* 2003; Bahadur *et al.* 2004; Reichmann *et al.* 2005; Reichmann *et al.* 2007). However, some residues located at the binding interface of proteins have been demonstrated (in the last decade) to contribute substantially to recognition, whereas others only play a marginal role (Clackson *et al.* 1995). These so called "hot-spots" are clusters of amino acids that dominate binding free energy and specificity (Clackson *et al.* 1995; Dall'Acqua *et al.* 1996). This was observed in the case of the GABPα-binding groove of the ankyrin repeat protein GABPβ, in which the binding free energy difference was determined for residues in the interface by characterising alanine mutants of the protein using ITC. The differences in binding free energy (ΔΔG)

obtained from the calorimetric analysis were plotted onto the structural profile in order to identify the hotspot residues (Desrosiers *et al.* 2005) (Figure 1.1). This illustrates that even though the binding grooves involved in protein-protein complexes are large, it may still be possible to interfere with them using small molecules or peptides by focusing on targeting key residues implicated in the interaction.

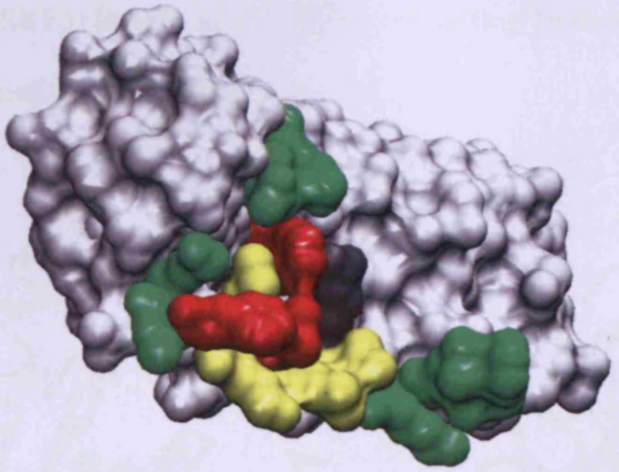

Figure 1.1: *Surface representation of GABPβ (light grey) (1AWC.pdb). The interface residues are displayed according to their ΔΔG values obtained from ITC measurements. The hot spot residues (ΔΔG > 2.0 kcal mol^{-1}) are coloured in red, moderately contributing residues (1.5 kcal mol^{-1} > ΔΔG > 0.8 kcal mol^{-1}) are coloured in yellow whilst residues with weak contributions (ΔΔG < 0.5 kcal mol^{-1}) are coloured in green. ΔΔG of residues shown in dark grey were not determined*

1.2.2 Protein-DNA interactions

Recombination, replication and transcription of genetic material are all dependent on the formation of specific DNA-protein interactions. A common feature shared by all of these is the large interaction interface (on average 3,100 Å^2), which has a high degree of shape, polarity and electrostatic complementarity (Hard *et al.* 1996). Protein-DNA

recognition is characterised mainly by a topological readout strategy. Defined secondary structural elements such as α-helices contact the major groove of double stranded DNA to distinguish cognate from non-cognate sequences (Jones *et al.* 1999; Pabo *et al.* 2000). Although most protein-DNA interactions rely on the major groove for recognition, there are also a number of important factors that interact with the narrow minor groove, such as the TATA box binding protein (TBP), integration host factor (IHF) or the male sex determining factor (SRY) (Bewley *et al.* 1998). The binding mode of the two classes of DNA targeting proteins is compared in Figure 1.2.

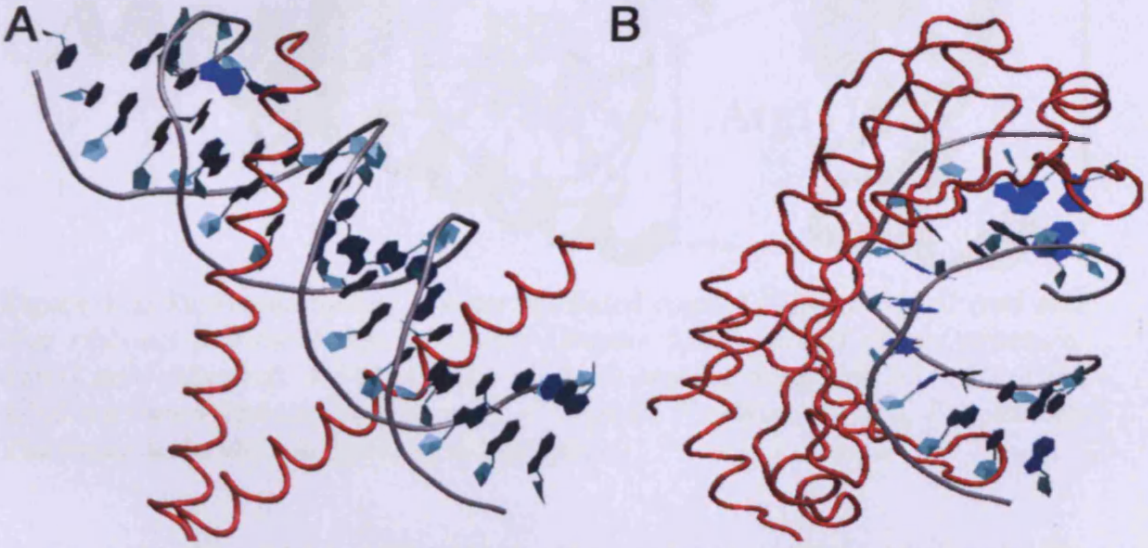

Figure 1.2: *DNA binding mode of A) a major groove binding protein (GCN4, 1YSA.pdb, (Ellenberger* et al. *1992)) and B) a minor groove binder (TBP, 1TGH.pdb, (Juo* et al. *1996)). The protein is shown in red and the DNA in blue.*

An induced fit mechanism for the binding of the protein component is frequently observed in DNA-protein interactions. In this case, the protein conformation changes substantially upon contact with the target DNA sequence in order to facilitate complex formation (Spolar *et al.* 1994). Protein binds to DNA by directly contacting the bases or the backbone with the amino acid side chains of certain secondary structural elements. These specific interactions are mediated by electrostatic contacts, van der Waals

interactions and hydrogen bonds (Allemann 1999). Protein-DNA complex formation is also commonly assisted by contacts between water and both polymers, for example, this kind of relationship is present in the basic helix loop helix (bHLH) domain of the transcriptional activator MyoD, where a nitrogen from the side chain of Arg111 contacts the oxygen (6') of a guanine in the binding region *via* a water molecule (Ma *et al.* 1994; Allemann 1999) (Figure 1.3).

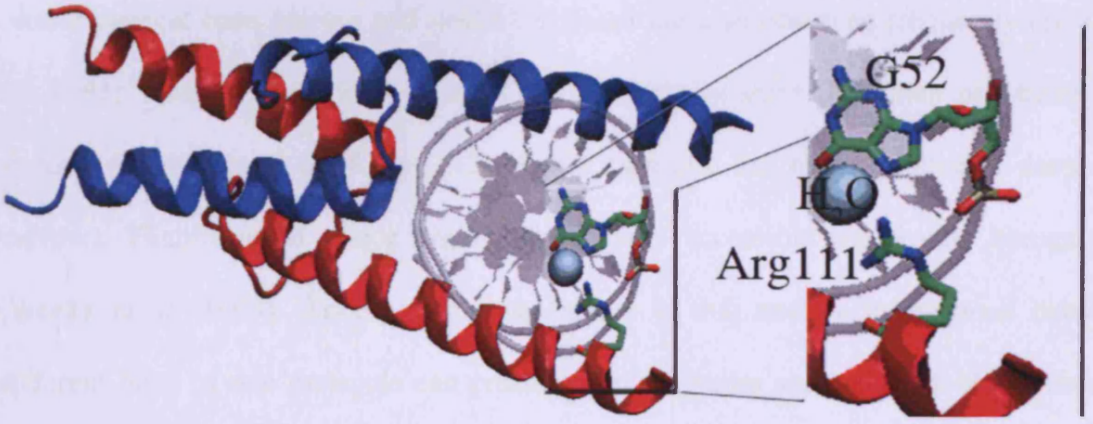

Figure 1.3: *Representation of a water mediated contact between MyoD (red and blue ribbons) and the E-box DNA (see Chapter 5.3.1) (silver) (X-ray structure, 1MDY.pdb) (Ma* et al. *1994). Arg111 of MyoD and the oxygen of G52 (6') of the DNA are shown with atom colour code (C = green, N = blue, O = red, P = yellow). The water molecule is depicted as a cyan sphere.*

Small molecules such as echinomycin, which inhibits sequence specific binding of hypoxia-inducible factor-1 DNA-binding activity have been successfully used to target DNA-protein interactions and are of great therapeutic interest (Kong *et al.* 2005).

1.2.3 Protein-RNA interactions

Ribonucleic acids are major players in many important biochemical processes. The formation of *specific* complexes between RNA and protein molecules is therefore crucial to a variety of cellular processes such as information transfer and storage, transcriptional activation, catalysis, post-transcriptional regulation of gene expression or

the assembly and function of ribonucleoprotein particles such as the splicesosome and the ribosome (Draper 1995; Moras *et al.* 1996; Lingel *et al.* 2005).

Single stranded RNA can adopt a much larger variety of conformations than double stranded DNA and is comparable to proteins in this respect. It structurally differs from B-DNA (right-handed form of double helix DNA that has 10.5 base pairs in each helical turn and two grooves on the external surface) in several significant ways. Bulges, hairpins and internal loops are found in between areas of Watson-Crick base pairing. Non-canonical base pairing and unstacked bases are also observed frequently (Heus *et al.* 1991; Varani *et al.* 1991). The helices are usually short (less than one turn) and A-form (similar to B-DNA but 11.0 bp per turn and the major groove is deep and narrow). Therefore the major groove is not very accessible for protein recognition (Weeks *et al.* 1993). Another common feature is that tertiary interactions between different parts of one molecule can create complex shapes such as the L-shape formed by tRNA hairpin loops (Shi *et al.* 2000) (Figure 1.4). Overall this gives rise to a lot more possibilities for indirect readout than in DNA recognition processes. Indirect readout is enabled by the unique flexibility and conformation such as the twist between base pairs or the width of the groove that is acquired by each nucleic acid sequence. It is not directly involved in the residue-base interaction, but is necessary as an overall facilitator of complex formation (Draper 1995). The phosphodiester group contributes less to the polar interactions than in DNA-complexes and the role of the sugar in DNA- and RNA-protein recognition is different. The deoxyribose plays no part in H-bonding to the protein moiety, unlike ribose (Lejeune *et al.* 2005). The 2'OH group of ribose comprises approximately 25% of the H-bonds to the protein while the 3'OH terminus contributes a further 6% to the protein. The bases account for a third of the H-bonds between protein and RNA (Lejeune *et al.* 2005). The contribution of guanine bases

among these is significantly lower than the average for DNA-protein complexes, where base recognition more frequently targets G than other bases.

Figure 1.4: *L-shaped tertiary structure of the yeast Phe tRNA (1EHZ.pdb) (Shi* et al. *2000).*

The interfaces are highly hydrated in a similar manner to DNA-protein interactions and water-mediated protein-RNA H-bonds are common (Bahadur *et al.* 2008). The positively charged amino acids Arg and Lys play a key role in binding to RNA as they do in the DNA-protein complexes. The average buried surface area in RNA-protein complexes is smaller than in DNA-protein complexes (2,500 $Å^2$ versus 3,100 $Å^2$) (Bahadur *et al.* 2008). Induced fit can be observed upon binding in both the RNA moiety or protein component. Mutually induced fit has also been described frequently (Williamson 2000). Overall protein-RNA recognition shares common features with protein-DNA recognition such as electrostatic complementarity and base recognition but it also shows similarity to protein-protein recognition such as shape recognition (Bahadur *et al.* 2008).

1.3 Stabilisation of α-helices

The α-helix is the most abundant structural element in proteins and is therefore an essential theme for modulating protein-nucleic acid and protein-protein interactions (about 30% of amino acid residues belong to this motif) (Barlow *et al.* 1988). However, isolated helical motifs and other small peptides are usually disordered in solution since the folding process is thermodynamically unfavourable (as a result, they seldom show optimal functional activity). Naturally occurring proteins typically depend on sophisticated folds to display a small number of functionally important amino acids. Many studies have therefore focused on pre-organising the structural elements such as α-helices to reduce the entropic penalty associated with folding.

In an α-helix motif, the hydrogen bonds between the amide NH group and the CO group of the amide backbone stabilise the structure. Each CO group contacts the NH group four residues ahead in the sequence. Each turn consists of 3.6 amino acids and the pitch per turn is 0.54 nm. The CO groups are parallel to the helical axis and the side chains point outwards from it. The amide groups of the first four residues and the carbonyl groups of the last four residues cannot participate in the hydrogen bonding of the helix and must form other H-bonds with the solvent or within the protein (Figure 1.5). Isolated helices are not stable since the entropically disfavoured process of folding of the polypeptide chain must be energetically compensated by stabilising interactions.

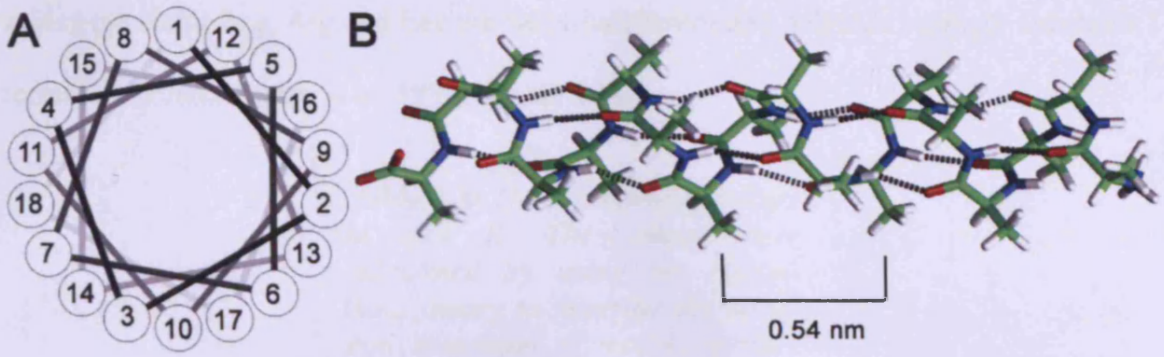

Figure 1.5: *A) Helical wheel representation from the* N*-terminal end of the helix. The positions of the residues are indicated. B) Model of an α-helix in a view perpendicular to the helix axis. Hydrogen bonds are shown as black dotted lines. Atoms are in standard colours (i.e. N = blue, C = green, H = white and O = red)*

The helix propensity of each amino acid was first estimated by observing the frequency of occurrence for each residue in different structural motifs (Davies 1964; Guzzo 1965; Chou *et al.* 1978). Subsequently, the helix propensity was investigated by studying the helical content of alanine based peptides in the absence of specific side chain interactions (Chakrabartty *et al.* 1994). The helix content of each peptide was determined by CD spectroscopy (222 nm) and the resulting data were fitted to the modified Lifson-Roig model (includes a parameter to account for the *N*-capping of amino acids since the original theory assumed that the *N*-terminal residue is always in a random coil state and therefore indifferent for helix formation). This theory was developed to describe the α-helix-random coil transition of polypeptides and describes each amino acid within a chain with three parameters: the statistical weight for helix nucleation, helix propagation and hydrogen bond formation (Doig *et al.* 1994). The helix propensity of each amino acid in Table 1.1 was defined as the calculated helix propagation parameter of the Lifson-Roig theory. Values greater than one indicate that helix formation is favored. Below one it is disfavoured. From the obtained values for the different amino acids, it was concluded that the helix propensities of most amino

acids oppose folding. Arg and Leu are helix-indifferent and only Ala strongly aids helix formation (Chakrabartty *et al.* 1994) (Table 1.1).

Table 1.1: *Helix propensity values at 273 K. The values were calculated by using the Lifson-Roig theory to describe the helix-coil transition of model peptides (Chakrabartty* et al. *1994).*

Residue	Helix propensity
Ala	1.54
Arg^+	1.04
Leu	0.92
Lys^+	0.78
Glu	0.63
Met	0.60
Gln	0.53
Glu^-	0.43
Ile	0.42
Tyr	0.37
His	0.36
Ser	0.36
Cys	0.33
Asn	0.29
Asp	0.29
Asp^-	0.29
Trp	0.29
Phe	0.28
Val	0.22
Thr	0.13
His^+	0.06
Gly	0.05
Pro	< 0.01

For short peptide sequences containing fewer than 16 amino acids the helical conformation is thermodynamically unstable because the strength of the backbone hydrogen bond network of a single helix must outweigh the unfavourable entropic loss upon helix formation (Scholtz *et al.* 1992). The ΔH for helix-random coil transition is about 1 kcal mol^{-1} and is independent of both the amino acid sequence and chain length (Scholtz *et al.* 1991; Lopez *et al.* 2002). A variety of other factors contributing to α-helix stability have been identified, such as *N*-capping, hydrogen bonds, hydrophobic and electrostatic interactions between side chains or side chain-peptide backbone interactions (Marqusee *et al.* 1987; Lyu *et al.* 1991; Kallenbach *et al.* 1998). Succinylation or acylation of the *N*-terminus stabilises α-helices (Presta *et al.* 1988; Richardson *et al.* 1988). The macrodipole created by the alignment of the amide bonds can be compensated by positively charged amino acids on the *N*-terminus (*N*-capping) and negatively charged ones on the *C*-terminus, leading to enhanced helix propensity.

Helical templates can serve as nucleation points to propagate the structure. A large number of strategies have been employed for stabilisation, such as the formation of helical bundles (Creighton 1993), lactam bridging (Osapay *et al.* 1992), unnatural amino acids (Rajashankar *et al.* 1995), disulphide formation (Pease *et al.* 1990; Jackson *et al.* 1991), multiple salt bridges (Mayne *et al.* 1998) and hydrazone linkages (Cabezas *et al.* 1999) (Figure 1.6).

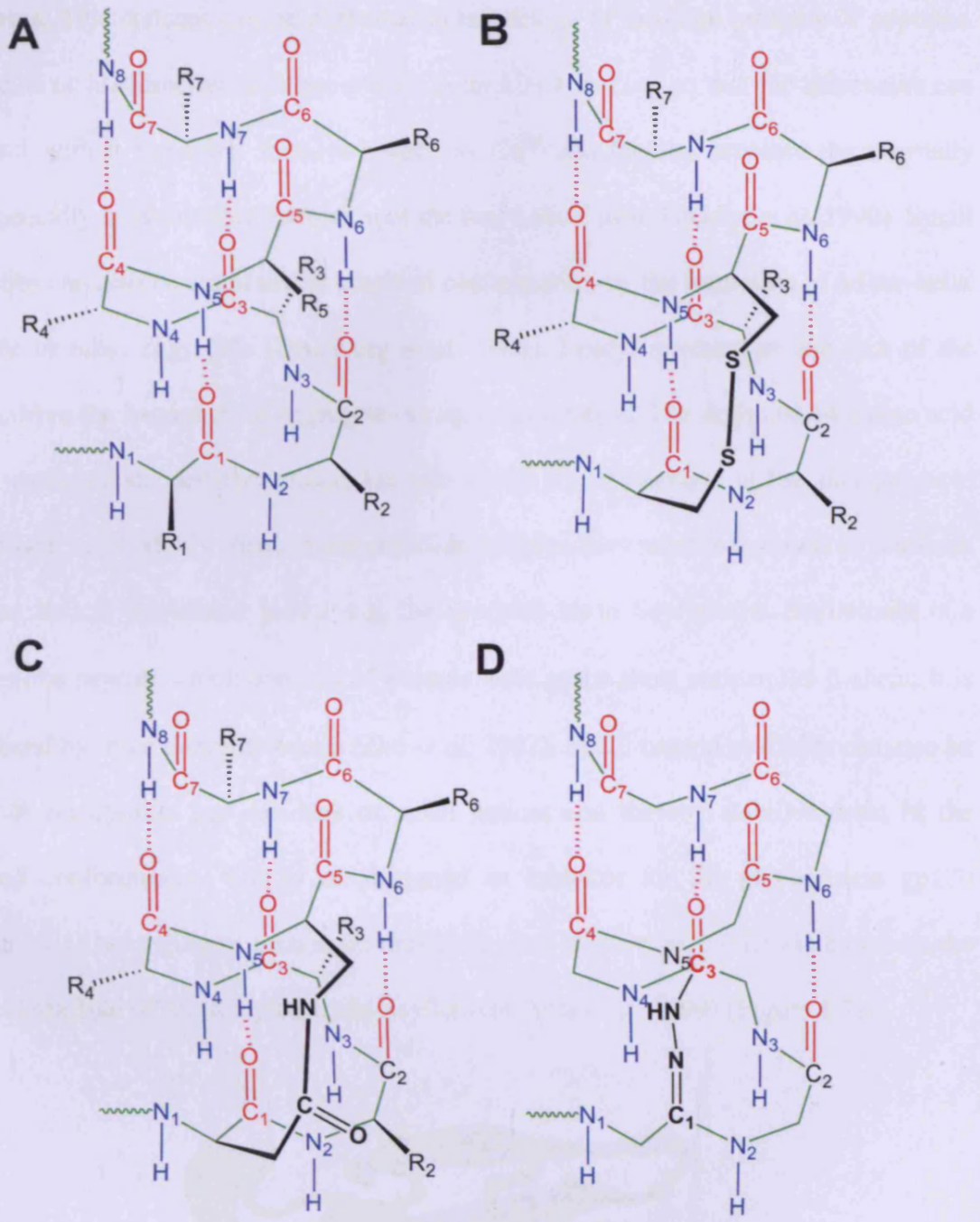

Figure 1.6: *The α-helical hydrogen bonding network and three different strategies for supporting this structure. Hydrogen bonds are shown in pink and the amide backbone in green. A) unmodified α-helix, B) disulfide bond, C) lactam and D) hydrazone.*

In nature, the coordination of amino acid residues to metal ions serves to stabilise helical sequences, examples of this include: haemoglobin, plastocyanin and zinc finger

domains. This concept can be exploited in the design of artificial proteins or peptides. Cysteine or histidine residues are placed in an *i, i+4* spacing so that the sidechains can interact with a transition metal ion such as Cu^{2+} and thereby promote the normally energetically unfavourable formation of the first helical turn (Ghadiri *et al.* 1990). Small peptides can also be stabilised in a helical conformation by the formation of a four-helix bundle or other aggregate (Eisenberg *et al.* 1986). Leucyl residues on one face of the helix drive the formation of aggregates in aqueous solution. The designed 14 amino acid long oxaloacetate decarboxylases, Oxaldie-1 and -2 for example utilise this principle (Johnsson *et al.* 1993). Small multi-disulfide proteins have often been used as scaffolds and as helical nucleation motifs e.g. the scorpion toxin Scyllatoxin. Scyllatoxin is a 31-residue peptide which consists of a single helix and a short antiparallel β-sheet. It is stabilised by three disulfide bonds (Zhu *et al.* 2002). Small natural scaffolds can also be used to incorporate key residues or small helices and thereby stabilise them in the desired conformation. Vita *et al.* designed an inhibitor for the glycoprotein gp120 (Figure 4.1) belonging to human immunodeficiency virus type-1 (HIV-1) based on the helical scaffold of the scorpion toxin Scyllatoxin (Vita *et al.* 1999) (Figure 1.7).

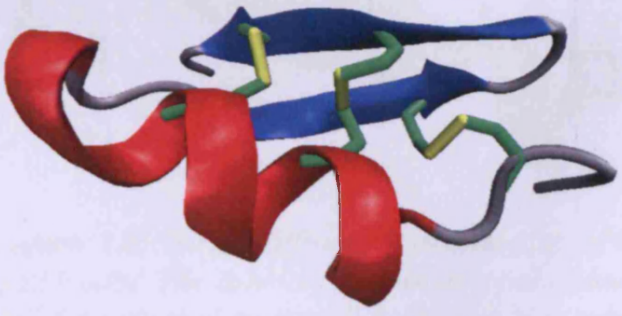

Figure 1.7: *NMR solution structure of Scyllatoxin (1SCY.pdb) (Martins* et al. *1995). The helix is coloured red, the β-sheet is shown in blue and the disulfide bonds are yellow.*

Avian pancreatic polypeptide (aPP) consists of an amphiphatic α-helix which is hydrophobically packed with a type II poly-proline helix (Figure 1.8). Schepartz *et al.* have reported potent inhibitors of proteins involved in apoptosis and cell cycle regulation (Bcl-2 and HDM2) based on small helical recognition motifs that were grafted onto this scaffold (Chin *et al.* 2001; Kritzer *et al.* 2006). Allemann *et al.* developed an oxaloacetate decarboxylase using the scaffold structure. Four lysine residues were incorporated on one site of the α-helix to form the active site. The enzyme displayed Michaelis-Menten saturation kinetics and the rate was significantly increased compared to simple amine catalysts, however, Oxaldie-3 displayed a molten globule-like structure. To improve upon this, bovine pancreatic polypeptide was used as an alternative scaffold to produce Oxaldie-4 which displayed a well defined tertiary structure, better stability towards thermal and urea denaturation whilst also exhibiting similar kinetic parameters (Taylor *et al.* 2001; Taylor *et al.* 2002).

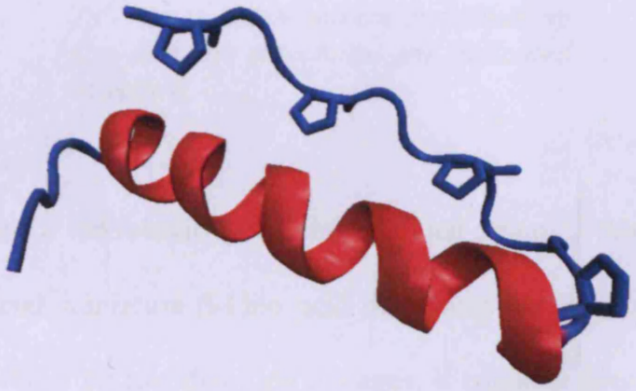

Figure 1.8: *X-ray diffraction structure of aPP (2BF9.pdb). The α-helix is shown as a red ribbon and the poly-proline type II helix as a blue tube (proline residues are displayed as sticks).*

The framework of C_2H_2-type zinc finger proteins (important class of nucleic acid binding proteins in eukaryotes that incorporate zinc ions *via* two Cys and His residues)

and a short sequence of the Rev protein has been successfully used in a number of studies to produce peptides that bind tightly (nano- and picomolar range), to the Rev Response Element (RRE) of HIV-1 in the presence of Zn^{2+} (McColl *et al.* 1999; Friesen *et al.* 2001; Mishra *et al.* 2006) (Figure 1.9).

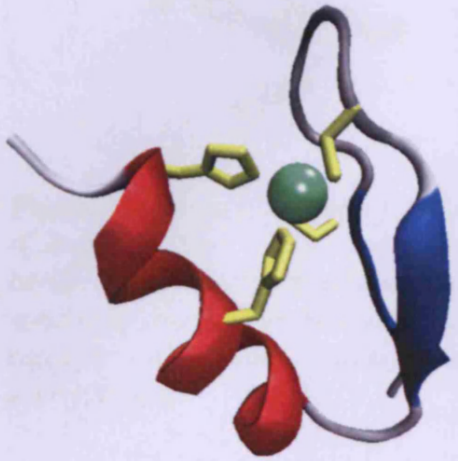

Figure 1.9: *NMR solution structure of an engineered HIV RRE IIB RNA (Chapter 4.1.5) targeting zinc finger protein (Mishra* et al. *2006) (2AB7.pdb). The helix is coloured red, the two β-sheet strands are blue, the Zn^{2+} ion is green and the coordinating Cys and His sidechains are indicated in yellow.*

Bee venom contains a neurotoxic polypeptide called apamin, this has been used to construct the artificial miniature β-keto acid decarboxylase Apoxaldie-1, which is a helical peptide stabilised by two disulfide linkages. It contains three lysine residues on one side of the helix which are responsible for the catalytic activity (Weston *et al.* 2004) (Figure 1.10).

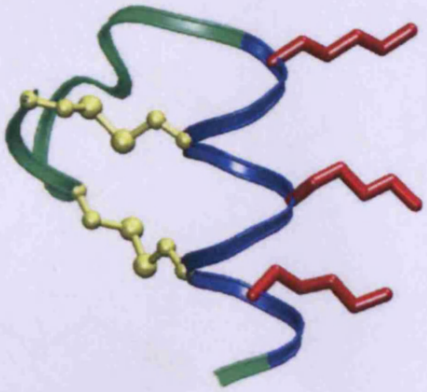

Figure 1.10: *Model of Apoxaldie-1 (Cureton 2003). The disulfide bonds are indicated in yellow, the α-helix is coloured in blue and the catalytic Lys side chains are shown in red.*

Another strategy involves conformationally constraining the peptide using cross-linkers. *Para*-substituted benzene rings and acetylenic cross-linking agents are important examples (Yu *et al.* 1999; Fujimoto *et al.* 2004; Fujimoto *et al.* 2007). *Para*-substituted amino acid derivatives of a benzene ring were utilised to link side chains of a model peptide in the *i, i+7* spacing. A non-proteinogenic 2,3-diaminopropionic acid residue within a short model peptide was linked to an aspartic acid by a bridge consisting of *p*-(aminomethylphenyl)acetic acid. The resulting bridged peptide showed enhanced helix stability. Fujimoto *et al.* used acetylenic cross-linkers of different lengths with the right compromise between rigidity and flexibility to modify two lysines within a sequence in either the *i, i+4* or *i, i+7* spacing. The side chain amine group of the lysines attacks the keto group of the succinimide part of the cross-linker, this results in ring opening and formation of a new amide bond (Fujimoto *et al.* 2004) (Figure 1.11).

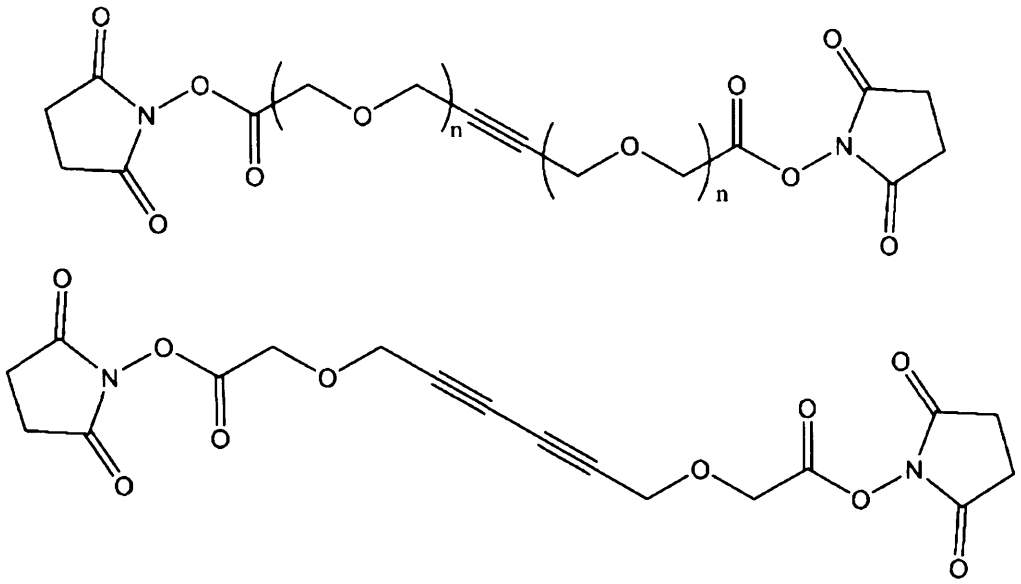

Figure 1.11: *Chemical structures of the acetylenic cross-linkers used to stabilise α-helices, where n corresponds to 1 or 2 (Fujimoto* et al. *2004).*

Other cross-linking reagents are based on methyl alkanethiosulfonate (MTS). These linkers are thiol reactive and can therefore be introduced using cysteine residues. They react rapidly and selectively with the sulfhydryl groups of proteins *via* thiol-disulfide exchange, upon addition of other thiols, the reaction is reversed (Kenyon *et al.* 1977; Dime 2002) (Figure 1.12).

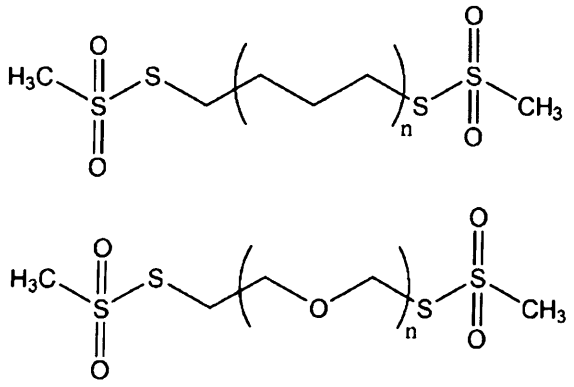

Figure 1.12: *General chemical structure of MTS cross-linkers.*

Verdine, Korsmeyer *et al.* have described the stabilisation of α-helical structure by hydrocarbon-stapling of the olefinic side chains of non-canonical amino acids that can be introduced either in the *i, i+4* or *i, i+7* spacing (Figure 1.13) (Schafmeister *et al.* 2000). The "staple" to constrain the peptide conformation is then formed through a ring closing metathesis reaction. This approach has been successfully applied to target protein-protein interactions such as Bcl-x_L/Bid and p53/HDM2 *in vitro* and *in vivo*. The peptides demonstrated enhanced affinity towards their target, protease stability and cell permeability (Walensky *et al.* 2004; Bernal *et al.* 2007).

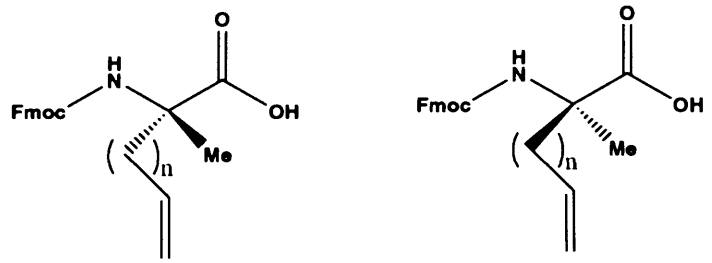

Figure 1.13: *Chemical structure of modified S- (left) and R-amino acids (right) with olefinic side chains of variable length (Schafmeister* et al. *2000).*

1.4 Photocontrol of peptide/protein conformation

As mentioned previously, one strategy for secondary structure stabilisation involves the use of a covalently bound cross-linker. An especially interesting case is the utilisation of photochromic compounds. Such cross-linkers can facilitate the light pulse dependent regulation of peptide or protein conformation. Examples of this include a mutated MscL protein from *E. coli* that was modified with a spiropyran compound using an alkylating cysteine-reactive photoswitchable reagent (Kocer *et al.* 2005). Upon irradiation with

UV light, charge separation occurs and the zwitterionic merocyanine state of the molecule is obtained (Scheme 1.1). Hydrophilic changes inside the narrow protein pore cause hydration and weakening of the hydrophobic van der Waals forces responsible for maintaining the closed channel conformation, so that the pore opens. Exposure to visible light leads to a 'ring closing' reaction resulting in the uncharged starting material, allowing for reversible control of the channel conductivity upon an optical signal. However the proportion of the merocyanine state of the channel obtained dropped substantially after the first illumination and the isomerisation process was also shown to progress slowly (Kocer *et al.* 2005).

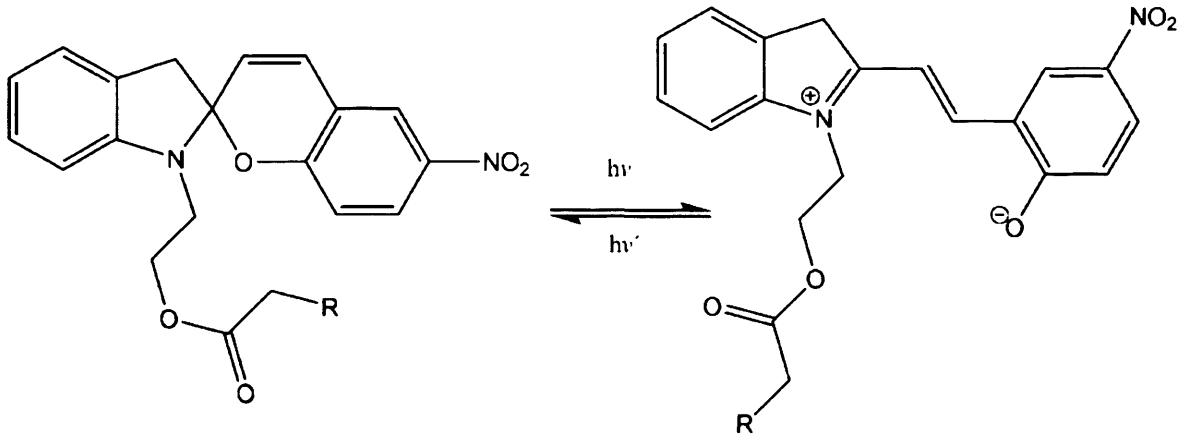

Scheme 1.1: *Structures of the spiropyran and merocyanine states of the 3',3'-dimethyl-1'-(2-iodoacetyloxyethyl)-6-nitrospiro[2H-1-benzopyran-2,2'-indoline] photoswitch (R = iodine or MscL protein).*

Stilbenes can be switched between the *trans* and the *cis* configuration using UV light. Cyclic β-hairpin peptidomimetic have been designed using this photoresponsive compound. β-hairpins are heavily involved in both protein-protein and protein-DNA interaction but difficult to characterise and structurally unstable. They consist of two anti-parallel strands of β-sheet that are linked by a small loop. The stilbene moiety (Figure 1.14) was incorporated during peptide synthesis. The β-hairpin mimetics were

studied by CD spectroscopy and the backbone conformation determined by NMR spectroscopy, which confirmed that only the *cis*-isomer had a β-hairpin structure.

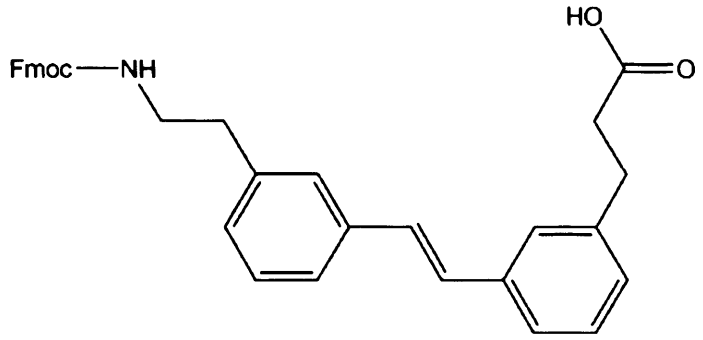

Figure 1.14: *Structure of the Fmoc protected stilbene amino acid used to generate the photoresponsive peptidomimetic.*

Azobenzene is the most widely used compound for the generation of photoresponsive systems (Renner *et al.* 2005). It can adopt the *cis* and the thermally stable *trans* conformation. In the dark there is greater 99% *trans* azobenzene. The *trans* conformation is about 50 kJ mol^{-1} lower in energy and the energy barrier to the photo-exited state is approximately 200 kJ mol^{-1}. The two isomers can be switched with light of particular wavelength (in the UV- or visible spectrum). The π-π* leads to the *trans-cis* isomerisation and the n-π* transition to the *cis-trans* isomerisation. The photo-isomerisation reactions occur rapidly at a picosecond timescale typically resulting in around 85-90% of the *cis* isomer (Satzger *et al.* 2004). The *cis* to *trans* isomerisation can also occur thermally (Scheme 1.2). The rates for this vary between seconds and hours. The barrier for this step is around 90 kJ mol^{-1}. Two mechanisms for the *trans* to *cis* isomerisation have been proposed: the rotation pathway involves an out of plane rotation around the CNNC dihedral angle (ϕ), the alternative inversion pathway proceeds *via* an in-plane inversion of the NNC angle (φ) (Schulze *et al.* 1977; Crecca *et*

al. 2006) (Scheme 1.2). Azobenzene has been frequently used to reversibly constrain and relax the peptide backbone by means of its isomerisation due to its rapid isomerisation, high quantum yield, the reversibility of the process and the strong change in geometry upon switching. The two isomers are 1.0 nm and 1.7 nm in length respectively. Azobenzene possesses high photostability so repeated switching does not lead to destruction of the compound (Behrendt *et al.* 1999a; Cattani-Scholz *et al.* 2001; Schutt *et al.* 2003; Zhao *et al.* 2004; Renner *et al.* 2005; Liu *et al.* 2006; Aemissegger *et al.* 2007; Boulegue *et al.* 2007; Kusebauch *et al.* 2007).

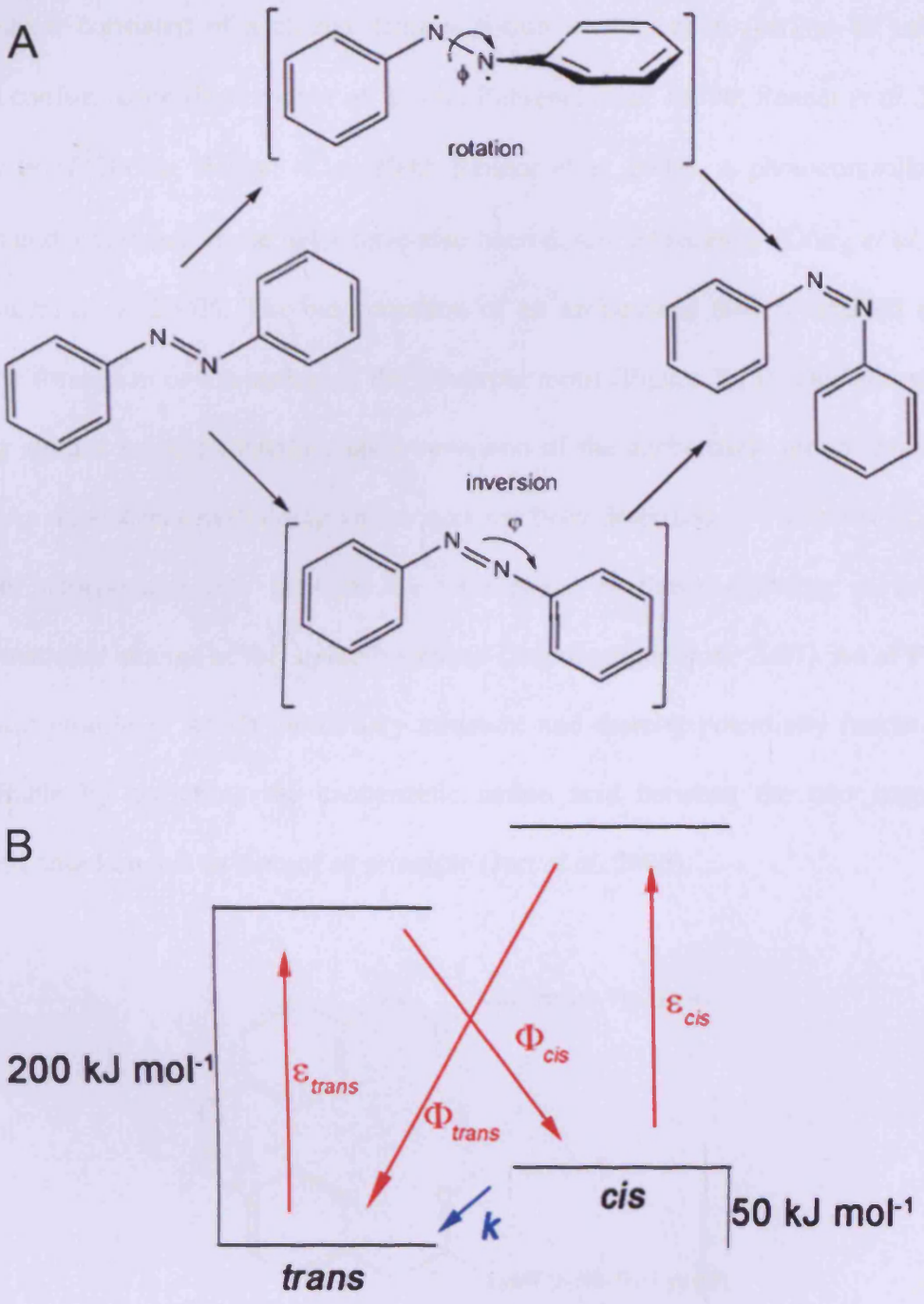

Scheme 1.2: *A) Conformational change of azobenzene and the two pathways of isomerisation and B) State model for the azobenzene chromophore. The rate of thermal relaxation is labelled k. Φ and ε denote quantum yield and extinction coefficient, respectively.*

A variety of structural motifs have been successfully modulated by azobenzene-containing agents. The conformation of cyclic peptides was controlled by incorporating an azobenzene moiety into the peptide backbone. The effect upon isomerisation of the

cross-linker consisted of a change from a β-turn conformation (*cis*) to an unfolded (*trans*) conformation (Behrendt *et al.* 1999a; Behrendt *et al.* 1999b; Renner *et al.* 2000a; Renner *et al.* 2000b; Renner *et al.* 2002; Renner *et al.* 2005). A photocontrollable β-hairpin and a collagen triple helix have also been described recently (Dong *et al.* 2006; Kusebauch *et al.* 2007). The incorporation of an azobenzene moiety enabled control over the formation or disruption of the β-hairpin motif (Figure 1.15). This allowed CD folding studies to be undertaken upon reversion of the azobenzene group from *cis* to *trans*. An azobenzene-containing amino acid has been described by Hilvert et *al.* which can be incorporated into peptides by solid-phase synthesis enabling a reversible conformational change of the amide backbone (Aemissegger *et al.* 2007). An aPP based miniature protein in which the tertiary structure and thereby potentially function was controllable by switching the azobenzene amino acid between the two states was designed based on this as a proof of principle (Jurt *et al.* 2006).

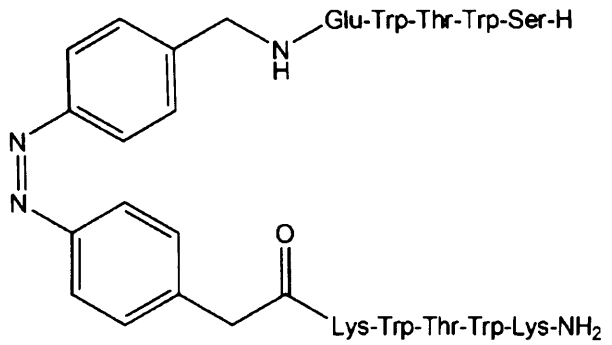

Figure 1.15: *A designed photocontrolled β-hairpin structure (*cis*-isomer).*

Light activatable ion channels have been developed which can aid in the study of the nervous system. The ligand is tethered to the channel *via* the azobenzene moiety and its effective concentration and binding to the receptor is modulated (Banghart *et al.* 2004; Volgraf *et al.* 2006; Gorostiza *et al.* 2007). The enzymatic activity of ribonuclease S

was controlled by photoresponsive S-peptide analogues containing phenylazophenylalanine residues (Liu 1997). Caamano *et al.* first described the photomodulation of DNA-binding affinity *via* an azobenzene cross-linker. Two basic leucine zipper (bZIP) domains were linked through the azobenzene moiety and so that their orientation became photoswitchable, enabling only the *cis*-form to interact tightly with the DNA major groove (Caamano *et al.* 2000).

Woolley and Smart *et al.* developed a cross-linking strategy that can be used to both stabilise and destabilise α-helix formation and initially applied it to regulating the structure of a model peptide (Kumita *et al.* 2000). This cross-linker used iodoacetamide groups which were then substituted by chloroacetamide groups in order to improve the light stability of the compound. Additionally, sulfonate groups were attached to the *meta* position of the benzene rings to enhance the water solubility (Zhang *et al.* 2003) (Scheme 1.3).

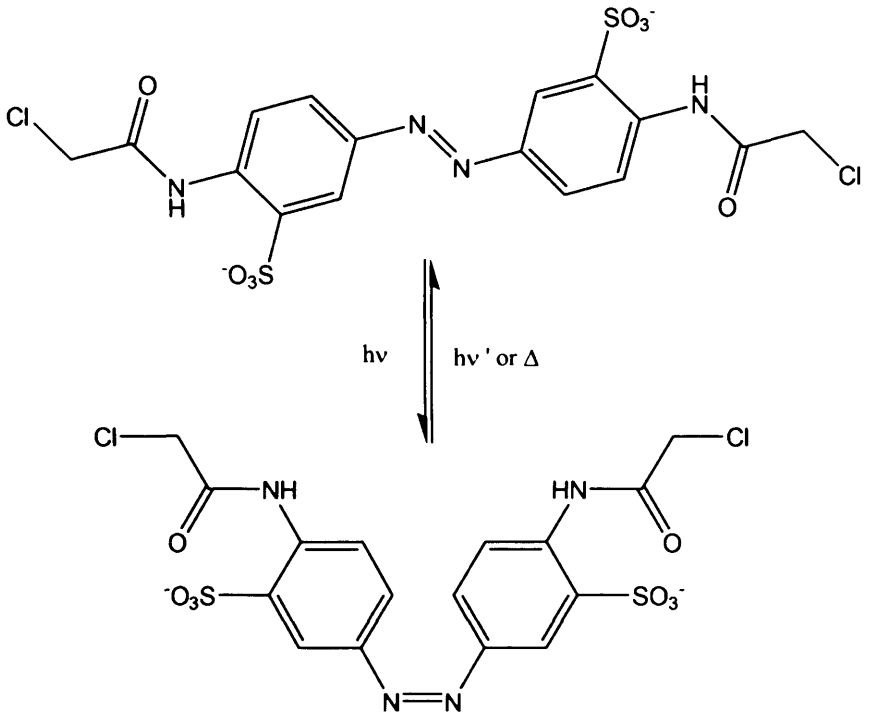

Scheme 1.3: *Structure of the azobenzene cross-linker designed and optimised by Zhang* et al.

The azobenzene cross-linker is incorporated into peptides *via* Sn2 reaction with two cysteines. It was established with the aid of molecular modelling that stabilisation of a helical motif in the *cis* form requires cysteines in the *i*, *i*+4 or *i*, *i*+7, whereas for the *trans* isomer a spacing of *i*, *i*+*11* is ideal. The light-induced state contains 70-90% *cis* isomer whereas the dark-adapted state comprises more than 99% *trans* (Zhang *et al.* 2003). In the *i*, *i*+*11* spacing, the cross-linker will be compatible with an α-helical peptide conformation in the *trans* form but the *cis* conformation it is too short to accommodate the structure. In the *i*, *i*+*7* and *i*, *i*+*4* spacing it is the other way round (Flint *et al.* 2002; Zhang *et al.* 2003) (Scheme 1.4).

Subsequent research into this strategy has shown that it is possible to regulate the DNA-binding specificity of two peptides by light. The 18 amino acid peptide HDH-3 which was based on the DNA recognition helix of the *engrailed* homeodomain was attached to

the azobenzene moiety in the *i, i+11* spacing (Figure 1.16). HDH-3 in the dark displayed the spectrum of an α-helix whereas the uncrosslinked peptide and HDH-3 in the light-induced state were mainly unstructured. HDH-3 in the dark-adapted state bound to the target sequence with high affinity (K_D = 7.5 nM) whereas in the light-induced state the affinity was reduced by one order of magnitude. Furthermore, dark-adapted HDH-3 displayed specificity similar to the full length protein. The *i, i+7* spacing, which allows helix-formation upon irradiation was tested using the bHLH domain of the transcription factor MyoD. The photochemical regulation of DNA binding specificity was achieved. PhotoMyoD displayed two orders of magnitude enhanced specificity for the target DNA sequence. This represents the first time this photocontrol strategy was used to modulate the functional properties of proteins (Guerrero *et al.* 2005a; Guerrero *et al.* 2005b).

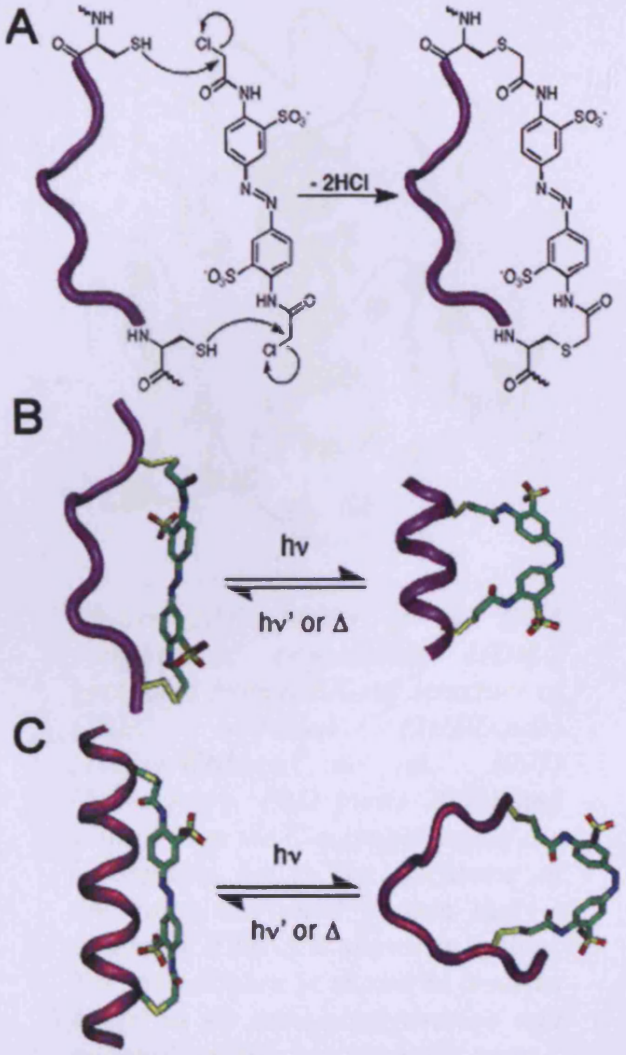

Scheme 1.4: *A) Mechanism of the cross-linking reaction between two sulfhydryl groups and the compound developed by Zhang* et al. *B) Conformational change upon isomerisation for the* i, i+7 *spacing. C) Conformational change upon isomerisation for the* i, i+11 *spacing.*

amino acid side chains have to be protected orthogonally so that they may be freed at a later point. A number of popular protecting groups are shown in Figure 1.17. Subsequently, the *N*-terminus of the peptide is deprotected again and can be therefore modified by acetylation or a fluorophore for example. The polymer is then cleaved from the solid support and the sidechain protection groups are removed (Scheme 1.5).

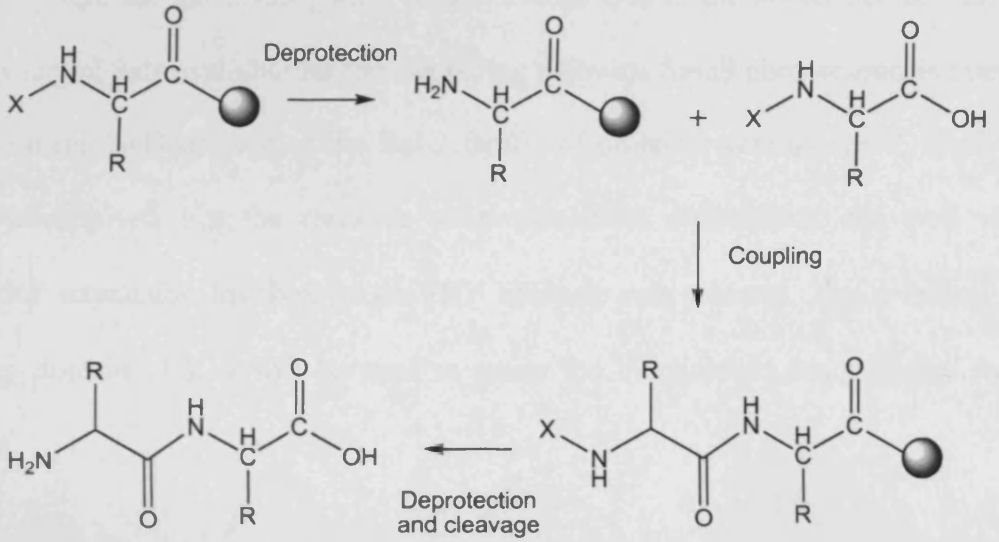

Scheme 1.5: *The solid phase peptide synthesis reaction scheme. The solid phase support is shown as a grey sphere (X = protecting group and R = amino acid side chain).*

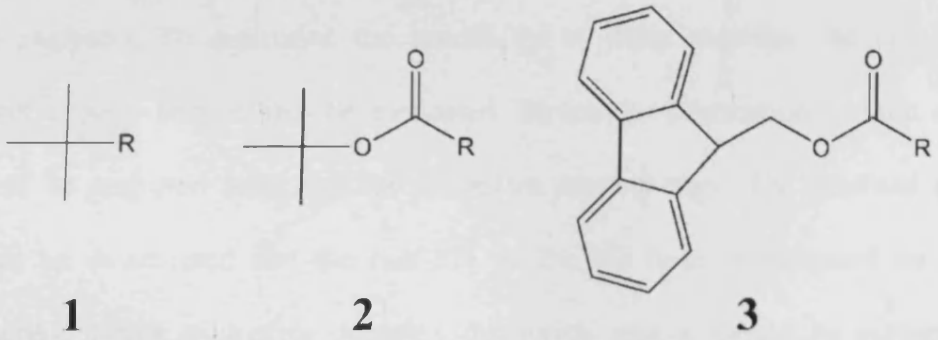

1 **2** **3**

Figure 1.17: *Popular* N*-terminal protecting groups.* t*-Butyl (*t*-Bu) (**1**), *t*-Butyloxycarbonyl (Boc) (**2**) and 9-Fluorenylmethoxycarbonyl (Fmoc) (**3**).*

1.6 Aim of the work described in this thesis

At the commencement of this study, protein-protein interactions and protein-RNA interactions had not been successfully photomodulated. The purpose of this study is to extend this approach to these two important types of biomacromolecular interactions. To test the feasibility of interfering with protein-protein interactions in the same manner as described for DNA-protein interactions, apoptosis signalling was chosen as a suitable model system for the investigation of this avenue due to the abundance of functional and structural data available for this signalling pathway. Small photoresponsive peptides based on the BH3 domain of the Bcl-2 family of proteins were designed, synthesised and characterised. For the research on protein-RNA interactions, the well studied Rev/RRE interaction involved in the HIV lifecycle was selected. The α-helical RNA binding domain of Rev will be used to create the biophotonic nanoswitches for this system.

The interaction of the obtained biophotonic nanoswitches with the target molecules is to be determined using fluorescence based assays and the differences in the binding affinities of the uncross-linked, light-induced and dark-adapted states of the peptides will be analysed. To determine the specificity of these peptides, the binding to a non-target protein should also be evaluated. Structural information for the different states will be acquired from circular dichroism spectroscopy. The obtained *cis/trans* ratio will be determined and the half-life of the *cis* form investigated by UV/Vis spectroscopy. NMR studies or complex disruption assays should be carried out to determine if the biophotonic nanoswitches target the same interaction interface as the wild-type peptides.

The controllable activation of transcription by PhotoMyoD or any other peptide inside a cell has not been demonstrated to date. Therefore PhotoMyoD and a peptide developed during the studies described in Chapter 3 were modified with a peptide transduction domain, to enable their future *in vivo* application.

CHAPTER 2:

Materials and methods

2.1 Materials

All chemicals were purchased from Fisher, Merck, Sigma-Aldrich, NovaBiochem, AGTC, New England BioLabs, GE Healthcare, QIAGEN or Fluka. The oligonucleotides were purchased from Operon.

2.1.1 Culture media

2.1.1.1 Luria Bertani (LB) medium

Bacto tryptone (10 g l^{-1}), yeast extract (5 g l^{-1}) and NaCl (10 g l^{-1}) were dissolved in deionised water. The pH was adjusted to 7.5 using 5 M NaOH, and the medium was autoclaved for 20 min at 15 lb $sqin^{-2}$ on a liquid cycle.

2.1.1.2 2× YT medium

Bacto tryptone (16 g l^{-1}), yeast extract (10 g l^{-1}) and NaCl (5 g l^{-1}) were dissolved in deionised water. The pH was adjusted to 7.0 using 5 M NaOH and the medium was autoclaved for 20 min at 15 lb $sqin^{-2}$ on a liquid cycle.

2.1.1.3 SOB medium

Yeast extract (5 g l^{-1}), tryptone (20 g l^{-1}), NaCl (0.58 g l^{-1}), KCl (0.186 g l^{-1}), $MgCl_2$ (2.0 g l^{-1}) and $MgSO_4$ (2.5 g l^{-1}) were dissolved in deionised water and the medium was autoclaved for 20 min at 15 lb $sqin^{-1}$ on a liquid cycle.

2.1.1.4 M9 minimal medium

To 900 ml of sterile water are added the following sterilised solutions:

100 ml of 10 x M9 salt (60g l^{-1} Na_2HPO_4, 30g l^{-1} KH_2PO_4, 5g NaCl, pH 7.4)

10 ml of 100 g l^{-1} NH_4Cl

2.0 ml of 1.0 M $MgSO_4$

12.5 ml of 20% (w/v) D-Glucose

0.2 ml of 0.5 M $CaCl_2$

1 mg Biotin

0.5 ml 2 mg ml^{-1} Thiamine hydrochloride

1.0 ml 15 mg ml^{-1} $FeCl_2$ in 1.0 M HCl

1.0 ml 15 mg ml^{-1} $ZnCl_2$ in slightly acidic water

(1 drop of 12 M HCl for 10 ml solution)

2.0 ml 10% (w/v) yeast extract

2.1.2 Agar plates

Agar plates were prepared with autoclaved LB medium containing agar (40 g l^{-1}) and the appropriate antibiotic concentration. The solution was poured into 90 mm Petri dishes under aseptic conditions. Once set, the agar plates were inverted and stored at 4 °C. For cell growth, a solution of bacterial culture was spread over the plate with a sterile glass rod and incubated at 37 °C overnight.

2.1.3 *E. coli* strains

The *E. coli* strains used in this work were: BL21(DE3), BL21(DE3)pLysS and XL1-Blue.

Table 2.1: *Genotype of the* E. coli *strains used in this work (Studier* et al. *1986).*

Strain	Genotype
BL21(DE3)	F⁻ *ompT* *hsdS*$_B$ (r_B^- m_B^-) *gal dcm* (DE3)
BL21(DE3)pLysS	F⁻ *ompT* *hsdS*$_B$ (r_B^- m_B^-) *gal dcm* (DE3) pLysS (Cam^R)
XL1-Blue	*end*A1 *rec*A1 *gyr*A96 *thi*-1 *hsd*R17 *sup*E44 *rel*A1 *lac* [F' *pro*AB $lacI^qZ\Delta M15$ Tn10 (Tet^r)]

The BL21 strains are designed for protein expression (Studier *et al.* 1986). The DE3 designation denotes that the strain contains the λDE3 lysogen carrying the gene for T7 RNA polymerase under the control of the *lac*UV5 promoter allowing induction of the expression of recombinant proteins with isopropyl-β-D-thiogalactopyranoside (IPTG). The pLysS plasmid produces T7 lysozyme to reduce basal levels of T7 RNA polymerase and thereby reducing the basal expression level of the gene of interest (Studier *et al.* 1986). This is essential in the cases where the protein produced is toxic to the cell. XL1-Blue strain (Table 2.1) is a host for optimal propagation of plasmids. This strain is used for cloning where high transformation efficiencies are required.

2.1.4 Preparation of antibiotic solutions

Stock solutions were prepared by dissolving each antibiotic in the appropriate solvent; filter sterilised using a 0.2 μm syringe filter, aliquoted and finally stored at -20 °C. Ampicillin stocks were prepared to a final concentration of 50 mg ml^{-1} in deionised water and used at a concentration of 100 μg ml^{-1}. Chloramphenicol stocks were diluted to a final concentration of 34 mg ml^{-1} in ethanol and used at a concentration of 34 μg ml^{-1}.

Table 2.1: *Genotype of the* E. coli *strains used in this work (Studier* et al. *1986).*

Strain	Genotype
BL21(DE3)	F⁻ *ompT* *hsd*S_B (r_B^- m_B^-) *gal dcm* (DE3)
BL21(DE3)pLysS	F⁻ *ompT* *hsd*S_B (r_B^- m_B^-) *gal dcm* (DE3) pLysS (Cam^R)
XL1-Blue	*end*A1 *rec*A1 *gyr*A96 *thi*-1 *hsd*R17 *sup*E44 *rel*A1 *lac* [F' *pro*AB $lacI^qZ\Delta M15$ Tn10 (Tet^r)]

The BL21 strains are designed for protein expression (Studier *et al.* 1986). The DE3 designation denotes that the strain contains the λDE3 lysogen carrying the gene for T7 RNA polymerase under the control of the *lac*UV5 promoter allowing induction of the expression of recombinant proteins with isopropyl-β-D-thiogalactopyranoside (IPTG). The pLysS plasmid produces T7 lysozyme to reduce basal levels of T7 RNA polymerase and thereby reducing the basal expression level of the gene of interest (Studier *et al.* 1986). This is essential in the cases where the protein produced is toxic to the cell. XL1-Blue strain (Table 2.1) is a host for optimal propagation of plasmids. This strain is used for cloning where high transformation efficiencies are required.

2.1.4 Preparation of antibiotic solutions

Stock solutions were prepared by dissolving each antibiotic in the appropriate solvent; filter sterilised using a 0.2 μm syringe filter, aliquoted and finally stored at -20 °C. Ampicillin stocks were prepared to a final concentration of 50 mg ml^{-1} in deionised water and used at a concentration of 100 μg ml^{-1}. Chloramphenicol stocks were diluted to a final concentration of 34 mg ml^{-1} in ethanol and used at a concentration of 34 μg ml^{-1}.

Kanamycin was prepared as a 35 mg ml^{-1} stock solution in deionised water and used at a final concentration of 50 μg ml^{-1}.

2.1.5 Preparation of reagents and buffers

All buffers were made as stock solutions according to Sambrook *et al.* (1989).

2.1.5.1 50× TAE (Tris-acetate/EDTA) electrophoresis buffer

Per litre,

242 g Tris base (pH 8.0)

27.1 ml glacial acetic acid

100 ml 0.5 M ethylene diamine tetraacetic acid (EDTA)

2.1.5.2 10× SDS running buffer

Per litre,

30.3 g Tris base (pH 8.3)

144 g glycine

10 g sodium dodecyl sulfate (SDS)

2.1.5.3 SDS gel-loading buffer

Per 10 ml,

1.25 ml 0.5 M Tris-HCl (pH 6.8)

2 ml 10% SDS

0.2 ml of a 0.5% (w/v) bromophenol blue solution

2.5 ml glycerol

0.5 ml β-mercaptoethanol

3.55 ml deionised water

2.1.5.4 Staining buffer for SDS-PAGE

0.25% (w/v) Coomassie brillant blue

45% (v/v) methanol: deionised water

10% (v/v) glacial acetic acid

2.1.5.5 Destaining buffer for SDS-PAGE

10% (v/v) glacial acetic acid

12% (v/v) isopropanol

in deionised water

2.1.5.6 Gel-loading buffer for agarose gel electrophoresis

0.25% (w/v) bromophenol blue

15% glycerol (v/v)

2.1.5.7 1 M IPTG

2.383 g IPTG was dissolved in 10 ml deionised water and sterilised by filtration through a 0.2 µm syringe filter.

2.1.5.8 0.5 M phenylmethylsulfonylfluoride (PMSF)

87 mg PMSF was dissolved in 1 ml isopropanol and stored at 4 °C.

2.1.5.9 Phosphate buffered saline (PBS)

Per litre of deionised water

8.12 g NaCl

0.75 g KCl

0.88 g $Na_2HPO_4 \times 2H_2O$

0.35 g KH_2PO_4

2.1.5.10 TB solution

To 100 ml water the following was added:

0.30 g Piperazine-1,4-bis(2-ethanesulfonic acid) (PIPES)

0.22 g $CaCl_2$

1.86 g KCl

The pH was adjusted to 6.7 and 1.08 g of $MnCl_2$ dissolved.

The solution was filtered through a 0.22 µm filter for sterilisation.

2.1.5.11 RNase free solutions

RNase free water and buffers were obtained by adding 0.1% diethylpyrocarbonate (DEPC) to the respective solution prior to incubation at 37 °C for 1 hour. The remaining DEPC was destroyed by autoclaving. Amine group containing compounds such as 2-(4-(2-hydroxyethyl)-1-piperazinyl)-ethanesulfonic acid (HEPES) were added after this step.

2.1.5.12 FRET buffer

Per litre:

7.14 g HEPES (pH 7.5)

7.46 g KCl

2.32 g NaCl

0.77 g NH_4Ac

0.24 g guanidinium hydrochloride

0.19 g $MgCl_2$

0.19 g EDTA

100 µl Triton X-100

2.2 Molecular biology methods

2.2.1 Preparation of competent cells

The desired *E. coli* strain was aseptically streaked out from a frozen glycerol stock onto an agar plate containing appropriate antibiotics. The plate was incubated overnight at

37 °C. Ten large colonies were picked and cultured with vigorous shaking in 250 ml SOB medium in a 1 litre flask at 20 °C. Upon reaching an OD_{600} of 0.5 (after 24 h to 36 h), the flask was placed on ice for 10 min. The cells were pelleted by centrifugation at 4 °C and gently resuspended in ice-cold TB medium and stored on ice for 10 min. The cells were pelleted again and resuspended in 20 ml of TB and 1.4 ml of dimethylsulfoxide (DMSO). 100µl aliquots were flash frozen and stored at -80 °C.

2.2.2 Transformation

A sample of plasmid DNA (1µl-10µl) and 100 µl of competent cells were mixed in an Eppendorf tube and incubated on ice for 30 min. The cells were then subjected to heat shock (40 °C) for 45 s before being placed on ice for a further 2 min. The cells were incubated at 37 °C for 1 h with shaking at 180 rpm in 1 ml LB medium. The solution was then centrifuged for 1 minute at maximum speed (~16,000 *g*) in a bench top microcentrifuge and the supernatant was discarded. The cells were resuspended in fresh LB medium (100 µl) and the solution was plated on a prewarmed at 37 °C agar plate containing the appropriate antibiotic(s). The plate was incubated at 37 °C overnight.

2.2.3 DNA isolation and purification

2.2.3.1 QIAprep Spin Miniprep Kit™

The QIAprep Spin Miniprep Kit™ was used for purification of up to 20 µg of high-copy plasmid DNA from 5 ml overnight cultures of *E. coli* in LB medium. The procedure was followed according to the manufacturer's instructions.

2.2.3.2 Agarose gel electrophoresis

Agarose gels were used for analysis and isolation of DNA fragments. Powdered agarose was dissolved in 50 ml 1× TAE buffer to a final concentration of 1% using a microwave oven to melt the agarose and the mixture was poured into the minigel kit (CBS Scientific) and left to set. Samples were mixed with the gel-loading buffer and loaded into the gel. Gels were run in 1× TAE buffer at 60 mA for 60 min after which the DNA was stained with ethidium bromide and visualised with a UV lamp at 254 nm. The DNA fragment of interest was excised from an agarose gel with a clean, sharp scalpel. The QIAquick Gel Extraction Kit was used according to the manufacturer's instructions (QIAGEN).

2.2.4 Quantification of DNA and oligonucleotides in solution

The concentration of nucleic acids was determined spectrophotometrically using a Shimadzu BioSpec-mini spectrophotometer to determine the optical density (OD) of a solution of DNA or oligonucleotide at 260 nm. An OD_{260} reading of 1.0 corresponds to a concentration of approximately 50 μg ml^{-1} for double-stranded DNA and 20 μg ml^{-1} single-stranded oligonucleotides. The ratio of the absorbencies measured at 260 and 280 nm (OD_{260}/OD_{280}) gives an indication of the purity of the nucleic acid in the sample. A ratio of around 1.8 indicates a DNA sample is pure. If the sample is contaminated with proteins and/or lipids the ratio will be lower.

2.2.5 Storage of plasmids

2.2.5.1 Ethanol precipitation of nucleic acids

To precipitate the purified DNA, 50 µl 7.5 M ammonium acetate and 2.5 volumes of absolute ethanol were mixed with the DNA solution and the mixture was left for 10 min at room temperature. The solution was then centrifuged for 15 min at maximum speed (~16,000 *g*) in a bench top microcentrifuge. The supernatant solution was discarded and the pellet was washed with 250 µl 80% ethanol. The solution was centrifuged for 10 min as before and the supernatant discarded. The pellet was dried at 37 °C in an oven and stored at -20 °C.

2.2.5.2 Glycerol stocks

To prepare glycerol stocks a sample (0.8 ml) of cells from an overnight culture was aseptically mixed with 0.2 ml of sterile glycerol. Glycerol stocks were stored at -80 °C.

2.2.6 Digestion with restriction enzymes

Digestion reactions were performed with the desired volume of DNA (usually 10 µl) and the restriction endonucleases in their recommended buffers (New England Biolabs and Pharmacia). The total volume of the reactions was 20 µl. Reactions were incubated at 37 °C for 4 hours. For double digestions the buffer used was as per manufacturer's instructions in order to provide the highest digestion efficiency for both enzymes. The DNA products from digestion were analysed by agarose gel electrophoresis.

2.2.7 Dephosphorylation of DNA fragments

Following digestion with a single restriction enzyme, the vector should be dephosphorylated at the 5'-end with calf alkaline phosphatase (CAP) to avoid self-ligation, to this end, the DNA (0.05 μg μl^{-1}) was suspended in 1× NEBuffer (supplied by New England Biolabs). Next, 0.5 U μg^{-1} of vector DNA of alkaline phosphatase (from calf intestinal mucosa) was added to the mixture. The solution was incubated at 37 °C for 60 min, followed by purification of the DNA using gel purification.

2.2.8 Phosphorylation of DNA fragments (kinase reaction)

Oligonucleotides were phosphorylated at the 5'-end with 0.5 μl T4 Polynucleotide Kinase in T4 ligase buffer (50 mM Tris-Cl (pH 7.5 at 25 °C), 10 mM $MgCl_2$, 10 mM dithiothreitol (DTT), 1 mM adenosine triphosphate (ATP), 25 μg ml^{-1} bovine serum albumin (BSA)) and 2 mM $MgCl_2$. The solutions were incubated at 37 °C for 2 h. The success of the reaction was not analysed at this stage.

2.2.9 Annealing oligonucleotides

Equimolar quantities of oligonucleotides were mixed in an Eppendorf tube that was placed in a heat block at 95 °C. After 5 min at 95 °C, the heat block was switched off and the sample left to cool to RT. The annealed oligonucleotides were stored at -20 °C.

2.2.10 Ligation reaction

The desired gene was ligated into an appropriate expression vector. The digested plasmid and the insert were mixed together with 1 µl T4 DNA ligase (10 U μl^{-1}) and 1× T4 DNA ligase buffer (400 mM Tris-HCl (pH 7.8 at 25 °C), 100 mM $MgCl_2$, 100 mM DTT, 5 mM ATP). The solution was then incubated at 16 °C for 4 h. Products were stored at -20 °C.

2.2.10.1 PCR Script ligation kit

The kit was used according to the manufacturer's instructions.

2.2.11 Polymerase chain reaction (PCR)

Each reaction mixture was prepared in a 0.5 ml PCR tube and composed of 5 U *Pfu* Turbo DNA Polymerase, 0.2 ng DNA template, 0.5 mM of each primer, 10 mM dNTP mix (0.2 mM of each: dATP, dCTP, dGTP, dTTP), 1× PCR buffer (200 mM Tris-Cl (pH 8.4) and 500 mM KCl) and 2 mM $MgCl_2$. Sterile deionised water was added to give a final volume of 50 µl. The temperatures were determined in each case considering the melting temperatures of the primers being used. The typical cycle implemented was as follows: 1 min at 95 °C (denaturation), 1 min at 55 °C (annealing) and 1 min/1,000 bps at 72 °C (extension). This thermal cycle was repeated 30 times. Amplification of the desired DNA fragment was confirmed by agarose gel electrophoresis and the products were stored at -20 °C.

2.2.12 Mutagenesis

The QuikChange™ Site-Directed Mutagenesis Kit was used to achieve single amino acid mutations. The procedure was followed according to the manufacturer's instructions.

2.2.13 DNA sequencing

All sequencing reactions were carried out by Lark.

2.2.14 Reactions with modifying enzymes

Reactions with the modifying enzymes T7 polymerase and T4 polynucleotide kinase polymerase were carried out according to manufacturer's procedures. Reaction volumes were 20 µl.

2.3 General methods for protein preparation and purification

2.3.1 Growth of bacterial cultures

Overnight cultures were grown in sterile conditions by inoculating a single colony from an agar plate into 5 ml LB medium containing the appropriate antibiotic(s). The cultures were incubated at 37 °C with constant shaking at 180 rpm.

2.3.2 Protein expression using the T7 system

The desired competent cells were transformed with plasmid DNA. For large scale expression, the colonies were grown overnight in 10 ml LB medium containing the

appropriate antibiotic(s). The entire contents of each of the overnight cultures were transferred to separate 500 ml of fresh LB medium or 2× YT medium containing antibiotics in 2 litre conical flasks, and incubated until they reached an OD_{600} ~0.5. The cells were then induced with IPTG to a final concentration of 0.8 mM and left to grow for 4 to 6 h. 1 ml samples were taken from each flask (including a sample prior to induction) and SDS-PAGE was used to analyse the extent of the expression of the target protein. The cells were then centrifuged at 6,800 g for 10 min at 4 °C and pellets were stored at -20 °C.

2.3.3 Lysis of cells

Pellets from a large-scale expression were thawed on ice and resuspended by vortexing in the appropriate lysis buffer. PMSF was added to a concentration of 0.5 mM and the suspension was sonicated for 10 min (5 s on, 20 s off) on ice using a Sonicator W-37 (Heat Systems Ultrasonics Inc.). The resulting lysate was centrifuged at 40,000 g for 20 min and the protein-containing supernatant decanted.

2.3.4 Dialysis and storage of pure protein

To remove undesired components, the samples were dialysed using Medicell International Ltd. dialysis membranes (12,500 and 3,500 molecular weight cut off (MWCO), respectively) into the appropriate buffer with stirring at 4 °C. The dialysis buffer was changed in 12 hour intervals until the desired dilution was obtained. Purified protein was either transferred into appropriate buffers, flash frozen and stored at -20 °C or lyophilised and stored at -20 °C.

2.3.5 Measurement and calculation of protein concentration

2.3.5.1 Determination of the concentration of protein

The concentration of Bcl-x_L and HDM2 was determined spectrophotometrically. Absorbance measurements were taken at 210 nm using a Shimadzu UV-2401PC UV/Vis Recording Spectrophotometer. A clean quartz cuvette was used to hold the samples.

Protein concentration was calculated using the equation:

$$C(mg ml^{-1}) = \frac{A}{dX_{210}} \qquad \textbf{Equation 2.1}$$

where A is the absorbance, d is the pathlength in cm and $X_{210} = 20$.

2.3.5.2 Determination of peptide concentration

The concentration of FAM-labelled peptide was determined using an extinction coefficient at 494 nm of 83,000 $M^{-1}cm^{-1}$. The concentration of TMR-labelled peptides was determined using an extinction coefficient at 550 nm of 96,900 M^{-1} cm^{-1}. Peptide concentrations for cross-linked peptides were calculated using an extinction coefficient at 363 nm of 24,000 M^{-1} cm^{-1} (Lucia Guerrero, PhD thesis 2005). The concentration of uncross-linked and unlabelled peptide was obtained from the absorbance at 210 nm after dialysis of the peptide.

2.3.6 Sodium dodecyl sulfate polyacrylamide gel electrophoresis

A 10 ml volume of 15% resolving gel (2.4 ml deionised water, 5 ml 30% degassed acrylamide/bis-acrylamide, 2.5 ml 1.5 M Tris-Cl (pH 8.8), 0.1 ml 10% w/v SDS) was mixed with 10% APS (100 µl) and TEMED (10 µl). The solution was immediately poured in between the assembled glass plates up to a height of 5 cm and left to polymerise at room temperature. A 3 ml aliquot of 5% stacking gel (5.7 ml deionised water, 1.7 ml 30% degassed acrylamide/bis acrylamide, 2.5 ml 0.5 M Tris-Cl (pH 6.8), 0.1 ml 10% w/v SDS) containing the same polymerising agents (10% APS (100 µl) and TEMED (10 µl)) was pipetted on top of the resolving gel. A comb possessing either 10 or 15 teeth was immediately inserted between the plates and the stacking gel was left to polymerise at room temperature. The comb was then removed and the wells rinsed with 1× SDS running buffer. Samples, mixed with 1× SDS gel-loading buffer, were loaded into the gel (15 µl in the 10-well gels and 8 µl in the 15-well gels) and ran at 200 volts for 50 min. After electrophoresis, the gel was stained then destained using the appropriate buffers, followed by visualisation of the protein bands on a light box.

2.3.7 Mass spectrometry

Matrix Assisted Laser Desorption Ionisation Time of Flight (MALDI-TOF) mass spectrometry was performed to identify the purified proteins and peptides. Either a sinapinic acid or an α-cyano-hydroxy-cinnamic acid matrix containing 0.1% trifluoroacetic acid (TFA) were used for MALDI-TOF experiments. The peptides were ionised on a thin film of one part peptide solution to one part matrix, using a Waters Micro MX mass spectrometer.

2.4 Purification of Bcl-x_L

The cells were lysed in 100 mM sodium phosphate buffer (pH 7.5) containing 100 mM β-mercaptoethanol. The clarified lysate was dialyzed against 100 mM sodium phosphate buffer (pH 7.5) containing 5 mM β-mercaptoethanol to allow purification on a Ni-Sepharose column. Following loading of the protein solution, the column was washed with 100 mM sodium phosphate buffer (pH 7.5) containing 500 mM NaCl, 5 mM β-mercaptoethanol and 50 mM imidazole, and bound Bcl-x_L was eluted using the same buffer containing 500 mM imidazole. The purity of the resulting protein was analyzed by SDS polyacrylamide gel electrophoresis and the correct mass was verified by MALDI-TOF mass spectrometry (measured: 25,922; calculated: 25,985 Da). The full protein sequence is given in the appendix section.

2.5 ^{15}N-Labelling of Bcl-x_L

For the ^{1}H ^{15}N HSQC NMR experiments ^{15}N-labelled protein was produced. Due to the lower aggregation tendencies of the truncated loop protein this was used for these experiments. A pET vector coding for residues 1 to 212 (Δ45-84) of Bcl-x_L and a *C*-terminal His-tag was obtained from Dr. Matt Crump (University of Bristol) and BL21(DE3) cells were transformed with the plasmid. These cells were grown at 37 °C in M9 minimal medium to an OD_{600} of 0.5 and induced at that point with IPTG (0.4 mM). After 4 hours of incubation, the cells were harvested and the purification protocol described for the non-truncated protein followed. The elution of the protein from the column was done in a step-wise manner (50 mM, 100 mM and 250 mM imidazole) to enhance the purity of the obtained protein.

2.6 Purification of HDM2

The HDM2 (1-125) protein was obtained from Thomas Fricke. It was expressed and purified as described by Nicholas Taylor (PhD thesis 2009).

2.7 Purification of TAT Bid KSI protein

The cells were lysed in 100 mM sodium phosphate buffer (pH 7.5) containing 100 mM β-mercaptoethanol. The protein was either directly cleaved using cyanogen bromide at this step or extracted from the pellet with sodium phosphate buffer (pH 7.5) containing 6 M guanidinium hydrochloride and 5 mM β-mercaptoethanol and the resulting protein solution applied to a Ni-sepharose column, depending on the obtained expression level. Following the loading of the protein solution, the column was washed with 100 mM sodium phosphate buffer (pH 7.5) containing 500 mM NaCl, 5 mM β-mercaptoethanol and 50 mM imidazole and 6 M guanidinium hydrochloride. The bound protein was eluted using the same buffer containing 500 mM imidazole. The protein was dialysed into water and the resulting precipitate used in the cyanogen bromide cleavage step. The full protein sequence is given in the appendix section.

2.8 Purification of PhotoMyoD penetratin

2.8.1 Cation exchange chromatography

The full protein sequence of PhotoMyoD penetratin is given in the appendix section. After expression, the cells were lysed in 50 mM potassium phosphate buffer (pH 8.0) containing 100 mM β-mercaptoethanol and dialysed against the same buffer. A CM

cation exchange column was equilibrated with 50 mM potassium phosphate buffer (pH 8.0) containing 100 mM β-mercaptoethanol and the protein solution loaded directly onto the column with the help of a pump. Once all the protein solution was loaded and the spectrophotometer reached a steady 280 nm reading, the bound protein was eluted with a NaCl gradient from 0 to 1.5 M using a 50 mM potassium phosphate buffer (pH 8.0) containing 100 mM β-mercaptoethanol and 1.5 M NaCl with a flow rate of 3 ml min^{-1}. The fractions were collected and analysed by SDS-PAGE.

2.8.2 Size exclusion chromatography

The cells were lysed in 100 mM sodium phosphate buffer (pH 7.5) containing 100 mM β-mercaptoethanol and 100 mM sodium chloride and dialysed against the same buffer. The solution was concentrated using a Vivaspin centrifugal concentrator (MWCO 10,000 Da) and applied to an equilibrated Sephadex G-75 size exclusion column. The obtained protein was passed through a Vivaspin centrifugal concentrator (MWCO 30,000 Da) to remove remaining impurities.

2.9 Purification of His-tagged PhotoMyoD penetratin

The cells were lysed in 100 mM sodium phosphate buffer (pH 7.5) containing 100 mM β-mercaptoethanol. The protein was extracted from the pellet with sodium phosphate buffer (pH 7.5) containing 6 M guanidinium hydrochloride and 5 mM β-mercaptoethanol and the resulting protein solution applied to a Ni-sepharose column. Following loading of the protein solution, the column was washed with 100 mM sodium phosphate buffer (pH 7.5) containing 500 mM NaCl, 5 mM β-mercaptoethanol, 50 mM

imidazole and 6 M guanidinium hydrochloride. The bound protein was eluted using the same buffer containing 500 mM imidazole.

2.9.1 Enterokinase cleavage

The protein was dialysed into 50 mM Tris buffer (pH 8.0) containing 1 mM DTT and 2 M urea. 50 units enterokinase were added to 3 ml of the protein solution and incubated at 20 °C for 20 hours. The success of the reaction was analysed by SDS-PAGE.

2.10 Peptide synthesis and purification

$Bak_{72\text{-}87}^{wild\text{-}type}$, $Rev_{33\text{-}50}^{wild\text{-}type}$ $Rev_{33\text{-}50}^{i+7}$ and $Bak_{72\text{-}87}^{i+7}$ were synthesised on Rink amide resin using a CEM Liberty microwave synthesiser, solid phase peptide synthesis and standard Fmoc chemistry (0.1 mM scale). For the synthesis of $Rev_{33\text{-}50}^{wild\text{-}type}$ $Rev_{33\text{-}50}^{i+11}$, $Bak_{72\text{-}87}^{i+11}$ and $Bid_{91\text{-}111}^{i+4}$ peptides; Rink amide 4-methylbenzhydrylamine (MBHA) resin was used. The sidechains were protected by the following groups: Arg (Pbf), Asn (trt), Asp (OtBu), Cys (trt), His (trt), Gln (trt), Glu (tBu) and Trp (boc). 20% piperidine in DMF was used to deprotect the N-terminus after each coupling. 0.45 M 2-(1H-benzotriazole-1-yl)-1,1,3,3-tetramethyluronium, 0.45 M hydroxybenzotriazole (HBTU/HOBt) in DMF and 2 M diisopropylethylamine (DIEA) served as the coupling mixture. The peptide was cleaved from the resin using 10 ml of a 95:2.5:2.5 mixture of TFA, water and triisopropylsilane (TIPS). After 2 hours incubation at room temperature, the resin was filtered off and 90% of the solvent was removed by rotary evaporation. 10 ml of cold diethyl ether was then added to precipitate the peptide. After one hour in the freezer (-20 °C) the peptide was isolated from the mixture by

centrifugation at 16,000 g. Subsequent purification was accomplished by Reverse Phase HPLC using a Phenomenex Luna 10u C18(2) 100 Å column (250 x 10 mm). Either a 0% to 60% or 0% to 100% acetonitrile linear gradient was run over 60 min. The flow rate was 5 ml min^{-1}.

2.11 Fluorophore labelling of the peptides

For the fluorescence-based binding studies the peptides had to be modified with an appropriate fluorophore. Carboxyfluorescein (FAM) and carboxytetramethylrhodamine (TMR) were selected because their absorbance and emission wavelength region will not interfere with the absorbance of the cross-linker. FAM and TMR can also be used as a Fluorescence Resonance Energy Transfer (FRET) donor and acceptor pair since they possess favourable spectral overlap.

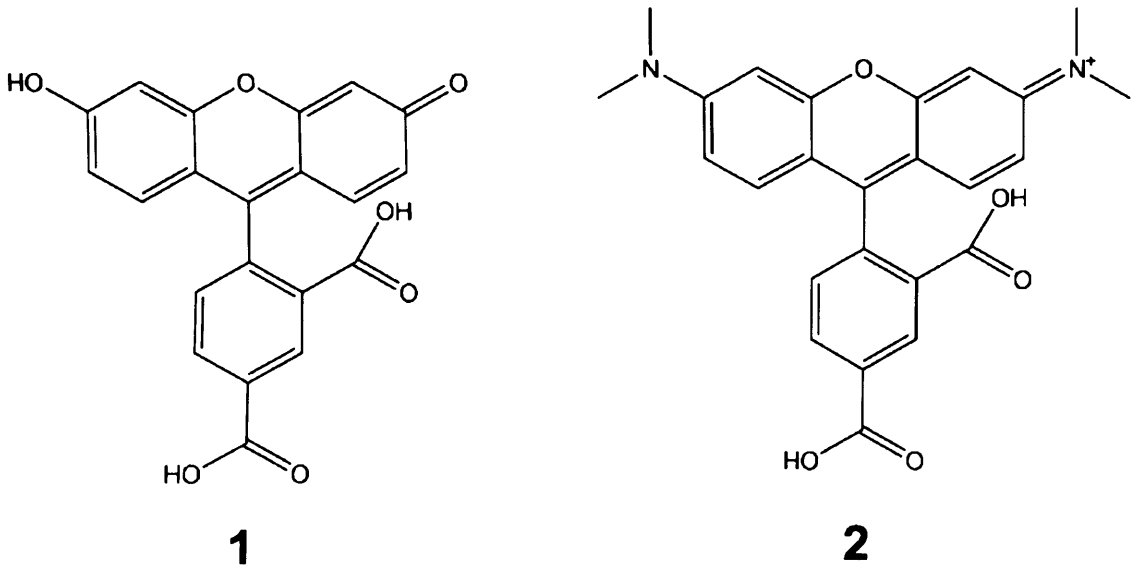

Figure 2.1: *Structure of 5-Carboxyfluorescein (5-FAM) (1) and 5-Carboxytetramethylrhodamine (5-TMR) (2).*

2.11.1 FAM-labelling

50 mg of 5(6)-FAM, 20 mg of HOBt and 26 µl of diisopropylcarbodiimide (DIPCDI) were incubated in 1 ml dimethylformamide (DMF) for 10 min. This solution was then added to the peptide on the resin and left to react at room temperature for 2 hours with agitation. The resin was filtered off and washed with dichloromethane (DCM).

2.11.2 TMR-labelling

50 mg of 5(6)-TMR, 20 mg of HOBt and 26 µl of DIPCDI were incubated in 1 ml DMSO for 10 min. This solution was then added to the peptide on the resin and left to react on a shaker at room temperature for 6 hours. The resin was filtered off and washed with DCM.

2.12 Cyanogen bromide cleavage

The fusion protein pellet was dissolved in 6 ml of 80% formic acid and transferred to a 50 ml round-bottomed flask. 0.2 g of cyanogen bromide was added and the solution bubbled with nitrogen. The flask was wrapped in aluminium foil and the reaction stirred for 18-22 h. The mixture was desiccated on a rotary evaporator and the resultant gel extracted and centrifuged repeatedly with small volumes of PBS. The peptide was then purified by HPLC using a 0-100% acetonitrile gradient over 60 min. To open the lactone ring, 0.2 N NaOH was added until a pH of 12.5 was reached. The solution was neutralised with dilute HCl after this.

2.13 Synthesis of the azobenzene cross-linker

The cross-linker (BSBCA) was synthesised and purified according to the procedure described previously (Zhang *et al.* 2003; Burns *et al.* 2007). Briefly, 2,5-diaminobenzenesulfonic acid (**1**) was acetylated and compound (**2**) was isolated from the product mixture by repeated wash steps with acetic acid (~80 °C). The compound (**2**) is oxidised under basic conditions to give the azobenzene core structure (**3**). The acetyl groups are removed to give product (**4**) and the reaction with chloroacetic acid yields the final product (**5**) (Scheme 2.1). The intermediates and the end product were analysed by ^{1}H NMR spectroscopy. The end product was further characterised by ESI-MS (calculated (*m/z*) 522.95, observed (*m/z*) 522.96). ^{1}H NMR (500 MHz, D_2O) δ 4.42 (s, 2H, CH_2), 7.95 (dd, 1H, H_b), 8.07 (d, 1H, H_a), 8.27 (d, 1H, H_c).

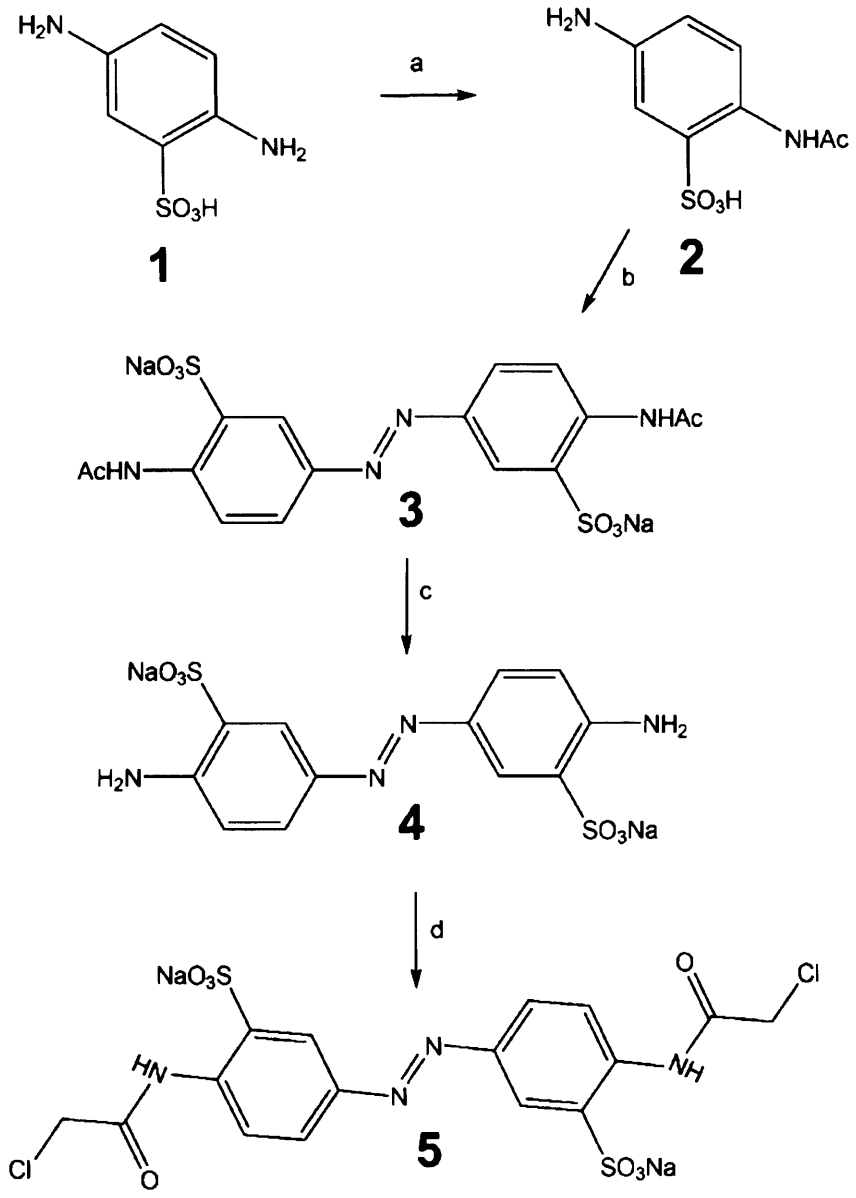

Scheme 2.1: *Synthesis of 3,3'-bis(sulfo)-4,4'-bis(chloroacetamido)-azobenzene (BSBCA): a) glacial acetic acid, acetic anhydride (1.2 eq.); b) i. H_2O, sodium carbonate ii. sodium hypochlorite; c) i. H_2O, HCl ii. NaOH and d) chloroacetic acid (24 eq.), chloroacetic anhydride (24 eq.).*

2.14 Cross-linking

2.14.1 Reaction at 4 °C

The peptides were incubated in Tris buffer (pH 8.3) containing 0.5 mM TCEP for 15 min at 4 °C to ensure that the cysteine residues were in the reduced state. Then 1 ml of a 2 mM cross-linker solution in 50 mM Tris buffer (pH 8.3) was added in three portions in 20 min intervals. The reaction was allowed to proceed for 12 hours. The cross-linked peptides were purified by reverse phase HPLC using the same equipment and procedure as previously described for the uncross-linked peptides and the correct mass was verified by MALDI-TOF mass spectroscopy

2.14.2 Reaction at 50 °C

In the cases were the reaction at 4 °C failed the alkylation was performed at 50 °C with 2 hours incubation after each addition of the azobenzene compound. Purification was performed immediately afterwards as described for the procedure above (2.14.1).

2.15 Photoisomerisation

Photoisomerisation of dark-adapted BPNs was achieved by irradiating a solution of the peptide with a 250 W metal halide UV Light Point Source (UV-P 280) coupled to a 360 nm band pass filter (10 nm bandwidth). Photoisomerisation was complete in less than 5 min as judged by the absence of further changes in the UV/Vis spectra. The percentage of isomerisation was calculated by using the respective extinction coefficients for the pure *cis* from (ε_{363nm} = 1,100 M^{-1} cm^{-1}) (Zhang *et al.* 2003) and the *trans* form to determine the ratio from the obtained absorbance values before and after

irradiation (A_{dad} and A_{lid}).

$$A_{lid} = A_{cis} + A_{trans}$$

$$A_{lid} = x\ \varepsilon_{cis}\ d\ [BPN] + (1 - x)\ \varepsilon_{trans}\ d\ [BPN] \qquad (x = \text{fraction of } cis \text{ isomer})$$

$$x = \frac{A_{lid} - \varepsilon_{trans} d\ [BPN]}{d(\varepsilon_{cis} - \varepsilon_{trans})}[BPN]$$

$$x = \frac{A_{lid} - A_{dad}}{d(\varepsilon_{cis} - \varepsilon_{trans})}[BPN] \qquad \textbf{Equation 2.2}$$

2.16 UV/Visible absorption experiments

All spectra were recorded in 5 mM potassium phosphate buffer (pH 8.0) at 5 °C using a Shimadzu UV-2401PC UV/Vis spectrometer or a Jasco V-660 spectrophotometer, running a 5 mm or 1 mm path length cuvette. The concentration was typically 100 μM. First order kinetics for the thermal *cis* to *trans* reversion were assumed since the rate of reversion should only depend on the concentration of *cis*-peptide (*cis*-P). The corresponding integrated first-order rate law is:

$$[cis\text{-}P] = [cis\text{-}P]_0\ e^{-kt} \qquad \textbf{Equation 2.3}$$

Since [*cis*-P] is directly proportional to the percentage of non-reverted irradiated peptide ($\%_{lid}$), the rate constant k for the thermal relaxation process could be calculated from a plot of ln $\%_{lid}$ (t) versus t. $\%_{lid}$ (t) is defined as:

$$\%_{lid}(t) = \frac{100 A_{363}(t)}{A_{363}^{\ dark} - A_{363}^{\ lid}} \qquad \textbf{Equation 2.4}$$

where A_{363} is the measured absorbance at 363 nm at time t and A_{363}^{dark} and A_{36}^{lid} are the values for the absorbance immediately before and after irradiation.

The activation energy for the isomerisation reactions was determined using the Arrhenius equations:

$$k = Ae^{\frac{-E_a}{RT}}$$ **Equation 2.5**

where E_a is the activation energy and A is the pre-exponential factor.

2.17 Circular dichroism (CD) spectroscopy

Chiral molecules, for instance sugars, amino acids and certain asymmetric elements of secondary or tertiary structure, interact specifically with certain types of circularly polarised light. The extent to which this occurs depends on the rotational direction of the polarised light as well as on the conformation of the compound. CD spectroscopy employs equal amounts of left and right handed circularly polarised light, which are absorbed differently depending on the structure. The remainder of the circularly polarised light combines to elliptically polarised light. This no longer possesses an oscillation along a straight line but along an ellipsoid path. The extent to which this occurs gives a value for the angle of ellipticity (θ).

Each amino acid residue in a polyamide possesses two degrees of backbone rotational freedom. The angle denoted φ corresponds to the rotation of the C_α-N bond and the angle Ψ to rotation of the bond linking the C_α and the carbonyl carbon. The CD signal of proteins and peptides is dependent upon the rotation of the φ and Ψ dihedral angles along the amide backbone (Figure 2.2). This results in different structural motifs exhibiting specific patterns of ellipticity. The α-helix for instance causes a positive value for ellipticity at 192 nm and negative at 208 nm and 222 nm in the spectrum.

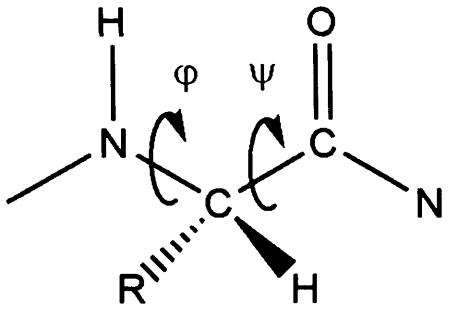

Figure 2.2: *The two degrees of backbone rotational freedom, Ψ and φ.*

All spectra were recorded in 5 mM potassium phosphate buffer (pH 8.0) in a 1 mm path length cuvette using an Applied Photophysics Chirascan spectrometer. The peptide concentration was typically 100 μM. Spectra were also acquired in the presence of 20% 2,2,2-trifluoroethanol, which promotes helix formation (Storrs *et al.* 1992). Mean residue ellipticities in deg cm^{-2} $dmol^{-1}$ were calculated according to the equation:

$$[\Theta]_r = \frac{\Theta}{10ncl} \qquad \textbf{Equation 2.6}$$

where Θ is the measured ellipticity in mdeg, n is the number of backbone amide bonds, c is the concentration in M and l is the path length in cm.

The percentage of helical structure was calculated using the equation:

$$\%helicity = \frac{-100n[\Theta]_{r,222}}{40{,}000(n-4)} \qquad \textbf{Equation 2.7}$$

where n is the number of amide bonds in the peptide.

2.18 Fluorescence anisotropy and FRET measurements

Fluorescence anisotropy assays are based on the detecting of the decorrelation of polarisation between the exciting and emitted state of photons. A fluorophore excited by polarised light will emit light with retained polarisation. However, if a molecule is moving during this time the emitted light will be depolarised. This "scrambling" effect is maximal with fluorophores that freely tumble in solution; it decreases as an inverse function of the tumbling rate. Hence, macromolecular interactions can be monitored using this approach if one of the interacting compounds is fused to a fluorophore. Upon binding to a partner molecule, a larger complex is formed which will tumble more slowly and therefore increase the polarisation of the emitted light (Figure 2.3). This technique is most sensitive if a smaller molecule is fused to a fluorophore and binds to a large partner (Heyduk *et al.* 1996).

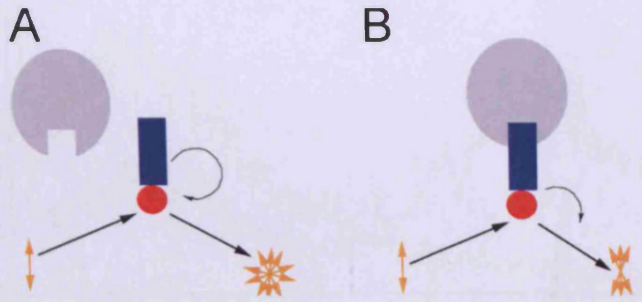

Figure 2.3: *Principle of a fluorescence polarisation assay. A) unbound molecule B) ligand bound molecule. Red: Fluorophore, blue: target molecule and grey: binding partner. The orange arrows indicate the direction of the polarisation of the light.*

FRET is based on the non-radiative transfer of energy between a donor fluorophore and an acceptor. This occurs through dipole-dipole coupling if the two compounds are in a suitable distance which is usually between 1 and 10 nm. The emission spectrum of the

donor and the absorbance spectrum of the acceptor must have sufficient overlap for this to be possible. The change in emission of the donor or acceptor molecule can then be monitored to follow the molecular interactions. Figure 2.4 shows the pronounced change in the emission spectrum of FAM upon addition of a peptide-linked FRET acceptor TMR. The small amount of fluorescence emission still present at 525 nm upon addition of the acceptor molecule is most likely due to incomplete transfer of energy between the donor and the acceptor fluorophore. Another possible explanation is the presence of a different FAM-RNA isomer which does not bind tightly to the peptide. The IC_{50} values would not be influenced by this since only the concentration of peptide is used to derive them. There would also be no error on the K_D for $Rev_{33\text{-}50}^{wt}$ since this is derived from the concentration of peptide. Therefore there would be no additional error on the calculation of K_i.

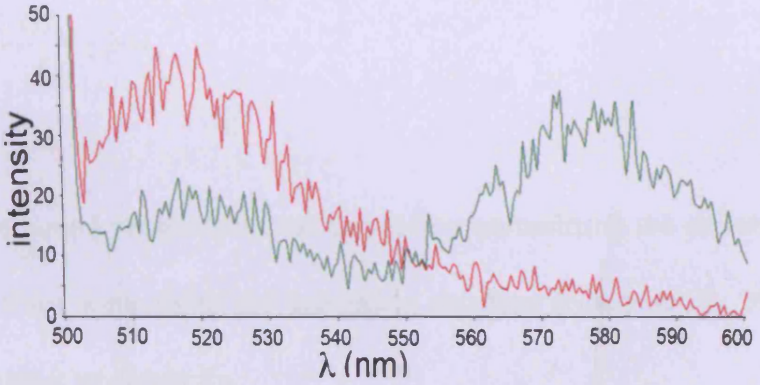

Figure 2.4: *Fluorescence emission spectra for FAM-RRE (red) and the FAM-RRE/TMR-$Rev_{33\text{-}50}^{wt}$ complex (green).*

2.18.1 Bcl-x_L/Bak-based BPN binding assay

Fluorescence anisotropy measurements were carried out on a Perkin-Elmer LS55 luminescence spectrometer at 15 °C (excitation at 494 nm and emission at 525 nm; slit width 5 nm, integration time 5 s). All measurements were performed in a 1 ml fluorescence quartz cuvette using 10 nM FAM-labelled peptide. The assay was

performed in 100 mM sodium phosphate buffer (pH 7.5) containing 10 mM NaCl. Defined volumes of a typically 4 μM or 40 μM Bcl-x_L solution were added to the FAM-labelled peptide and the change in fluorescence anisotropy measured. For experiments using light-induced peptides the solution in the cuvette was re-irradiated for 30 s every 5 min to keep the maximum amount of azobenzene cross-linker in the *cis* form. The G factor (ratio of monochromator sensitivity for horizontally and vertically polarised light) was calculated for each measurement using the equation

$$G = \frac{I_{\perp}}{I_{\parallel}},$$

where $I_{\parallel}$ and $I_{\perp}$ are the intensities of the fluorescence emission in parallel and perpendicular planes, respectively to the excitation plane. Values for fluorescence anisotropy (A) were then determined from the equation (Heyduk *et al.* 1996):

$$A = I_{\parallel} - \frac{GI_{\perp}}{I_{\parallel}} + 2GI_{\perp}.$$

The fraction of bound peptide (Φ) was derived by normalizing the anisotropy data. The resultant Φ values were fit to the Langmuir equation (Neely *et al.* 1959) using the program Sigmaplot to obtain K_D.

$$\Phi_{Fit} = \left(1 + \frac{K_D}{[L]^n}\right)^{-1} \qquad \textbf{Equation 2.8}$$

All binding curves were acquired independently four times and the resulting K_D values averaged. Reported errors are standard errors of the mean at 2σ.

2.18.2 RRE/Rev-based BPN binding assay

The binding of $Rev_{33\text{-}50}{}^{wt}$ to the RRE RNA was measured using a FRET based assay. 10nM of FAM-RNA was dissolved in FRET buffer and the decrease in fluorescence intensity upon addition of defined volumes of different TMR-labelled BPN stock solutions monitored. The excitation wavelength was 490 nm, the emission wavelength 518 nm, the excitation slit width was 2.5 nm, the emission slit width was 2.5 nm and the integration time 5 s. The binding data were normalised and fit to Equation 2.8.

2.18.3 RRE/Rev-based BPN disruption assay

The IC_{50} values for the two BPNs were determined using a FRET-based disruption assay. 10 nM of FAM-RNA was dissolved in FRET buffer and 80 nM of TMR-$Rev_{33\text{-}50}{}^{wt}$ was added. The decrease in fluorescence intensity upon addition of defined volumes of different BPN stock solutions was monitored. The excitation wavelength was 494 nm, the emission wavelength 580 nm, the excitation slit width was 2.5 nm, the emission slit width was 5.0 nm and the integration time 10 s. All experiments were performed at 15 °C using a Perkin-Elmer LS55 luminescence spectrometer. For experiments using light-induced peptides the stock solution was irradiated and kept on ice additionally the solution in the cuvette was re-irradiated for 30 s every 5 min to keep the maximum amount of azobenzene cross-linker in the *cis* form.

The data were normalised and fit to the following equation to obtain values for IC_{50}:

$$\Phi = \frac{1}{1+\left(\frac{[BPN]}{IC_{50}}\right)^{Hill\ slope}}$$

Equation 2.9

where Φ is the bound fraction and the Hill coefficient refers to the largest absolute value of the slope of the curve. It equals 1.0 for one ligand that binds with no cooperativity to one site. If it is greater than 1.0, the receptor or ligand has multiple binding sites with positive cooperativity. A Hill slope of less than 1.0 is observed if there are multiple binding sites with different affinities for the ligand or in the case of negative cooperativity. Alternatively, a mixture of ligands could also result in a Hill slope of less than 1.0.

In the case of a competitive inhibitor (Hill slope close to 1), the IC_{50} values can be precisely related to the inhibitory constant (K_i) by applying the Cheng-Prusoff equation:

$$K_i = \frac{IC_{50}}{1 + \frac{[\mathrm{Re}\, v_{33-50}{}^{wt}]}{K_D}}$$ **Equation 2.10**

where K_D refers to the dissociation constant of TMR-labelled ligand.

2.19 NMR experiments

2.19.1 ^{1}H ^{15}N Heteronuclear single quantum correlation (HSQC) NMR spectroscopy

The HSQC NMR spectrum correlates the nitrogen atom of an NH_x group with the directly attached proton. Therefore each signal corresponds to one proton that is bound to a nitrogen atom. Each amino acid (except Pro) will be represented by their backbone NH group. Additionally, the sidechains of Asn, Gln, His and Trp give rise to signals.

2.19.2 ^{1}H ^{15}N HSQC total correlation spectroscopy (HSQC TOCSY)

In a TOCSY experiment the magnetisation is transferred over a complete spin system of an amino acid by consecutive scalar coupling therefore all protons of that spin system are correlated. The transfer is stopped by small or zero proton-proton couplings and heteroatoms that also disrupt the TOCSY transfer. Hence, a specific signal pattern can be observed for each residue and the amino acid can be identified. However, a few of the amino acids display identical spin systems and therefore yield the same patterns such as Glu, Gln and Met.

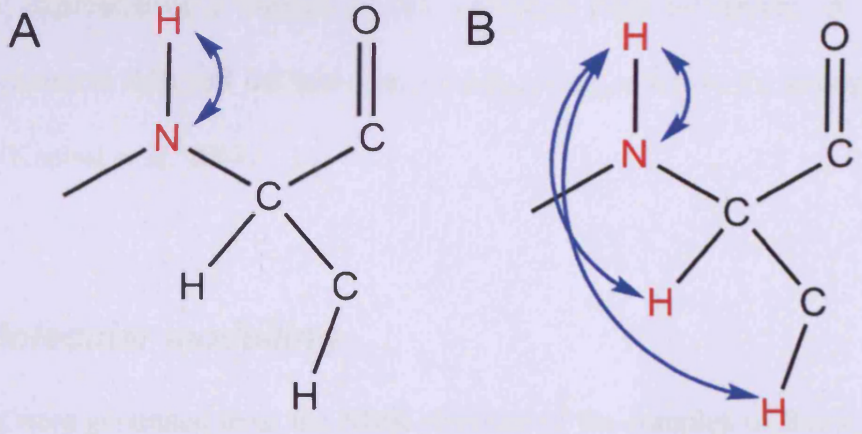

Figure 2.5: *Transfer of magnetisation in A) an HSQC NMR experiment and B) an HSQC TOCSY NMR experiment. Red: chemical shift of the atoms is observed and blue: transfer of magnetisation.*

2.19.3 Bcl-x_L NMR experiments

All experiments were performed in 10 mM sodium phosphate buffer (pH 7.3) containing 5 mM β-mercaptoethanol. ^{15}N-labelled Bcl-x_L was concentrated to 300 mM and D_2O (to 5% v/v) added. ^{1}H ^{15}N HSQC spectra of free Bcl-x_L and its complexes with wild-type Bak and cross-linked, dark-adapted, $Bak_{72\text{-}87}^{i+7}$ and $Bak_{72\text{-}87}^{i+11}$ (1:1.1 protein to peptide ratio) were acquired on a Varian INOVA 600 MHz NMR spectrometer. For the complex with $Bak_{72\text{-}87}^{i+11}$, a ^{1}H ^{15}N HSQC TOCSY spectrum was also acquired

(Kneissl *et al.* 2008). Spectra were processed using NMRPipe and analysed using the Analysis 1.0.15 software for Linux (Delaglio *et al.* 1995; Vranken *et al.* 2005). HSQC peaks for the complex with $Bak_{72\text{-}87}^{i+11}$ were assigned by comparison with the published assignments for the complex of Bcl-x_L with Bad, and assignment of residue types verified using the HSQC TOCSY spectrum. Peak movements were calculated by the following equation (Kneissl *et al.* 2008):

$$\omega = \sqrt{\Delta(\delta H)^2 + \left(\frac{\Delta(\delta N)}{5}\right)^2}$$ **Equation 2.11**

They were expressed as a fraction of the maximum peak movement. A significant change in chemical shift was defined as $\omega > 0.4\omega_{max}$ (ω_{max} refers to the strongest change observed) (Kneissl *et al.* 2008).

2.20 Molecular modelling

All models were generated from the NMR structure of the complex of Bcl-x_L and wild-type $Bak_{72\text{-}87}$ (1BXL.pdb) (Sattler *et al.* 1997) and the Rev/RRE complex (Battiste *et al.* 1996), respectively. The program used for this was the Molecular Operating Environment (MOE) software for Linux (Vilar *et al.* 2008). Following the necessary amino acid substitutions and incorporation of the cross-linker, the forcefield MMFF94 was used to energy minimise the peptide conformation and a 4.5 Å region around it. The MMFF94 Force Field is a combined "organic/protein" force field so it is equally applicable to small molecules as well as proteins and other systems of biological relevance (Halgren 1996).

The software Visual Molecular Dynamics (VMD) was used to create graphical representations from the respective pdb files (Humphrey *et al.* 1996).

CHAPTER 3:

Photocontrol of protein-protein interactions

3.1 Introduction

3.1.1 Apoptosis

3.1.1.1 Definition and physiological role of apoptosis

The term 'programmed cell death' was introduced to describe a specific form of cell death occurring during the development and homeostasis of multicellular organisms (Lockshin *et al.* 1965; Lockshin *et al.* 1974). Apoptosis is the primary mechanism of programmed cell death; it was initially recognised as a distinct morphological form of cell death by Kerr *et al.* in 1972. The term *apoptosis* is derived from the Greek word literally meaning "to drop off" in analogy to the falling of leaves from trees (Kerr *et al.* 1972). The process was first studied mechanistically in *Caenorhabditis elegans*. 1,090 cells are generated during the development of this nematode; exactly 131 of these cells are eliminated at precise times during morphogenesis. Subsequently key genes involved in morphogenesis were identified and the orthologues of these in higher mammals discovered (Horvitz 1999) (Figure 3.1).

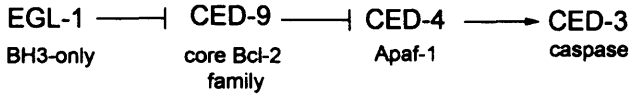

Figure 3.1: *Apoptotic pathway in* C. elegans *and mammalian gene orthologues.*

Apoptosis is a highly regulated active (i.e. energy-dependent) process in which cells die in a defined way characterised by certain biochemical events and morphological

features. It is distinct from necrotic death, which is an unregulated passive process caused by extreme changes in the cellular microenvironment, such as heat.

Programmed cell death is critical for tissue homeostasis to balance the number of cells being created by proliferation (Renehan *et al.* 2001). It has a crucial role in development, morphogenesis and the immune system. The nervous and immune systems are formed through an initial overproduction of cells followed by subsequent elimination of members of the population that do not form appropriate synaptic connections or generate antigen specificities, respectively (Nijhawan *et al.* 2000; Opferman *et al.* 2003). Apoptosis is also involved in processes such as wound healing as it plays a role in the conversion of granulation tissue into scars and in the removal of inflammatory cells (Greenhalgh 1998). Furthermore, this signalling cascade removes damaged or pathogen-invaded cells that could eventually endanger the organism. Apoptosis therefore requires tight control; otherwise it can have consequences such as autoimmune disease, neurodegenerative conditions or developmental defects. Some of these pathologies are caused by insufficient apoptosis whereas others feature excessive apoptosis. The ability to modulate the life and death of specific cells would have enormous therapeutic potential. Impaired apoptosis is now also recognised to be a key step in tumourigenesis (Cory *et al.* 2003).

3.1.1.2 Morphological features of apoptosis

Unlike necrosis, apoptosis occurs without tissue inflammation and is usually confined to a small number of cells. During the early stages of apoptosis, the cell will lose contact with its neighbours and shrink. This is followed by chromatin condensation and nuclear fragmentation (karyorrhexis). The plasma membrane starts "budding" and the cell falls

apart into apoptotic bodies. These bodies are then phagocytosed resulting in the complete removal of the cell (Figure 3.2) (Kerr *et al.* 1972) (Jiang *et al.* 2004) (Ziegler *et al.* 2004).

Necrosis on the other hand is characterised by cell swelling, ruptured organelles and finally the loss of cell membrane integrity. Cellular contents then leak into the surrounding tissue eliciting an immune response and damaging neighbouring cells. Necrosis is caused mainly by problems with the energy supply of the cell or direct damage to the membrane, it normally affects larger areas of tissue than apoptosis (Majno *et al.* 1995; Trump *et al.* 1997) (Figure 3.2).

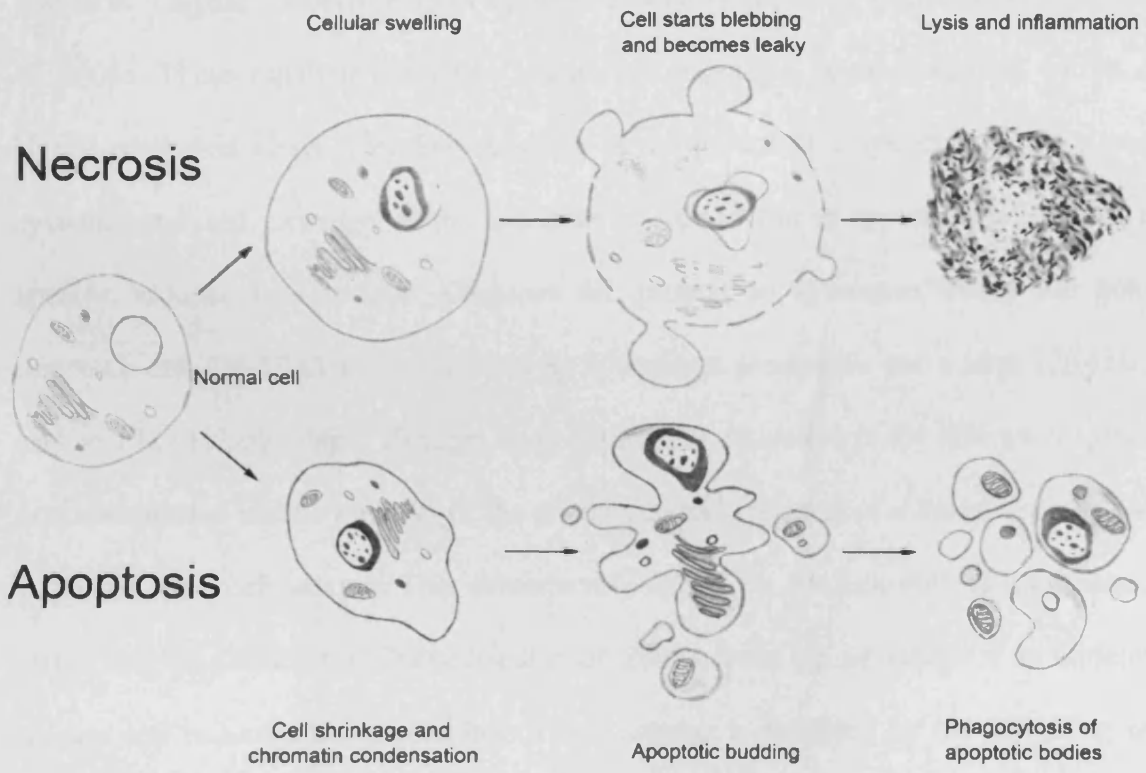

Figure 3.2: *Apoptosis and necrosis can be distinguished by their respective morphological changes.*

3.1.1.3 Apoptotic pathways

There are two main signalling pathways of apoptotic cell death, the intrinsic or mitochondrial pathway and the extrinsic (death receptor) pathway. They can be distinguished by the type of caspase (a protease) that is crucially involved in their activation and by the requirement for the proteins of the Bcl-2 family (Figure 3.5). The pathways converge at the point of the activation of effector caspases; they modify a variety of structural and regulatory proteins such as lamins or cytokeratins and activate cytoplasmatic proteases and endonucleases. This ultimately leads to the biochemical and morphological changes observed during apoptosis (Youle *et al.* 2008).

The term 'caspase' is derived from cysteine-dependent aspartate protease (Salvesen *et al.* 2008). These aspartate proteases contain an important cysteine residue within a highly conserved active site. The substrate is recognised at a specific sequence and cysteine-catalysed cleavage of the substrate is carried out at the carbonyl site of a specific aspartic acid residue. Caspases are present as zymogens inside the non-apoptotic cell (30-50 kDa). These carry an *N*-terminal prodomain and a large (20 kDa) and small (10 kDa) subunit (Bratton *et al.* 2000). The activation of the effector caspases is accomplished *via* the removal of the prodomain and cleavage of a linker between the large and the small subunit. This subsequently allows for the assembly of the dimeric active enzyme (Riedl *et al.* 2004; Riedl *et al.* 2007). Once the activation of an initiator caspase has occurred the processing of one caspase is followed by the activation of multiple others leading to signal amplification (Salvesen *et al.* 2008).

3.1.1.3.1 Extrinsic pathway

The extrinsic pathway is, for instance, engaged in the deletion of activated T-cells after an immune response (Andersen *et al.* 2006), it is triggered by extracellular ligands such as Fas and tumour necrosis factor-α (TNF-α) (Ashkenazi *et al.* 1998; Peter *et al.* 1998). The ligands bind to the corresponding transmembrane receptors that contain an intracellular death domain (DD). The death signal is transmitted to the cytosol by receptor oligomerisation and by recruitment of cytosolic adaptor proteins. These then associate with procaspase 8 *via* dimerisation of the death effector domains (DED). The death inducing signalling complex (DISC) is formed, leading to the assembly of multiple procaspase 8 molecules and the subsequent autocatalytic cleavage to give caspase 8 (Kischkel *et al.* 1995). This initiator caspase then triggers a cascade of activation of downstream executioner caspases such as caspase 3, caspase 6 or caspase 7 (Thornberry *et al.* 1998) (Figure 3.3) (Figure 3.5).

There are two cell types with different apoptotic potential. Type I cells are hallmarked by the presence of large amounts of active caspase 8 and 3 and have the ability to induce apoptosis *via* the extrinsic pathway. Type II cells have lower caspase 8 and 3 levels and therefore reduced DISC formation. They cannot undergo apoptosis exclusively by induction through the death receptor pathway and signal amplification *via* the intrinsic pathway is required (Li *et al.* 1998; Scaffidi *et al.* 1999). In type II cells (e.g. hepatocytes), the extrinsic pathway can intersect the mitochondrial pathway by activating the BH3-only protein Bid. Caspase 8 cleaves the full-length protein and the truncated form (tBid) translocates to the mitochondrion and triggers further caspase activation through the intrinsic pathway (Yin *et al.* 1999; Kaufmann *et al.* 2007).

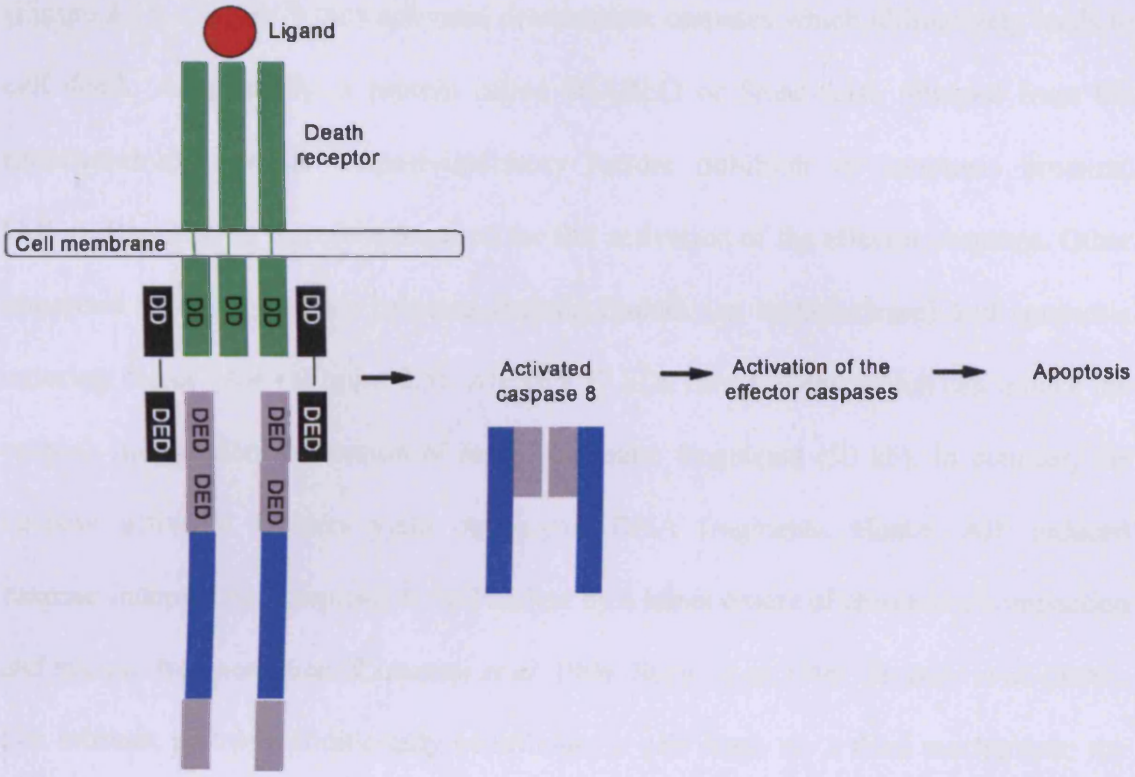

Figure 3.3: *The extrinsic pathway of apoptosis. Caspase 8 is autocatalytically activated at the DISC.*

3.1.1.3.2 Intrinsic pathway

This pathway is triggered in response to a variety of stimuli such as viral infection, growth factor deprivation, oxidative stress or DNA damage (Rich *et al.* 2000). Cytochrome C is released from the intermembrane space of the mitochondria upon activation from a death signal. This process is controlled by the pro- and anti-apoptotic members of the Bcl-2 family (see Chapter 3.1.2 for details). The cytosolic protein Apaf1 senses the release of cytochrome C which triggers oligomerisation upon binding providing that dATP is also present. Apaf1 will form a wheel-shaped signalling platform with seven-fold symmetry called the apoptosome. This is the key event in the activation of caspase 9. The caspase recruitment domain (CARD) of Apaf1 will recruit procaspase 9 and induce autocatalytic cleavage to yield the active caspase dimer

(Figure 3.4). Caspase 9 then activates downstream caspases which ultimatively leads to cell death. Additionally, a protein called DIABLO or Smac (also released from the mitochondria) removes caspase-inhibitory factors (inhibitor of apoptosis proteins, IAP's). DIABLO is therefore required for full activation of the effector caspases. Other important proteins that are released include EndoG (an endonuclease) and apoptosis inducing factor (AIF) (Figure 3.5). AIF is a 57 kDa flavoprotein, which can induce the caspase independent formation of large chromatin fragments (50 kb). In contrast, the caspase activated DNases yield oligosomal DNA fragments. Hence, AIF induced caspase-independent apoptosis is hallmarked by a lesser extent of chromatin compaction and nuclear fragmentation (Zamzami *et al.* 1996; Susin *et al.* 1999; Strasser *et al.* 2000). The intrinsic pathway additionally contributes to cell death *via* a third mechanism; the release of cytochrome C, the only water-soluble compound in the electron transfer chain (occurring in the mitochondria), can therefore stop electron transfer and lead to failure in maintaining the mitochondrial membrane potential followed by ATP synthesis termination. Since cytochrome C functions in shuttling electrons from complex III to complex IV, by which oxygen is reduced to water, blocking this step generates reactive oxygen species (ROS), this leads to lipid peroxidation and damage to the cell (Hockenbery *et al.* 1993; Cai *et al.* 2000; Wang 2001).

The mechanism of mitochondrial outer membrane permeabilisation (MOMP) is controversial. In the first theory, upon a stimulus, opening of the permeability transition (PT) pore increases the inner mitochondrial membrane permeability, allowing molecules smaller than 1.5 kDa to pass through. This leads to the influx of water into the mitochondrial intermembrane space increasing of the inner transmembrane potential ($\Delta\Psi$), resulting in organelle swelling and finally rupture of the outer mitochondrial

membrane and release of content from the mitochondrial intermembrane space into the cytoplasm. The second mechanism does not involve a major role for the mitochondrial inner membrane. Instead, members of the Bcl-2 family act directly on the outer mitochondrial membrane. The anti-apoptotic family members block MOMP, whereas the numerous pro-apoptotic members function to promote it (Green *et al.* 1998).

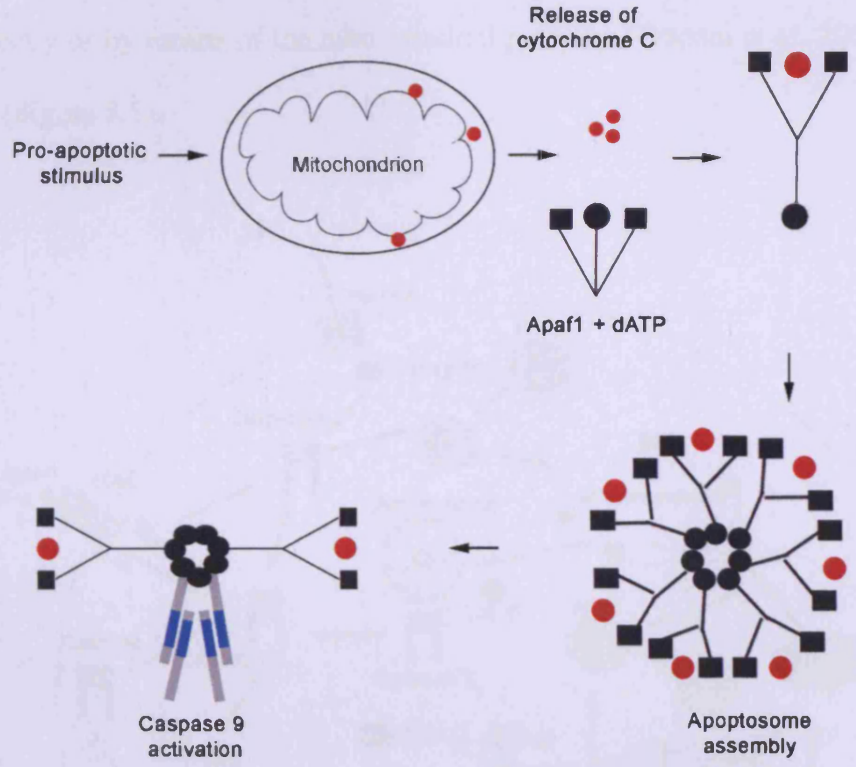

Figure 3.4: *Apoptosome assembly in the intrinsic pathway of apoptosis. Cytochrome C: red circle, CARD: charcoal circle and WD40 domain: charcoal square. (The WD40 domain is an about 40 amino acids long sequence which often terminates in Trp Asp. WD40 repeats form circular β-propeller structures that serve as scaffolds for protein-protein interactions.)*

3.1.1.3.3 Perforin/granzyme pathway

There exists an additional pathway that involves perforin and granzyme mediated killing of tumours or virus infected cells. This signalling cascade is triggered by cytotoxic T-cells that exert their effect by secretion of a transmembrane pore forming substance, named perforin. Through this pore cytoplasmic granules are released which contain the serine proteases granzyme A and B. These proteins then activate caspases, either directly or by means of the mitochondrial pathway (Trapani *et al.* 2002; Pardo *et al.* 2004) (Figure 3.5).

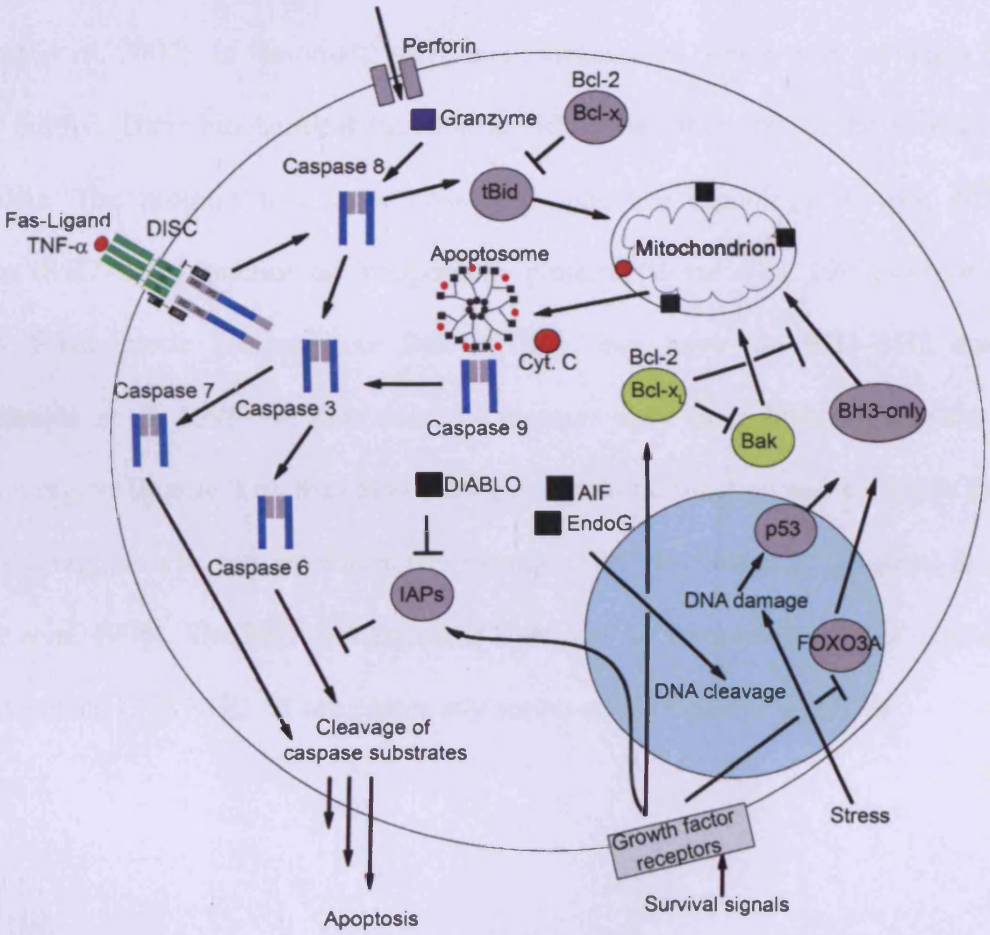

Figure 3.5: *Schematic representation of important apoptosis signalling processes (the nucleus is shown in cyan)*

3.1.2 Structure and function of the Bcl-2 family of proteins

The bcl-2 gene was first cloned from the breakpoint of the t(14:18) chromosomal translocation often found in follicular lymphoma, where it was under the control of the immunoglobulin heavy chain promoter and enhancer. This leads to excessive expression of the gene and therefore to inhibition of apoptosis (Tsujimoto *et al.* 1984; Bakhshi *et al.* 1985; Tsujimoto *et al.* 1985; Cleary *et al.* 1986). Bcl-2 established a new type of oncogene that does not act by increasing cell proliferation similar to previously identified oncogenes, but by inhibiting programmed cell death. It has been demonstrated that many mutations leading to constitutive activation of cell proliferation require a second mutation that counteracts cell death to ultimately promote tumour development (Adams *et al.* 2007). In mammals, there is a minimum of twelve core members of the Bcl-2 family. Their biochemical function is either the inhibition or the activation of apoptosis. The proteins that show conserved sequence homology in four different regions (BH1-BH4) function as antiapoptotic proteins (Boise *et al.* 1993; Gibson *et al.* 1996). Proapoptotic proteins like Bak or Bax only have the BH1-BH3 domains (Chittenden *et al.* 1995). A third class of proteins only share homology in the BH3 domain region (Figure 3.6), they also show pro-apoptotic function and are likely to have arisen through convergent evolution (for example Bid, Bim and Bik) (Boyd *et al.* 1995; Wang *et al.* 1996). The BH3 domain motif is defined by the presence of the core amino acid sequence LXXXGD (X represents any amino acid) (Youle *et al.* 2008).

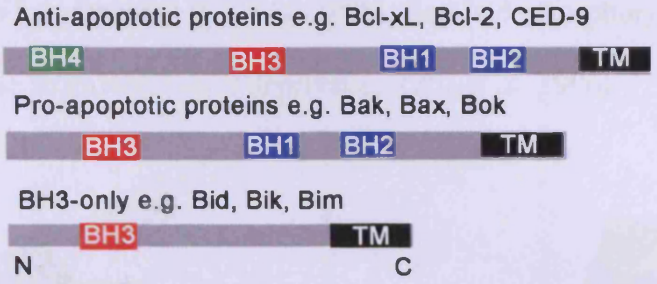

Figure 3.6: *Domain structure of the Bcl-2 family of proteins (Walensky 2006).*

The pro- and antiapoptotic members of the Bcl-2 family can form homo- and hetero-dimers. The relative concentration of these two groups determines the apoptotic potential of the cell. The proapoptotic members such as Bak are important for the induction of outer mitochondrial membrane permeabilisation and the following release of cytochrome C. The antiapoptotic members such as Bcl-x_L inhibit this by binding to these proteins. Bak interacts with Bcl-x_L *via* its BH3 domain. By using a peptide with the BH3 domain sequence it is possible to keep Bcl-x_L from binding Bak and the cell can go into apoptosis (Finnegan *et al.* 2001) (Figure 3.7).

The BH3-only proteins are initial sensors of apoptotic stimuli that function downstream of various biochemical processes. Noxa and Puma production for instance is activated by the transcription factor and tumour suppressor protein p53 in response to DNA damage (Oda *et al.* 2000; Nakano *et al.* 2001; Chipuk *et al.* 2005). Bim expression is induced by the transcription factor forkhead box O3A (FOXO3A) upon the withdrawal of growth factors or through C/EBP homologous protein (CHOP) in the case of endoplasmic reticulum (ER) stress (Puthalakath *et al.* 2007). The activation of this protein class can also be regulated post-translationally. Bid, for example, is activated

through proteolysis by caspase 8 (Li *et al.* 1998). Bad is dephosphorylated and thereby activated in response to growth-factor deprivation (Zha *et al.* 1996).

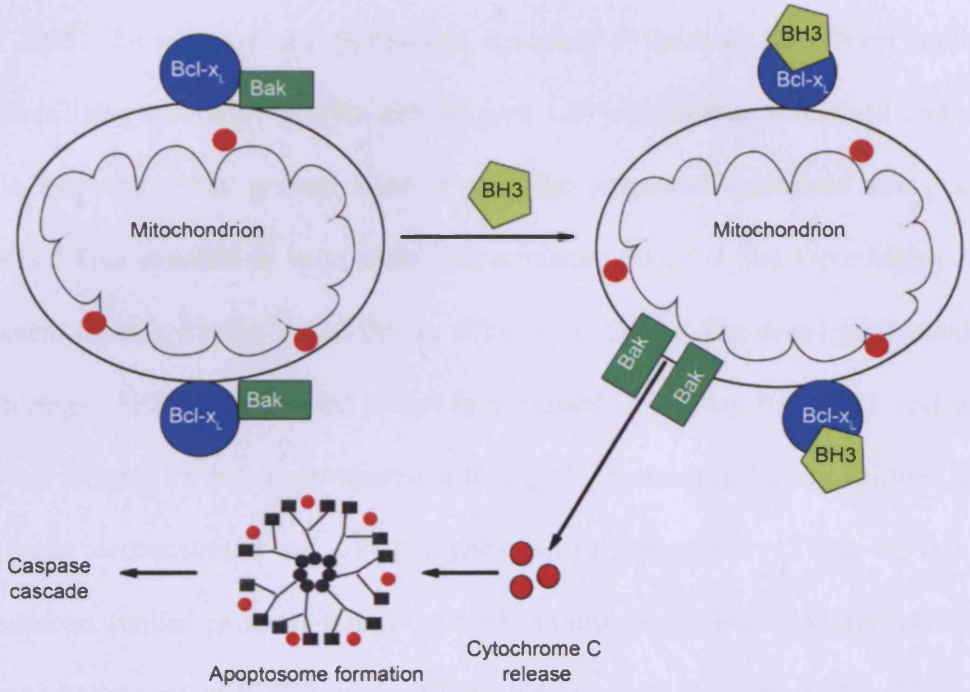

Figure 3.7: *Regulation of apoptosis by the Bcl-2 family of proteins.*

The induction of antiapoptotic protein expression is another means by which apoptotic modulation may occur. For example, Bcl-x_L protein levels are upregulated in response to growth factors, *via* the JAK-STAT pathway (a signalling cascade involved in development and homeostasis) (Grad *et al.* 2000). The core pro-apoptotic proteins such as Bak or Bax are mainly controlled post-translationally by the other components of the Bcl-2 family and their expression levels are relatively constant (Youle *et al.* 2008).

3.1.3 Controlling/mimicking the α-helical conformation of BH3 peptides

Isolated BH3 peptides generally show less than 25% α-helicity in aqueous solution (Letai 2005). To increase this percentage, a variety of methods have been applied; the helix stabilising miniature protein aPP (Figure 1.8) was used as a scaffold and the Bak peptide sequence was grafted onto it and the sequence optimised using directed evolution. This resulted in helix-stabilised miniature proteins that were highly specific and potent ligands for Bcl-2 and Bcl-x_L (Chin *et al.* 2001). The best ligand obtained by this strategy, PPBH3-1, showed a 100-fold enhanced affinity for Bcl-2 and a 7-fold improved affinity for Bcl-x_L compared to $Bak_{72\text{-}87}{}^{wt}$. A series of lactam-bridged peptides have been demonstrated to adopt highly helical structures (Yang *et al.* 2004). Hydrocarbon stapled peptides based on the BH3 domain of Bid (SAHBs) also showed increased helix content (87%), high affinity binding to Bcl-x_L (K_D = 39 nM) and their cell permeability and protease stability were also enhanced. Good biological activity was demonstrated by the administration of SABHs to Jurkat T cell leukemia cells and to human leukemia xenografts. It was shown with the help of HSQC NMR spectra that these peptides target the same cleft on Bcl-x_L as the wild-type Bid peptide (Walensky *et al.* 2004). Foldamers are designed scaffolds that mimic the conformation of natural oligomers to fold into defined structural motifs. They are more proteolytically stable than α-helices and therefore of interest as antagonists for protein-protein interactions. A number of different foldamers using α- and β-amino acids have been designed. However, the actitvity of the exclusively β-amino acid peptide was low (IC_{50} > 500 μM). Foldamers based on a scaffold consisting of α- and β-amino acids in contrast showed a very high affinity for Bcl-x_L (K_D = 1 nM) and some of them were active in Cytochrome C release assays (Sadowsky *et al.* 2005). Non-peptide based

scaffolds have also been developed as helix-mimetics. This is exemplified by: terephthalamide, terphenyl and oligoamide based compounds which are modified with appropriate functional groups to mimic key surface functionalities displayed on the α-helix (Kutzki *et al.* 2002; Ernst *et al.* 2003; Yin *et al.* 2004; Yin *et al.* 2005b; Yin *et al.* 2005c) (Figure 3.8). A number of Bcl-x_L/Bak antagonists, based on this scaffold, have been designed to mimic the α-helical BH3 region of the $Bak_{72\text{-}87}{}^{wt}$ peptide and their binding mode was investigated by NMR spectroscopy. Some of these molecules displayed activity in HEK-293 cells and K_i values in the high nanomolar range (Yin *et al.* 2005b; Yin *et al.* 2005c).

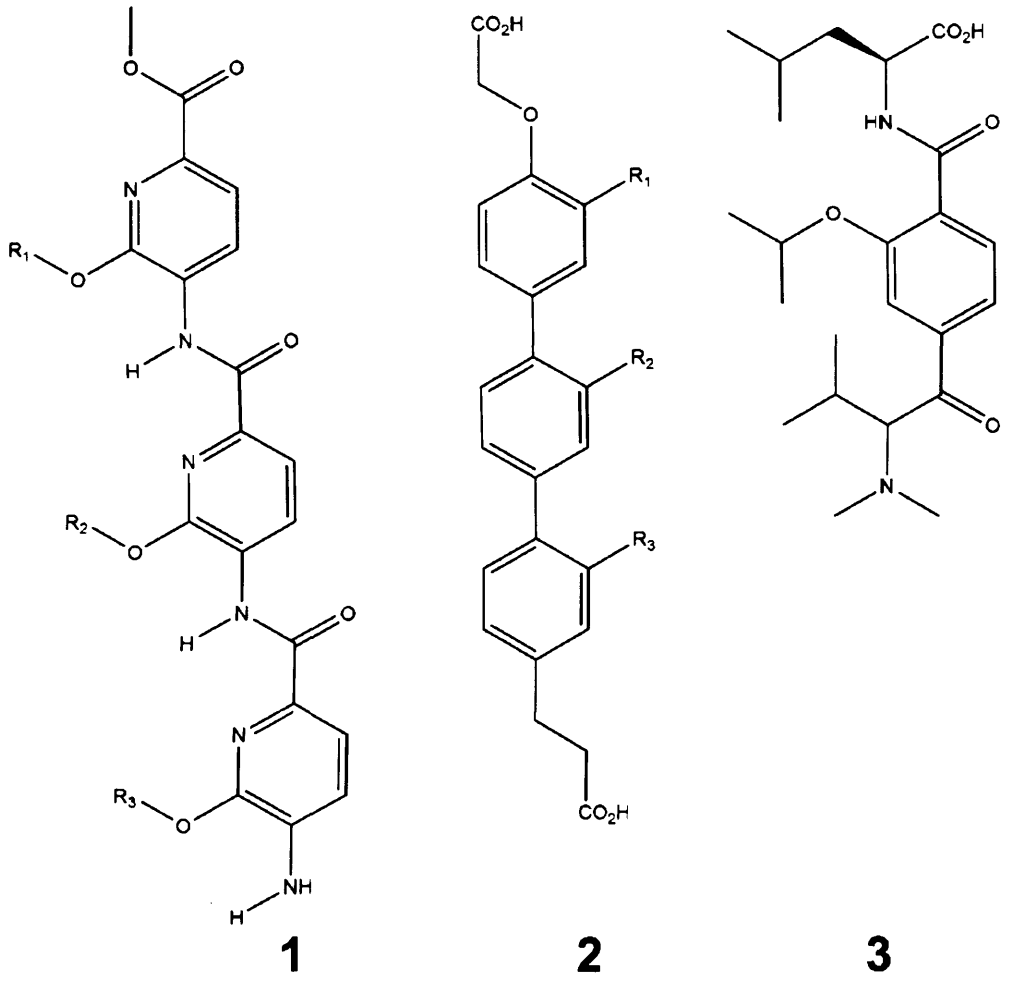

Figure 3.8: *Non-peptidic α-helix mimetics: oligoamide (1), terphenyl (2) and terephthalamide (3). $R_{1\text{-}3}$ = alkyl groups such as isopropyl or isobutyl.*

Small molecules avoid the problems associated with proteolysis observed in peptide based compounds and some of them are cell-permeable. Small molecules that mimic the BH3 motif such as (-)-gossypol, TW-37, ABT-737 and ABT-263 (an orally bioavailable analogue of ABT-737) have been discovered or developed recently (Figure 3.9). (-)-Gossypol is a natural product from the terpenoid family which is present in cottonseeds. It has been shown to execute proapoptotic activity in numerous cancer cell lines and acts by targeting Bcl-x_L and additionally by upregulation of Puma and Noxa (Meng *et al.* 2008). A structure-based design strategy was employed to develop new potent small molecule inhibitors starting from the gossypol structure. The resulting compound, TW-37 targets Bcl-2 with nanomolar affinity and Bcl-x_L and Mcl1 with micromolar affinity. It induces apoptosis in a dose-dependent manner. It has been successful in preclinical studies and could prove an effective therapeutic in the treatment of B-cell lymphoma (Wang *et al.* 2006; Mohammad *et al.* 2007; Wang *et al.* 2008). The third molecule, ABT-737, is a Bad peptide mimetic that makes several key hydrophobic and electrostatic contacts with the binding groove of the protein (Figure 3.10). It demonstrates subnanomolar affinity for Bcl-x_L and Bcl-2. Effective antitumour activity has been shown in cell culture and animal models (Kline *et al.* 2007) (Park *et al.* 2008). ABT-737 was developed by using structure-based design in combination with NMR screening (Oltersdorf *et al.* 2005).

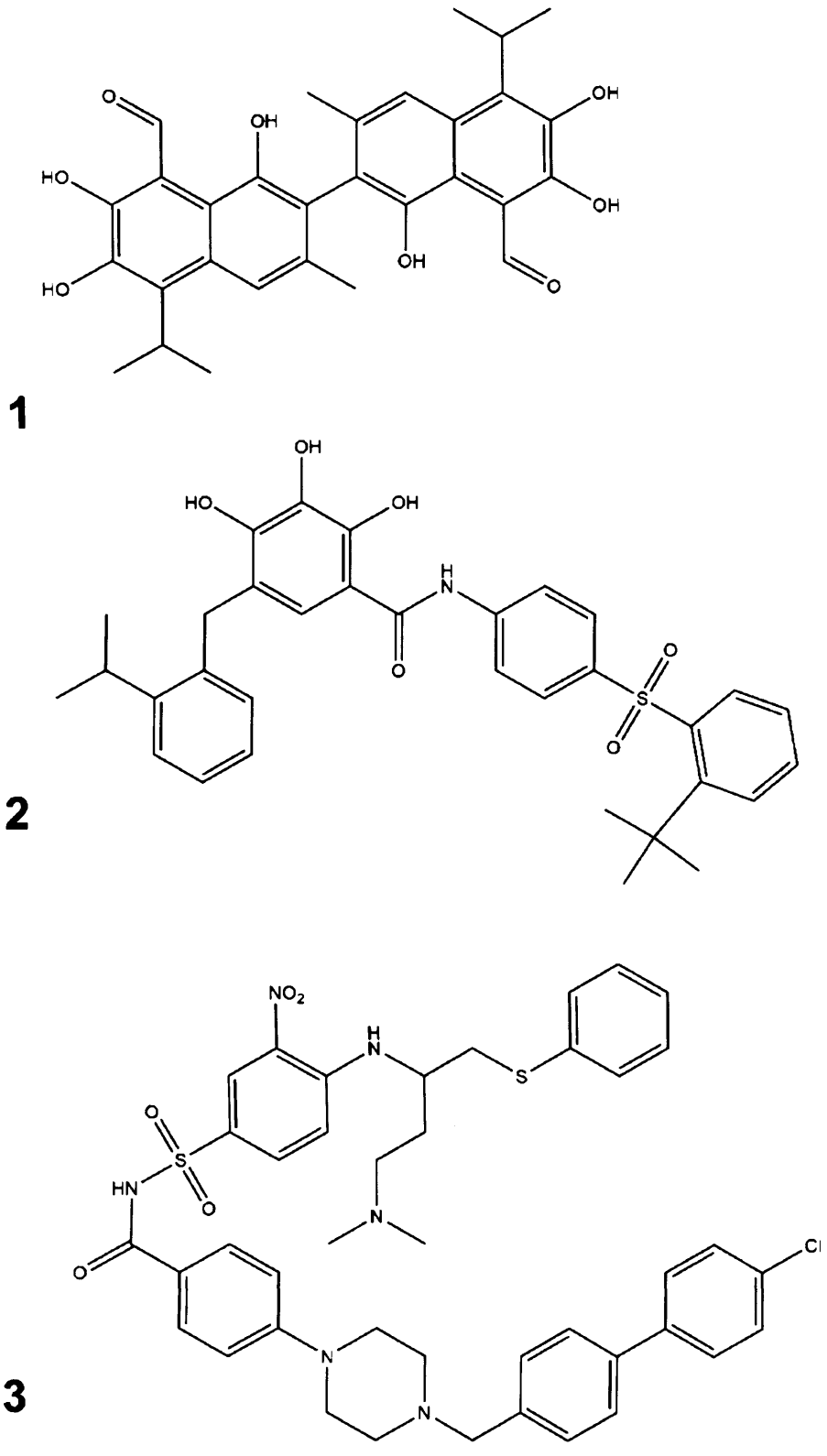

Figure 3.9: *Structure of three potent small molecule antagonists of the Bcl-2 protein family: (-)-gossypol (**1**), TW-37 (**2**) and ABT-737 (**3**)*

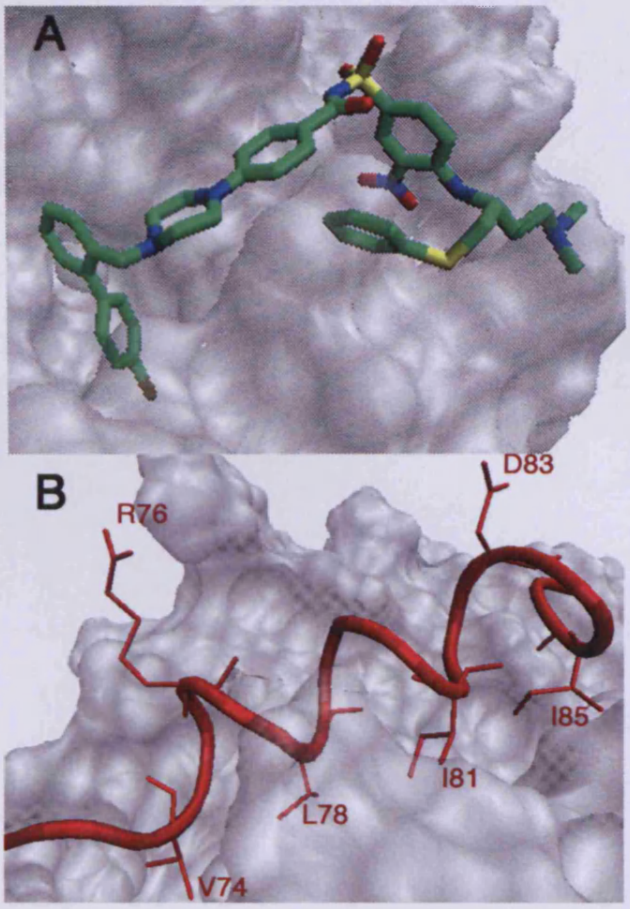

Figure 3.10: *Comparison of the binding mode of a small molecule inhibitor to Bcl-x_L and the Bcl-x_L/Bak$_{72\text{-}87}^{wt}$ complex. A) ABT-737 binds to the hydrophobic pocket of Bcl-x_L (2YXJ.pdb) (Oltersdorf* et al. *2005) and B) The Bak peptide binds to Bcl-x_L (1BXL.pdb) (Sattler* et al. *1997). Protein surface is shown in transparent grey. ABT-737 is shown as sticks (N = blue, C = green, O = red, P = yellow). The peptide is shown in red.*

3.2 Aim of the project

While several potent small molecule and peptide-based inhibitors of the Bcl-x_L/Bak complex or of other protein-protein interactions have been developed recently, none of these have the potential to program changes in discrete and critical intracellular protein-protein interactions through external stimuli and in a reversible manner.

The aim of the project was to develop small photocontrollable peptides (termed 'biophotonic nanoswitches') for the modulation of protein-protein interactions. The Bak/Bcl-x_L complex, involved in apoptotic signalling, was selected as a model system because of the abundance of structural and functional data available for this interaction. The aim was to make BH3-domain derived peptides with an azobenzene cross-linker in different spacings and to characterise them structurally and functionally.

3.3 Results and discussion

3.3.1 Subcloning of bcl-x_L

Human bcl-x_L was obtained in a pcDNA3 vector (expression vector used in mammalian cell culture). For protein expression in *E. coli* it was first subcloned into a pET vector. Two primers were designed to introduce new restriction sites and to delete the *C*-terminal transmembrane domain of the protein and the PCR performed (Figure 3.6) (Table 3.1). The resulting PCR product was cloned into a PCR Script vector by blunt end ligation. The resulting plasmid was digested with *Bgl*II and *Nde*I and the 640 bp fragment ligated into the pET19b expression vector, using the *Nde*I and the *Bam*HI restriction sites. The pET19b vector codes for an *N*-terminal His-tag and enterokinase cleavage site. A *Hind*III digest and DNA sequencing confirmed the presence of the bcl-x_L insert (Figure 3.11).

Table 3.1: *Primer sequences for the bcl-x_L PCR reaction. The restriction sites are underlined.*

Primer	Sequences
bcl-x_L fwd	5'-GTACGCATATGTCTCAGAGCAACCGGGAGC-3'
bcl-x_L rev	5'-CTAGTAGATCTTCAGCGTTCCTGGCCCTTTCG-3'

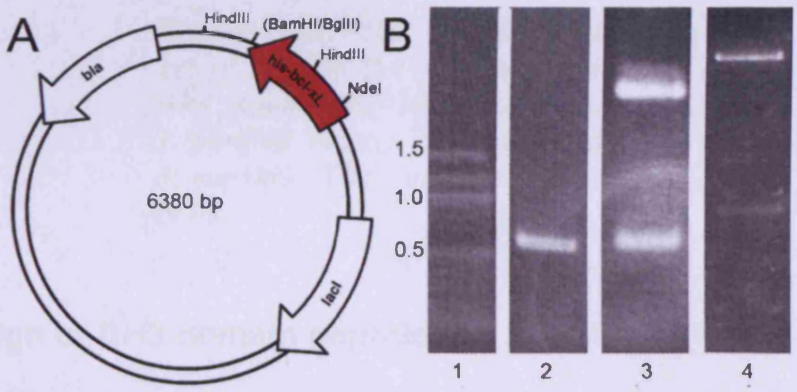

Figure 3.11: *A) Map of the pET19b bcl-x_L vector B) Agarose gel stained with ethidium bromide. Lane 1: Marker (fragment size is indicated in kbp), lane 2: bcl-x_L PCR product, lane 3:* Nde*I*/Bgl*II digest of the PCRscript bcl-x_L vector, lane 4:* Hind*III digest of the pET19b bcl-x_L vector (the presence of two fragments on the gel indicates the success of the ligation reaction).*

3.3.2 Expression and purification of Bcl-x_L

BL21(DE3) cells were transformed with the pET19b bcl-x_L vector, the gene was expressed in LB medium and the obtained protein was purified using a Ni-Sepharose column and analysed by SDS-PAGE (Figure 3.12). The cleavage with enterokinase resulted in multiple bands. Therefore, the uncleaved protein was used in all subsequent experiments.

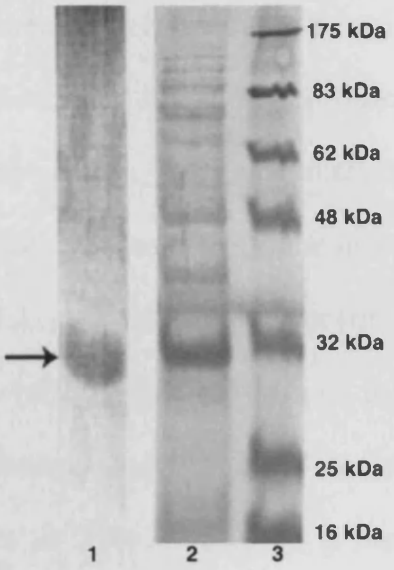

Figure 3.12: *SDS polyacrylamide gel of purified Bcl-x_L after staining with Coomassie blue. Lanes are 1: purified Bcl-x_L; 2: crude Bcl-x_L; 3: marker. The arrow indicates Bcl-x_L.*

3.3.3 Design of BH3 domain peptides

Bak peptides were designed by looking at the NMR structure of the Bcl-x_L/Bak complex (Sattler *et al.* 1997) (1BXL.pdb) (Figure 3.13) to identify positions for the cross-linker where it would not interfere with the binding. The importance of specific residues for the interaction with the target protein was judged using the data from an alanine scan (Sattler *et al.* 1997). A model of the BPNs in complex with Bcl-x_L was generated from the NMR structure of the complex of Bcl-x_L and wild-type Bak_{72-87} (1BXL.pdb) (Sattler *et al.* 1997) using the Molecular Operating Environment software for Linux. Following the necessary amino acid substitutions and incorporation of the cross-linker, the forcefield MMFF94 (Halgren 1996) was used to energy minimise the peptide conformation and a 4.5 Å region around it (Figure 3.14). Two appropriately spaced residues on the solvent exposed face of the Bak helix, opposite the residues

involved in Bcl-x_L-binding, were replaced with cysteines to allow for the introduction of the photo-activatable cross-linker 3,3'-bis(sulfo)-4,4'-bis(chloroacetamido)azobenzene. Gln73 was changed to cysteine in $Bak_{72\text{-}87}^{i+11}$ and to alanine in $Bak_{72\text{-}87}^{i+7}$. Asp84 was substituted by cysteine in $Bak_{72\text{-}87}^{i+7}$ and by alanine in $Bak_{72\text{-}87}^{i+11}$. In addition, Ile80 was changed to alanine in $Bak_{72\text{-}87}^{i+11}$ to prevent a possible steric clash with the cross-linker. Ile81 was replaced with phenylalanine in both peptides because of the higher hydrophobicity of phenylalanine, which has been shown to increase the affinity of $Bak_{72\text{-}87}$ for Bcl-x_L (Chin *et al.* 2001). Similarly, a peptide based on another pro-apoptotic protein (Bid) was designed to allow introduction of the azobenzene cross-linker in an *i, i+4* spacing of the cysteines to generate $Bid_{91\text{-}111}^{i+4}$. Bid has previously been successfully stabilised by a conformational restraint in the *i, i+4* position and is therefore a good starting point for the design (Walensky *et al.* 2004). One methionine residue was substituted with isoleucine because of its similar hydrophobicity and structure but higher stability towards oxidation (Figure 3.14). To produce the three peptide-based biophotonic nanoswitches (BPNs), $Bak_{72\text{-}87}^{i+11}$, $Bak_{72\text{-}87}^{i+7}$ and $Bid_{91\text{-}111}^{i+4}$ were alkylated with 3,3'-bis(sulfo)-4,4'-bis(chloroacetamido)-azobenzene (Figure 3.14) (Table 3.2 and Table 3.3) (Kneissl *et al.* 2008).

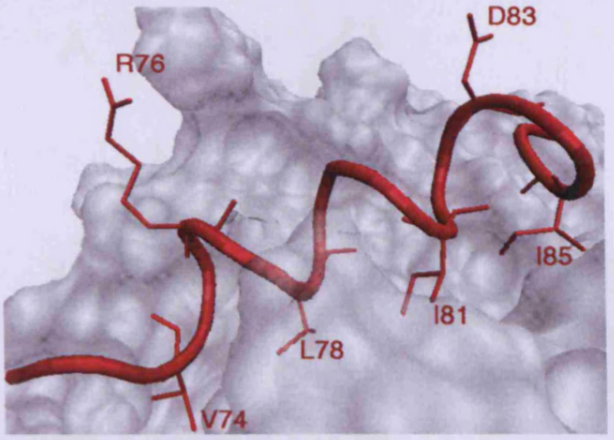

Figure 3.13: *NMR structure of the Bcl-x_L/Bak_{72-87}^{wt} complex (1BXL.pdb) (Sattler et al. 1997). The peptide is shown in red and the protein in grey. The important residues for binding affinity are shown as sticks.*

Table 3.2: *Sequences of the Bak peptides. Changed residues are shown in blue.*

	72 87
Bak_{72-87}^{wt}	GQVGRQLAIIGDDINR
Bak_{72-87}^{i+7}	GAVGRCLAIFGDCINR
Bak_{72-87}^{i+11}	GCVGRALAAFGDCINR

Table 3.3: *Sequences of the Bid peptides. Changed residues are shown in blue.*

	91 111
Bid_{91-111}^{wt}	DIIRNIARHLAQVGDSMDRSI
Bid_{91-111}^{i+4}	DIIRNIARHLACVGDCIDRSI

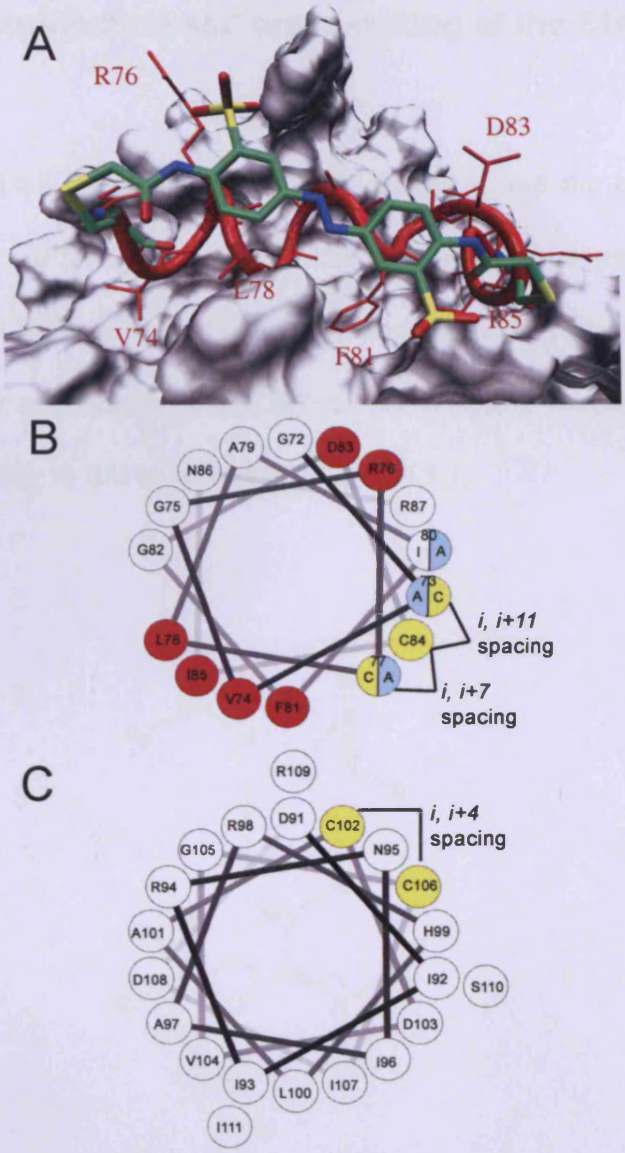

Figure 3.14: *A) Model of* $Bak_{72\text{-}87}^{i+11}$ *complexed with Bcl-*x_L *(based on 1BXL.pdb) (Sattler* et al. *1997) B) Helical wheel representation of* $Bak_{72\text{-}87}^{i+11}$ *and* $Bak_{72\text{-}87}^{i+7}$*, C) Helical wheel representation of* $Bid_{91\text{-}111}^{i+4}$*. Red: residues shown to result in > 10-fold loss of binding affinity upon replacement to an alanine. Yellow: cysteine residues and cyan: residues replaced by alanine to avoid steric clash (Kneissl* et al. *2008).*

3.3.4 Synthesis, purification and cross-linking of the BH3-domain peptides

Peptides were synthesised by using Fmoc SPPS chemistry and the pure compounds obtained after HPLC purification (Figure 3.15). The *N*-terminal modification with carboxyfluorescein (FAM) was carried out while the peptide was attached to the resin, using *N,N*-diisopropylcarbodiimide (DIPCDI) as the coupling reagent. The reaction mechanism corresponding to this is depicted in Scheme 3.1.

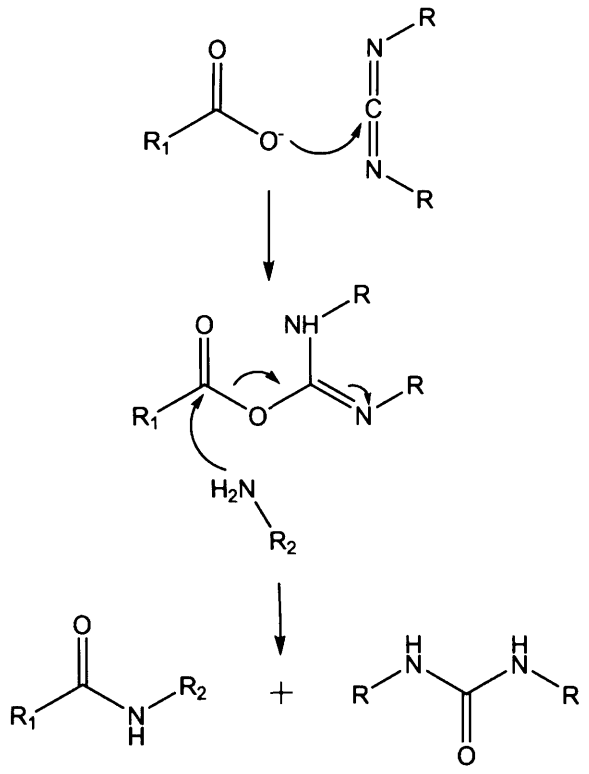

Scheme 3.1: *The mechanism of the carbodiimide mediated coupling of a fluorophore (R_1) to the* N*-terminus of a peptide (R_2).*

The cross-linking reaction with 3,3'-bis(sulfo)-4,4'-bis(chloroacetamido)azobenzene was performed by treating a solution of the peptide with 4 equivalents of the thiol-

reactive cross-linker, added in three consecutive aliquots, followed by stirring the mixture at 4 °C for 12 hours. The reaction was carried out under reducing conditions (TCEP) to avoid the formation of disulfide bonds. For $Bid_{91\text{-}111}{}^{i+4}$, the reaction was carried out at 50 °C over a period of 6 hours because the other method failed probably due to steric difficulties which are less pronounced at higher temperature. The cross-linked peptides were purified by HPLC and analysed by mass spectroscopy. A typical HPLC trace and mass spectrum for the purified peptides is shown in Figure 3.15. The retention times and molecular weight of all peptides can be found in Table 3.4.

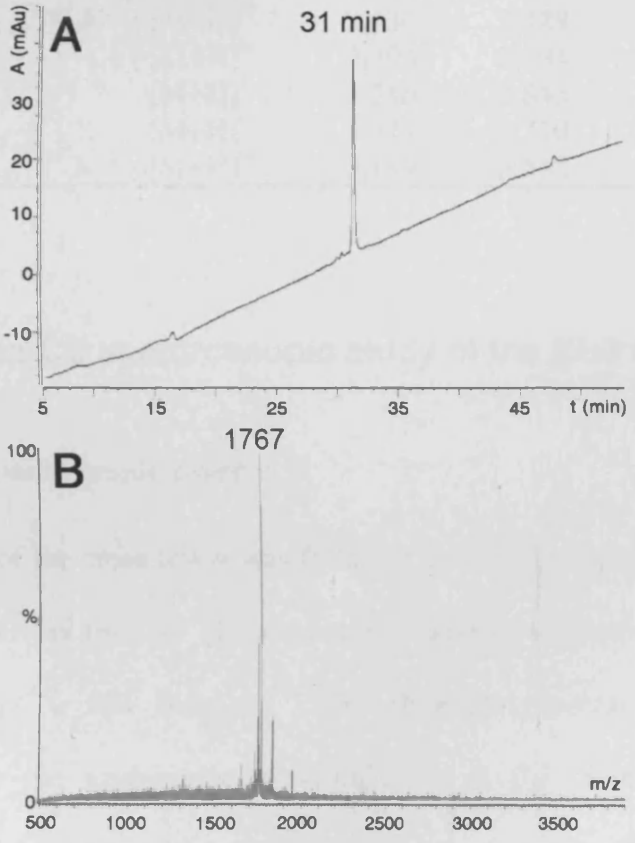

Figure 3.15: *Typical HPLC trace (A) and typical mass spectrum (B) of a purified BPN ($Bak_{72\text{-}87}{}^{wt}$).*

Table 3.4: *Molecular weight of the BH3 peptides (X = alkylated with the azobenzene cross-linker). Major MS peak corresponds to the species observed in the mass spectrum. The molecular weight calculated from that is given in the column to the right. Theoretical average MW corresponds to the anticipated mass of each molecule.*

Peptide	Ion	Major MS peak	MW (g mol^{-1})	Theoretical average MW (g mol^{-1})
$Bak_{72\text{-}87}^{wt}$	$[M+H]^+$	1,767	1,766	1,766
$Bak_{72\text{-}87}^{i+7}$	$[M+H]^+$	1,708	1,707	1,706
$Bak_{72\text{-}87}^{i+7}$ X	$[M+H]^+$	2,158	2,157	2,156
FAM $Bak_{72\text{-}87}^{i+7}$	$[M+H]^+$	2,024	2,023	2,023
FAM $Bak_{72\text{-}87}^{i+7}$X	$[M-H]^-$	2,472	2,473	2,473
$Bak_{72\text{-}87}^{i+11}$	$[M+H]^+$	1,664	1,663	1,663
$Bak_{72\text{-}87}^{i+11}$ X	$[M+Na]^+$	2,139	2,116	2,114
FAM $Bak_{72\text{-}87}^{i+11}$	$[M+H]^+$	1,983	1,982	1,980
FAM $Bak_{72\text{-}87}^{i+11}$ X	$[M+H]^+$	2,430	2,429	2,430
$Bid_{91\text{-}111}^{i+4}$	$[M+H]^+$	2,395	2,394	2,394
$Bid_{91\text{-}111}^{i+4}$ X	$[M+H]^+$	2,846	2,845	2,844
FAM $Bid_{91\text{-}111}^{i+4}$	$[M+H]^+$	2,711	2,710	2,704
FAM $Bid_{91\text{-}111}^{i+4}$ X	$[M+H]^+$	3,149	3,148	3,154

3.3.5 UV/Vis and CD spectroscopic study of the BH3 domain BPNs

3.3.5.1 UV/Vis spectroscopic study

The isomerisation of the cross-linker was followed by UV/Vis spectroscopy at different temperatures. This was used to characterise the thermal isomerisation of irradiated $Bak_{72\text{-}87}^{i+7}$, $Bak_{72\text{-}87}^{i+11}$, and $Bid_{91\text{-}111}^{i+4}$. The absorption spectrum of dark-adapted $Bak_{72\text{-}87}^{i+11}$, where the azobenzene cross-linker is in the thermally stable *trans*-configuration, was characterised by a strong maximum at 363 nm (Kneissl *et al.* 2008). This is typical of the π-π^* transitions in amide-substituted *trans*-azobenzenes (Rau 1990; Guerrero *et al.* 2005a; Guerrero *et al.* 2005b). Irradiation with 360 nm light led to the disappearance of this maximum and appearance of a new maximum at 262 nm (Figure 3.16). Irradiated $Bak_{72\text{-}87}^{i+11}$ reverted to the dark-adapted state in a non-

photochemical process that was characterised by isosbestic points at 250, 317 and 434 nm with a half-life of 30 min at 15 °C. This was similar to the half-life of a previously reported model peptide FK-11 (developed to test the helix stabilisation and destabilisation *via* an azobenzene cross-linker) (Zhang *et al.* 2003), when alkylated with 3,3'-bis(sulfo)-4,4'-bis(chloroacetamido)azobenzene, but significantly shorter than the 150 min observed for the thermal reversion from the irradiated state of HDH-3, an 18-residue peptide derived from the homeobox protein engrailed, linked to the azobenzene cross-linker in an *i, i+11* configuration (Kneissl *et al.* 2008). In all systems, the presence of more than one isosbestic point was observed, suggesting that the reversion follows first order kinetics. The isomerisation rates were therefore determined from a plot of ln ($\%_{lid}$) versus time (Figure 3.17). A high α-helical content of the stabilised peptide form probably leads to very high relaxation rates in the case of the *i, i+11* spacing and to slower reversion rates in the other spacings. For example, the shortest half-lives are displayed by the helical peptides $Bak_{33\text{-}50}^{i+11}$ and the model peptide FK-11. HDH-3 and $Rev_{33\text{-}50}^{i+11}$ (Table 4.5) are less helical and possess significantly longer half-lives. In agreement with this hypothesis, a modified non-helical $Bak_{72\text{-}87}^{i+11}$ peptide, which contained an A80I substitution showed a half-life that was one order of magnitude longer than the one of $Bak_{72\text{-}87}^{i+11}$ (522 min versus 44 min at 5 °C). The UV/Vis spectra of dark-adapted and light-induced $Bak_{72\text{-}87}^{i+7}$ were similar to those observed for $Bak_{72\text{-}87}^{i+11}$, but the thermal reversion from the irradiated state of $Bak_{72\text{-}87}^{i+7}$ and $Bid_{91\text{-}111}^{i+4}$ occurred with a significantly longer half-life of 174 min and 190 min at 15 °C suggesting that the spacing of the cysteines influences this rate. Comparison of the reversion rates of $Bak_{72\text{-}87}^{i+7}$ with those measured for PhotoMyoD ($t_{½}$ = 193 min at 15 °C) (Guerrero *et al.* 2005a) and $Rev_{33\text{-}50}^{i+7}$ ($t_{½}$ = 154 min at 15 °C) (Table 4.5), where the cross-linker was also in *i, i+7* spacings, indicated that the rates of

thermal reversion are relatively similar for the *i, i+7* spacing. This could be explained by the smaller conformational constraint and therefore structural change that the cross-linker imposes in this spacing. This relatively small variance in structural change might lead to a less pronounced effect of the studied amino acid sequences on the rate.

The extent of the light-induced isomerisation was determined from the absorbance at 363 nm (Figure 3.16), using the difference between the extinction coefficients for the *cis* and *trans* azobenzene cross-linker (Zhang *et al.* 2003). 76%, 69% and 80% of the irradiated material was found to be in the c*is*-configuration for alkylated $Bak_{72\text{-}87}^{i+7}$, $Bak_{72\text{-}87}^{i+11}$, and $Bid_{91\text{-}11}^{i+4}$ respectively (Kneissl *et al.* 2008), values typically observed in the photoisomerisation of azobenzenes (Guerrero *et al.* 2005b; Renner *et al.* 2006) (Table 3.5).

Table 3.5: *Obtained percentage of* cis *isomer upon irradiation for different BH3-derived peptides.*

Peptide	*%cis* isomer
$Bak_{72\text{-}87}^{i+11}$	69
$Bak_{72\text{-}87}^{i+7}$	76
$Bid_{91\text{-}111}^{i+4}$	80

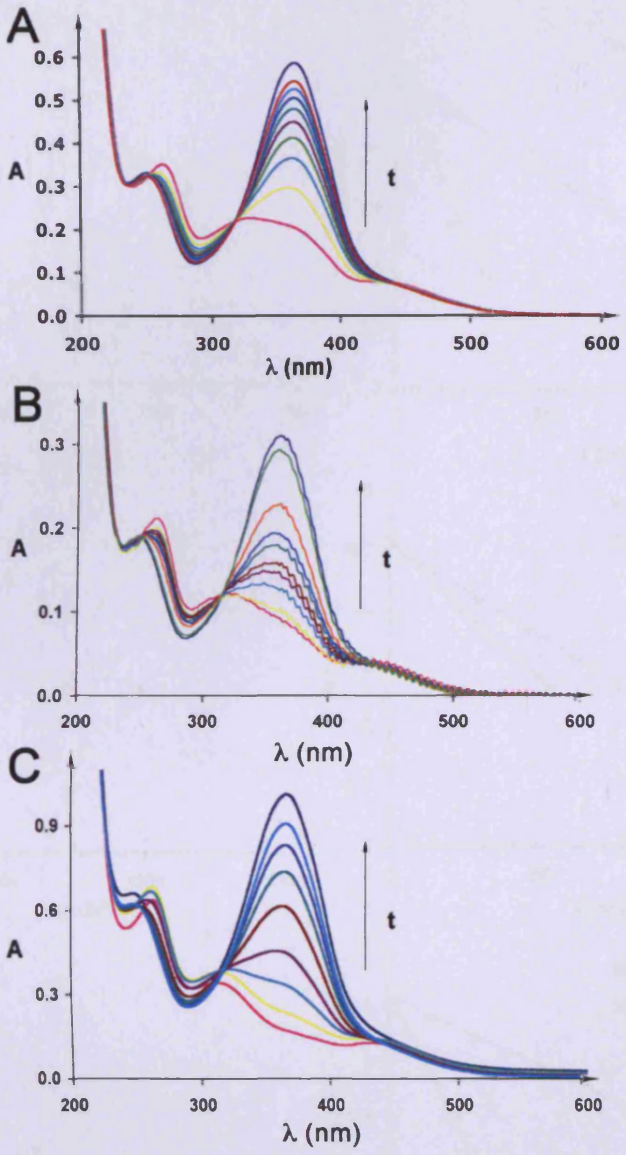

Figure 3.16: *UV/Vis spectra in the dark (dark blue), immediately after irradiation (pink) and at different times after irradiation. A) Bak_{72-87}^{i+11} B) Bak_{72-87}^{i+7} C) Bid_{91-111}^{i+4} (Kneissl* et al. *2008).*

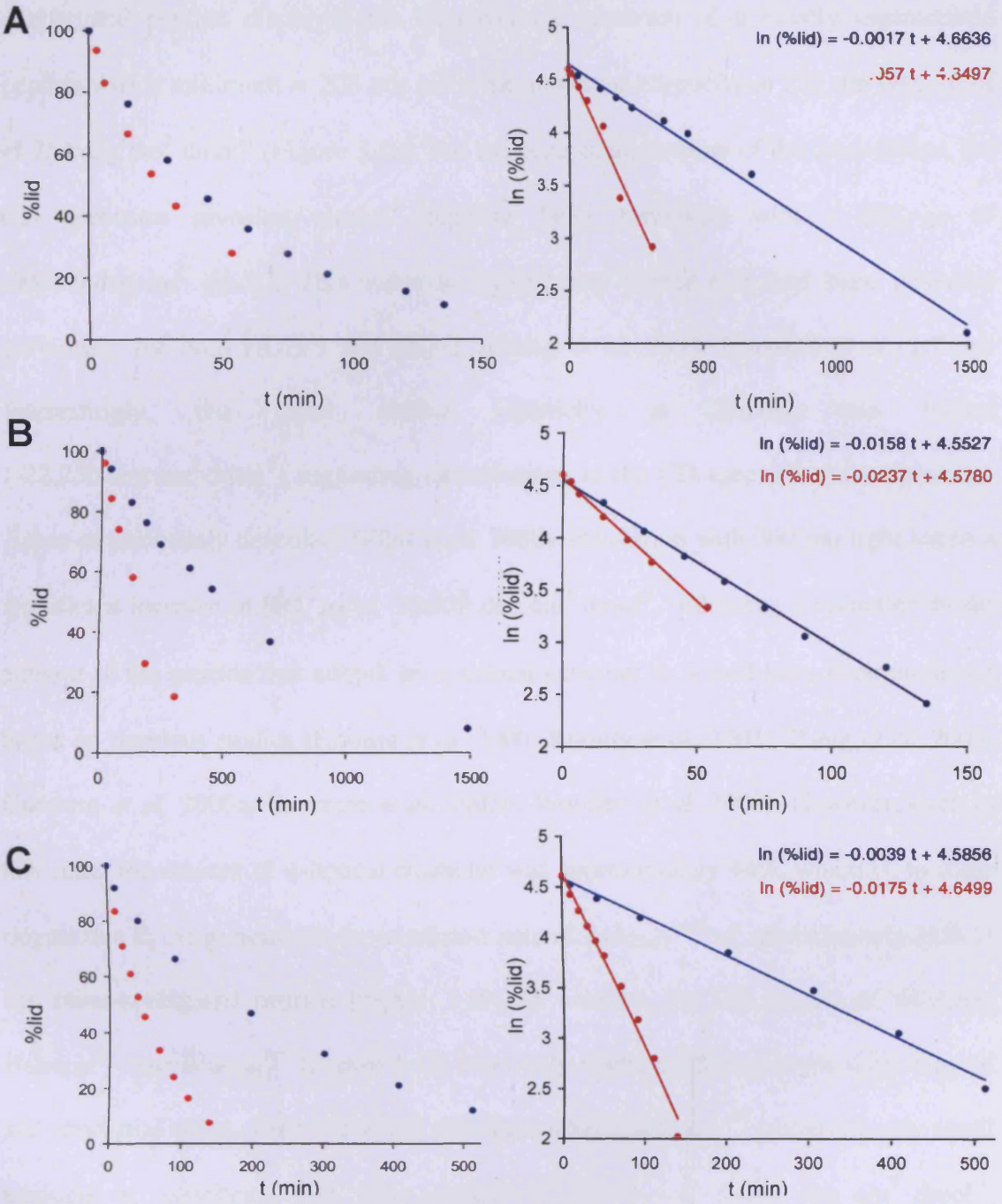

Figure 3.17: *Relaxation of different BH3-based peptides as a function of time in the dark as monitored by UV (363 nm). A) $Bak_{72\text{-}87}^{i+7}$ B) $Bak_{72\text{-}87}^{i+11}$ and C) $Bid_{91\text{-}111}^{i+4}$; Red: 15 °C and blue: 5 °C. The absorbance versus time plot is shown on the left and the corresponding linearised plot on the right.*

3.3.5.2 CD spectroscopic studies of the BH3 domain BPNs

CD spectroscopy indicated significant differences in the conformation of uncross-linked $Bak_{72\text{-}87}^{i+11}$ and its alkylated dark-adapted form (Figure 3.18) (Table 3.6). The

unalkylated peptide displayed the characteristic spectrum of a mostly unstructured peptide with a minimum at 203 nm and a mean residue ellipticity at 222 nm $[\Theta]_{r,\,222}$ of -4,752 deg cm^2 dmol^{-1} (Figure 3.18). For the *trans*-configuration of the cross-linker, the CD spectrum revealed almost complete helix formation with a $[\Theta]_{r,\,222}$ of -30,600 deg cm^2 dmol^{-1}. This value is significantly higher than had been observed previously for both HDH-3 and FK-11 (Zhang *et al.* 2003; Guerrero *et al.* 2005b). Interestingly, the mean residue ellipticity at 208 nm was higher (-22,250 deg cm^2 dmol^{-1}) suggesting contributions to the CD spectrum from the cross-linker as previously described (Flint *et al.* 2002). Irradiation with 360 nm light led to a significant increase in $[\Theta]_{r,\,222}$ to -13,458 deg cm^2 dmol^{-1}, indicating a reduction in the amount of the peptide that adopts an α-helical structure as would have been predicted based on previous studies (Kumita *et al.* 2000; Kumita *et al.* 2003; Zhang *et al.* 2003; Guerrero *et al.* 2005a; Guerrero *et al.* 2005b; Woolley *et al.* 2006). However, even in this state, the amount of α-helical character was approximately 44%, which is, to some degree due to the presence in the irradiated state of $Bak_{72\text{-}87}^{i+11}$ of approximately 31% of the *trans*-configured peptide (Figure 3.16). In contrast, the CD spectra of alkylated $Bak_{72\text{-}87}^{i+7}$ and $Bid_{91\text{-}11}^{i+4}$ (Figure 3.18) were only slightly different in the dark-adapted and irradiated states. Both irradiated and dark-adapted $Bak_{72\text{-}87}^{i+7}$ displayed only small amounts of α-helicity with $[\Theta]_{r,222}$-values of -8,808 and -6,056 deg cm^2 dmol^{-1}, respectively. This is similar to the behavior previously reported for PhotoMyoD, where DNA binding affinity could be modulated *via* an azobenzene linker introduced into the DNA recognition helix of MyoD by way of two cysteines in an *i, i+7* spacing. Irradiated PhotoMyoD showed only a modest increase in α-helicity compared to its dark-adapted and unalkylated forms (Guerrero *et al.* 2005a). However, upon addition of the DNA target sequence, the full conformational change was induced. Addition of

Bcl-x_L to irradiated $Bak_{72\text{-}87}^{i+7}$ and $Bid_{91\text{-}11}^{i+4}$ may have a similar helix-inducing effect. The dominant contribution from the elements of secondary structure of Bcl-x_L precluded studying this effect by CD spectroscopy. Hence, 2,2,2-trifluoroethanol (TFE) was used as a co-solvent to probe the α-helical potential of the different peptides (Figure 3.18). This led to the typical CD spectra of predominantly α-helical peptides ($[\Theta]_{r,\,222}$ of -24,100 and -17,100 deg cm^2 $dmol^{-1}$ for irradiated $Bak_{72\text{-}87}^{i+7}$ and $Bid_{91\text{-}11}^{i+4}$ respectively). As anticipated, addition of TFE to solutions of either dark-adapted $Bak_{72\text{-}87}^{i+7}$ or $Bid_{91\text{-}11}^{i+4}$ resulted in only a marginal reduction in mean residue ellipticity. These observations suggest that while irradiation of $Bak_{72\text{-}87}^{i+7}$ did not lead to a predominantly α-helical peptide as originally expected, it nevertheless generated a form that, upon addition of a helix-inducing co-solvent, was able to form the α-helical structure required for tight binding to Bcl-x_L, while dark-adapted $Bak_{72\text{-}87}^{i+7}$ did not exhibit this potential (Kneissl *et al.* 2008).

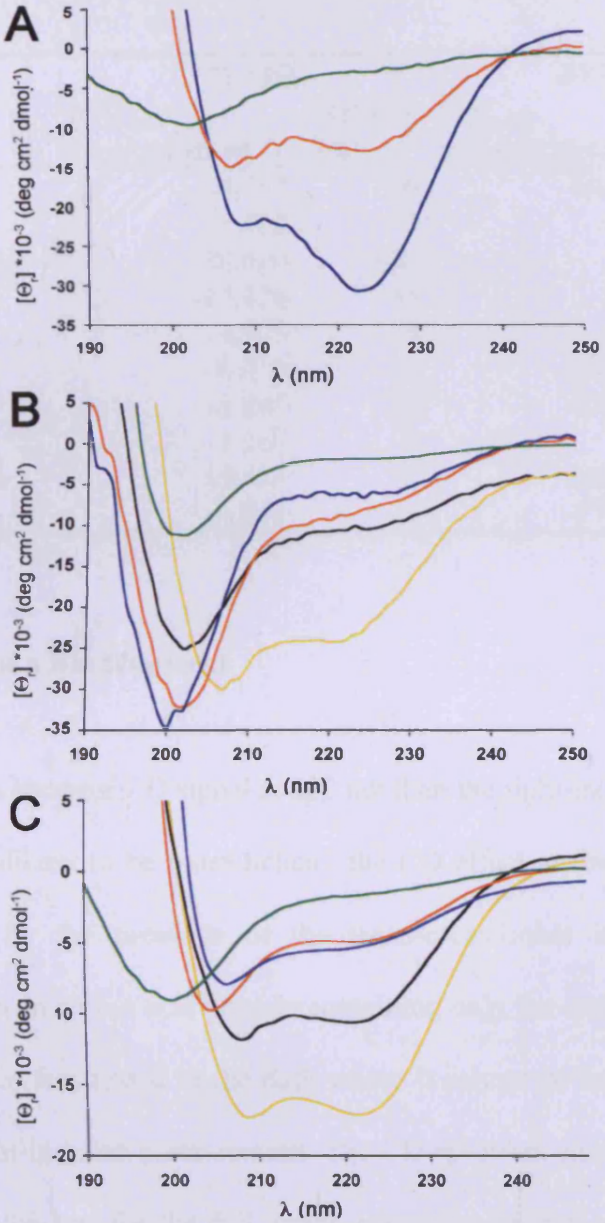

Figure 3.18: *CD spectra of the peptides at 5 °C (concentration was typically around 100 μM). A) $Bak_{72\text{-}87}^{i+11}$, B) $Bak_{72\text{-}87}^{i+7}$ and C) $Bid_{91\text{-}111}^{i+4}$; Green: unalkylated peptide, blue: dark-adapted, orange: irradiated, black: dark-adapted in 20% TFE, and gold: irradiated in 20% TFE (Kneissl* et al. *2008).*

Table 3.6: *Mean residue ellipticity and helical content of the BPNs at 5 °C.*

BPN	0% TFE		20% TFE	
	$[\Theta]_{r,222}$ (deg cm^2 dmol^{-1})	Helicity (%)	$[\Theta]_{r,222}$ (deg cm^2 dmol^{-1})	Helicity (%)
Bak_{72-87}^{wt}	-4,752	16	-14,800	48
Bak_{72-87}^{i+11}	-1,466	5	n.d.	n.d.
Bak_{72-87}^{i+11} dad	-30,600	100	n.d.	n.d.
Bak_{72-87}^{i+11} lid	-13,458	44	n.d.	n.d.
Bak_{72-87}^{i+7}	-1,926	5	n.d.	n.d.
Bak_{72-87}^{i+7} dad	-6,056	20	-10,100	33
Bak_{72-87}^{i+7} lid	-8,808	29	-24,100	79
Bid_{91-111}^{i+4}	-1,667	5	n.d.	n.d.
Bid_{91-111}^{i+4} dad	-5,281	16	-10,600	32
Bid_{91-111}^{i+4} lid	-4,918	15	-17,100	52

3.3.5.3 CD study of a Bid fragment

Bid_{91-111}^{i+4} showed a stronger CD signal at 222 nm than the light-induced peptide. Since this conformer is unlikely to be more helical, the CD effect at this wavelength might instead be caused by the presence of the *trans*-cross-linker in this spacing. To investigate this, a seven amino acid peptide containing only the cross-linked region and two flanking residues was tested in the dark where it cannot be helical and the results compared to the light-induced measurement. The CD spectrum shows a strong signal at 222 nm, similar to the one for the full length peptide even in the definite absence of helical structure (Figure 3.19). The distance between the two cysteine residues in an α-helical conformation is around 5.4 Å (Figure 1.5). The *trans* cross-linker is not able to accommodate that distance because it spans approximately 17 Å. This indicates that the same is true for the full length Bid_{91-111}^{i+4} peptide. IR spectroscopy could be utilised in future experiments to measure the helix content without the interference of the cross-linker in order to verify these results.

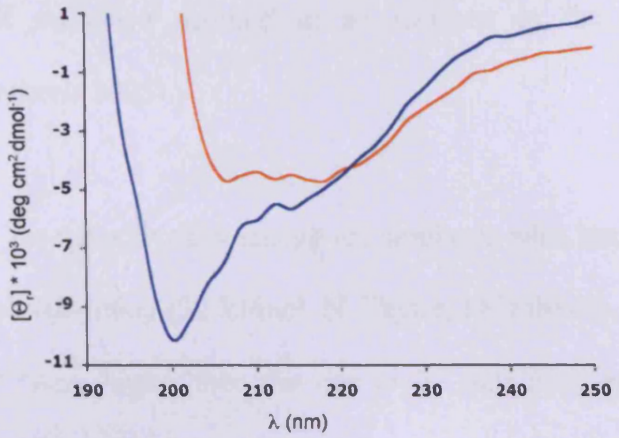

Figure 3.19: *CD spectra of Bid fragment at 5 °C. The dark-adapted form is shown in blue and the light-induced form in orange (the concentration was approximately 100 μM).*

3.3.5.4 Temperature dependence of the relaxation rate

To determine the effect of the Bcl-x_L protein on the relaxation rate, four different conditions were selected and the temperature dependence of the rates compared in an Arrhenius plot (ln k versus 1/T) (Equation 2.5) (see page 60). The isomerisation was followed by UV spectroscopy (363 nm) in the presence and in the absence of protein. Additionally, CD spectroscopy (222 nm) was used (in the absence of the protein) to compare the relaxation rate of the azobenzene moiety to the rate of structural change of the peptide. The observed structural change of the peptide is only pronounced enough for $Bak_{72\text{-}87}{}^{i+11}$ and therefore the rate could not be determined accurately in the other cases (Figure 3.18). The presence of Bcl-x_L did not have a significant effect on the relaxation rate and the obtained activation energy (E_a) and pre-exponential factor (A) values were similar in all cases (Table 3.7). The isomerisation is therefore also fully reversible in the presence of protein and not significantly slowed or speeded by its presence (Figure 3.20). This is in contrast to the findings for HDH-3, where the addition

of the DNA target sequence resulted in an increase in the isomerisation rate (Guerrero *et al.* PhD thesis 2005).

The obtained values for the activation energy are similar to what has been described for the free azobenzene cross-linker (32 kJ/mol, N. Taylor, PhD thesis). As anticipated, the values for $Bak_{72\text{-}87}^{i+7}$ were higher then this due to the stabilizing effect of the peptide secondary structure in for the *cis*-isomer. The values obtained for the other spacing were lower since the cis-conformation is probably sterically less favourable resulting in lower activation energy for the reaction. The pre-exponential factor for the peptides was significantly lower then for the free cross-linker in all cases. This suggests that the main effect of constraining the cross-linker conformationally is on the number of molecules that are in a reactive conformation and not on the activation energy.

The comparison of the CD- and UV spectroscopic results showed a significant difference in half-life at low temperature depending on the method used (more than one order of magnitude at 5 C) which disappears at higher temperatures (Figure 3.20). Errors in the experimental setup are very unlikely the cause for the difference in rate of more then one order of magnitude. Similar results have also been described previously by Guerrero *et al.* for the HDH-3 peptide (Guerrero *et al.* 2005b). This suggests the presence of more than two distinctive states of the peptide in the solution since the cross-linker isomerisation is not concerted with the isomerisation of the peptide. The cross-linker seems to isomerise first and the change in peptide secondary structure follows more slowly since the activation energy for this process is much higher (Table 3.7). The unusually low pre-exponential factor values obtained for $Bak_{72\text{-}87}^{i+11}$ suggests that only a small number of peptides are in a reactive conformation. This is

probably due to the very strong conformational constraints that the peptide secondary structure causes on the cross-linker in this spacing.

Table 3.7: *Arrhenius parameters for the relaxation of different peptides.*

BPN	Method	A (s^{-1})	E_a (kJ mol^{-1})
Cross-linker	UV (363 nm)	$3.25\ 10^8$	32.4
$Bak_{72\text{-}87}^{i+7}$	UV (363 nm)	$1.28\ 10^6$	56.0
$Bak_{72\text{-}87}^{i+7}$ + Bcl-x_L	UV (363 nm)	$7.76\ 10^5$	56.9
$Bak_{72\text{-}87}^{i+11}$	UV (363 nm)	0.02	13.7
$Bak_{72\text{-}87}^{i+11}$ + Bcl-x_L	UV (363 nm)	0.27	19.4
$Bak_{72\text{-}87}^{i+11}$	CD (222 nm)	$1.14\ 10^9$	76.2
$Bak_{72\text{-}87}^{i+7}$	CD (222 nm)	n. d.	n. d.

Table 3.8: *Half-life of the light-induced state for different peptides.*

BPN	Method	$t_{½}$ at 5 °C (min)	$t_{½}$ at 15 °C (min)	$t_{½}$ at 25 °C (min)	$t_{½}$ at 37 °C (min)
$Bak_{72\text{-}87}^{i+7}$	UV (363 nm)	448	174	89	34
$Bak_{72\text{-}87}^{i+7}$ + Bcl-x_L	UV (363 nm)	498	221	80	44
$Bak_{72\text{-}87}^{i+11}$	UV (363 nm)	44	30	32	22
$Bak_{72\text{-}87}^{i+11}$ + Bcl-x_L	UV (363 nm)	36	28	22	15
$Bid_{91\text{-}111}^{i+4}$	UV (363 nm)	178	40	n. d.	n. d.
$Bak_{72\text{-}87}^{i+11}$	CD (222 nm)	503	82	50	14

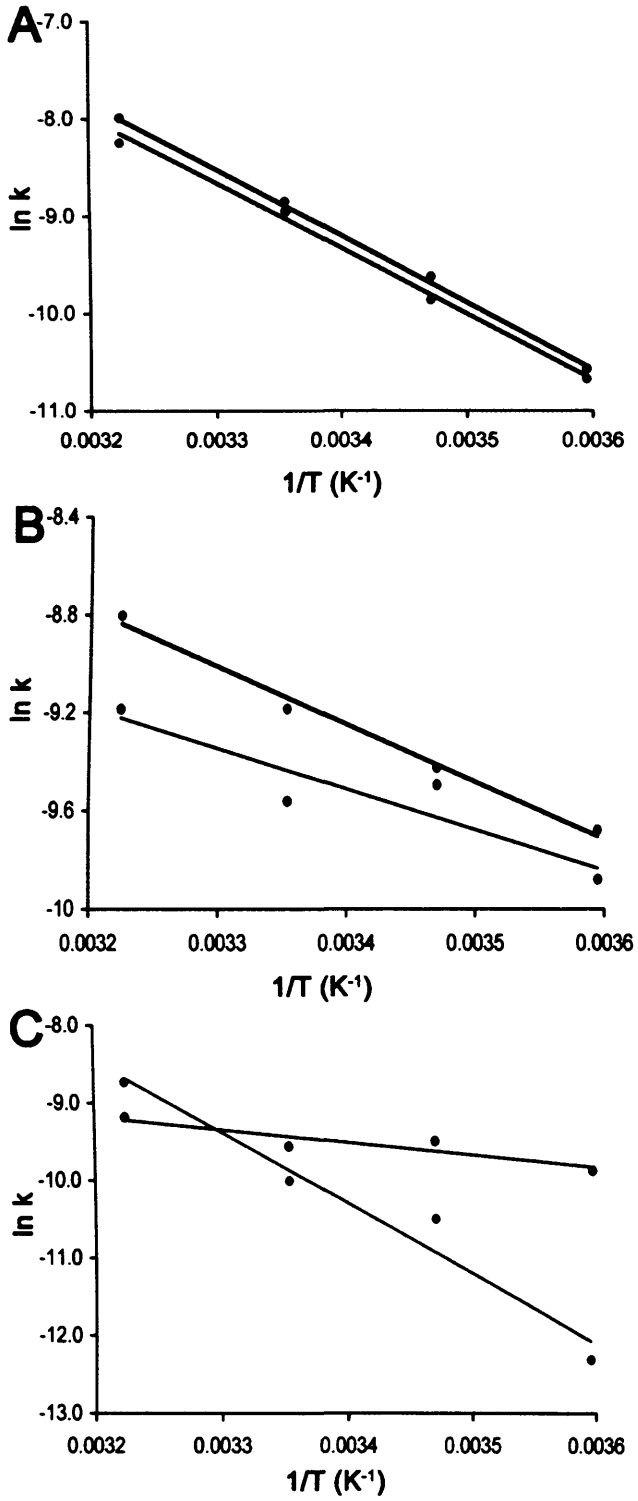

Figure 3.20: *Arrhenius plot of the UV relaxation rates of A) $Bak_{72\text{-}87}^{i+7}$ and B) $Bak_{72\text{-}87}^{i+11}$ and C) Arrhenius plot of the UV- and CD relaxation rates of $Bak_{72\text{-}87}^{i+11}$; Blue: absence of protein (UV), red: presence of protein (UV) and green: absence of protein (CD).*

3.3.6 Fluorescence anisotropy measurements of the peptides

Fluorescence anisotropy measurements (Heyduk *et al.* 1996) were carried out to determine the affinities of $Bak_{72\text{-}87}^{i+11}$, $Bak_{72\text{-}87}^{i+7}$ and $Bid_{91\text{-}111}^{i+4}$ for Bcl-x_L in their uncross-linked, dark-adapted and light-induced states. The addition of Bcl-x_L to a solution of fluorescently labelled peptide resulted in a 'saturatable' increase in the fluorescence anisotropy in all cases (Figure 3.21). Titration curves were fit to the Langmuir isotherm (Equation 2.8) (see page 64). For all complexes, the best fits were obtained for 1:1 binding (n = 1) as was expected from previous results with the wild-type peptide (Ernst *et al.* 2003; Gemperli *et al.* 2005) (Sattler *et al.* 1997; Walensky *et al.* 2004), these fits yielded the apparent dissociation constants in Table 3.9. The fits for $Bid_{91\text{-}111}^{i+4}$ in the two states were less accurate probably due to some degree of unspecific binding of this peptide to the protein.

The dissociation constant for the complex of Bcl-x_L and dark-adapted $Bak_{72\text{-}87}^{i+11}$ ($K_D = 21 \pm 1$ nM) was ~16-fold lower than that with the corresponding unalkylated peptide (Table 3.9). The K_D of 328 ± 19 nM obtained for the unalkylated peptide is similar to values previously reported for wild-type Bak peptide (Gemperli *et al.* 2005) (Sattler *et al.* 1997). The stability of the Bcl-x_L complex of irradiated $Bak_{72\text{-}87}^{i+11}$ was only decreased 2-fold relative to the complex with dark-adapted $Bak_{72\text{-}87}^{i+11}$. This high stability is most likely due to the incomplete *cis* to *trans* conversion of azobenzenes (Zhang *et al.* 2003) and hence the presence of 31% tightly binding *trans*-configured peptide in the irradiated state *(vide supra).*

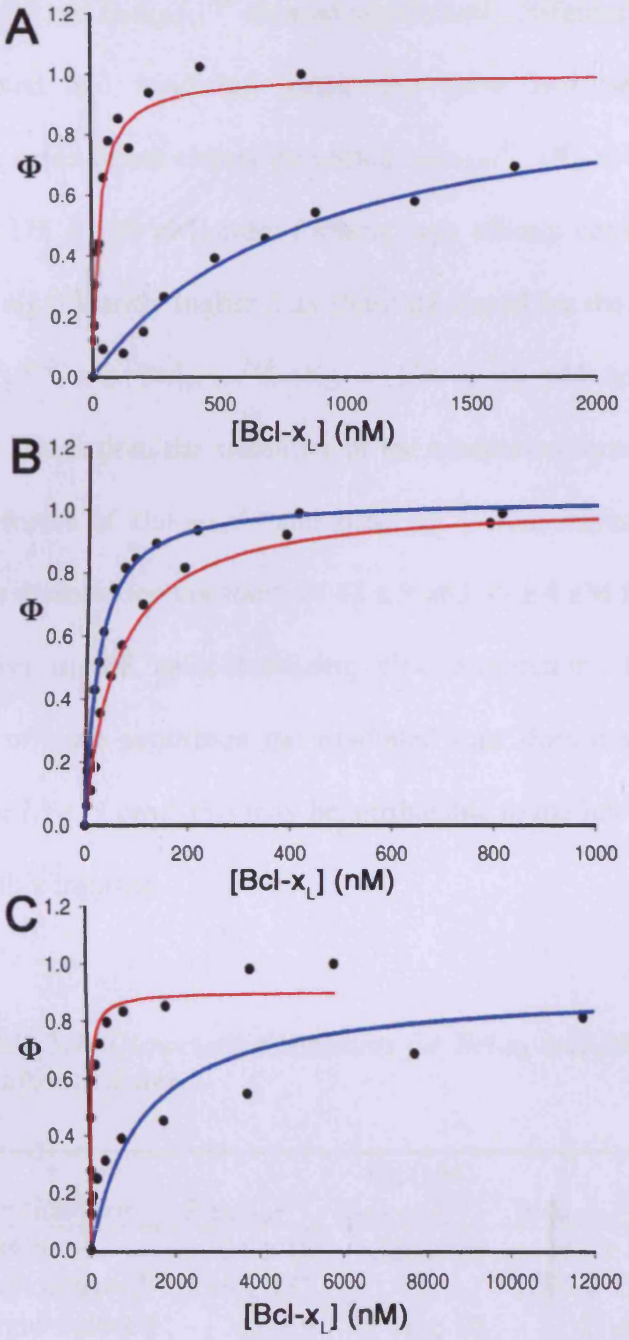

Figure 3.21: *Typical binding curves for A) $Bak_{72\text{-}87}^{i+7}$, B) $Bak_{72\text{-}87}^{i+11}$ and C) $Bid_{91\text{-}111}^{i+4}$. Φ indicates the bound fraction of Bcl-x_L in the cuvette. The blue line corresponds to the dark-adapted state of the BPNs and the red line to the irradiated state (Kneissl* et al. *2008).*

In contrast, $Bak_{72\text{-}87}^{i+7}$ and $Bid_{91\text{-}111}^{i+4}$ showed significantly different complex stabilities in their dark-adapted and irradiated forms. For these two peptides, the *trans*-configuration of the cross-linker clearly prevented $Bak_{72\text{-}87}^{i+7}$ (K_D = 825 ± 157 nM) and $Bid_{91\text{-}111}^{i+4}$ (K_D = 1275 ± 139 nM) from forming high affinity complexes (Table 3.9). These values were significantly higher than those measured for the unalkylated parent peptides of $Bak_{72\text{-}87}^{i+7}$ and $Bid_{91\text{-}111}^{i+4}$ (K_D = 134 ± 16 nM and 117 ± 48 nM, respectively). After irradiation, the stabilities of the complexes formed between Bcl-x_L and the irradiated forms of $Bak_{72\text{-}87}^{i+7}$ and $Bid_{91\text{-}111}^{i+4}$ were increased approximately 20-fold, resulting in dissociation constants of 42 ± 9 and 55 ± 4 nM for the two peptides with the cross-linker in the helix-stabilizing *cis*-configuration. The presence of a significant amount of *trans*-peptide in the irradiated state does not seem to have the same effect as in the *i, i+11* case; this may be attributable to the low binding affinity of the *trans*-isomer in this instance.

Table 3.9: *Dissociation constants for Bcl-x_L and BPNs in different states.*

	K_D (nM)		
Peptide form	$Bak_{72\text{-}87}^{i+7}$	$Bak_{72\text{-}87}^{i+11}$	$Bid_{91\text{-}111}^{i+4}$
Parent	134 ± 16	328 ± 19	117 ± 48
Dark-adapted	825 ± 157	21 ± 1	1275 ± 139
Light-induced	42 ± 9	48 ± 10	55 ± 4

The helix-stabilised forms of the BPNs bound to Bcl-x_L with much increased affinities when compared to the wild-type peptides or helical peptide mimetics, (Sattler *et al.* 1997; Petros *et al.* 2000; Yin *et al.* 2004; 2005a; Yin *et al.* 2005b) while the stabilities of the complexes of these BPNs rivalled those of the best designed Bcl-x_L-targeting miniature proteins reported so far (Chin *et al.* 2001; Walensky *et al.* 2004; Gemperli *et al.* 2005). However, unlike peptides in which the α-helical conformation is stapled

either through ruthenium-catalysed olefin metathesis of tethered amino acids (Walensky *et al.* 2004; Bernal *et al.* 2007) or through their introduction into a larger stable polypeptide fold such as pancreatic polypeptide (Gemperli *et al.* 2005), the activities of the biophotonic nanoswitches described here can be switched between high and low Bcl-x_L affinity states with external light pulses.

A key issue for a potential use of biophotonic switches to regulate cellular events is whether they demonstrate selectivity among different helix-binding proteins. We therefore determined the ability of alkylated $Bak_{72\text{-}87}^{i+11}$, $Bak_{72\text{-}87}^{i+7}$ and $Bid_{91\text{-}111}^{i+4}$ to bind to HDM2, a target of the tumour suppressor p53 (Joerger *et al.* 2007). The stability of the complex between HDM2 and p53 is the consequence of an α-helix of p53 binding to a deep cleft of the surface of HDM2 (Kussie *et al.* 1996). However, no binding activity for HDM2 was detected here in fluorescence anisotropy measurements for dark-adapted and irradiated $Bak_{72\text{-}87}^{i+11}$, $Bak_{72\text{-}87}^{i+7}$ and $Bid_{91\text{-}111}^{i+4}$ for concentrations up to 10 μM, indicating that the selectivity was more than 100-fold in their helical state (Kneissl *et al.* 2008) (Figure 3.22) (Table 3.10).

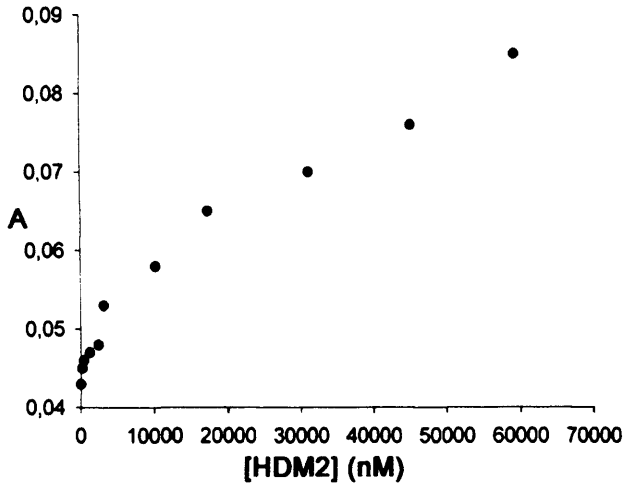

Figure 3.22: *Typical titration curve for BH3 domain BPNs and HDM2.*

Table 3.10: *Dissociation constants for the HDM2 and BPNs in different states.*

	K_D (nM)		
Peptide form	Bak_{72-87}^{i+7}	Bak_{72-87}^{i+11}	Bid_{91-111}^{i+4}
Parent	n.d.	n.d.	n.d.
Dark-adapted	> 10 μM	> 10 μM	> 10 μM
Light-induced	> 10 μM	> 10 μM	> 10 μM

3.3.7 Chemical shift perturbation NMR experiments

3.3.7.1 Expression of truncated Bcl-x_L in M9 minimal medium

To carry out NMR experiments, a loop deletion mutant (Δ45-84) of the protein was expressed since this resulted in less aggregation tendency. Expression was carried out in M9 minimal medium using $^{15}NH_4Cl$, the purification was accomplished using a Ni-Sepharose column and step-wise elution of 50 mM, 100 mM and 250 mM imidazole. Pure fractions were combined and analysed on an SDS gel (Figure 3.23).

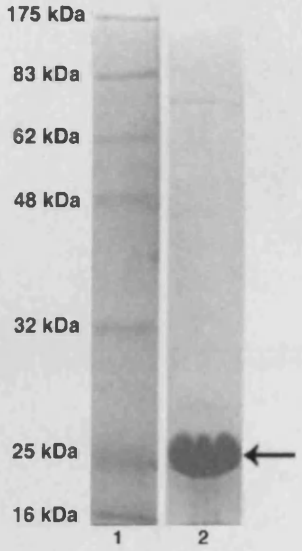

Figure 3.23: *SDS polyacrylamide gel electrophoresis of purified Bcl-x_L after staining with Coomassie blue. Lanes are 1: marker and 2: purified Bcl-x_L. The arrow indicates the band corresponding to Bcl-x_L.*

3.3.7.2 ^{1}H ^{15}N HSQC NMR experiments

^{1}H ^{15}N HSQC NMR measurements were carried out for the Bcl-x_L protein alone and in complex with the $Bak_{72\text{-}87}^{i+11}$, $Bak_{72\text{-}87}^{i+7}$ and $Bak_{72\text{-}87}^{wt}$ peptides. The assignments for the uncomplexed protein were obtained from Dr. Matt Crump (University of Bristol). A titration series was carried out so that the change in chemical shift could be monitored. Unfortunately, the dissociation of the complex was in slow exchange resulting in the formation of two sets of peaks instead of the expected gradual change in chemical shift (one set corresponding to the free protein and one to the complex). Comparison of the data for the different complexes strongly indicates that all peptides targeted the same binding cleft since the observed changes possess a high degree of similarity (Figure 3.24).

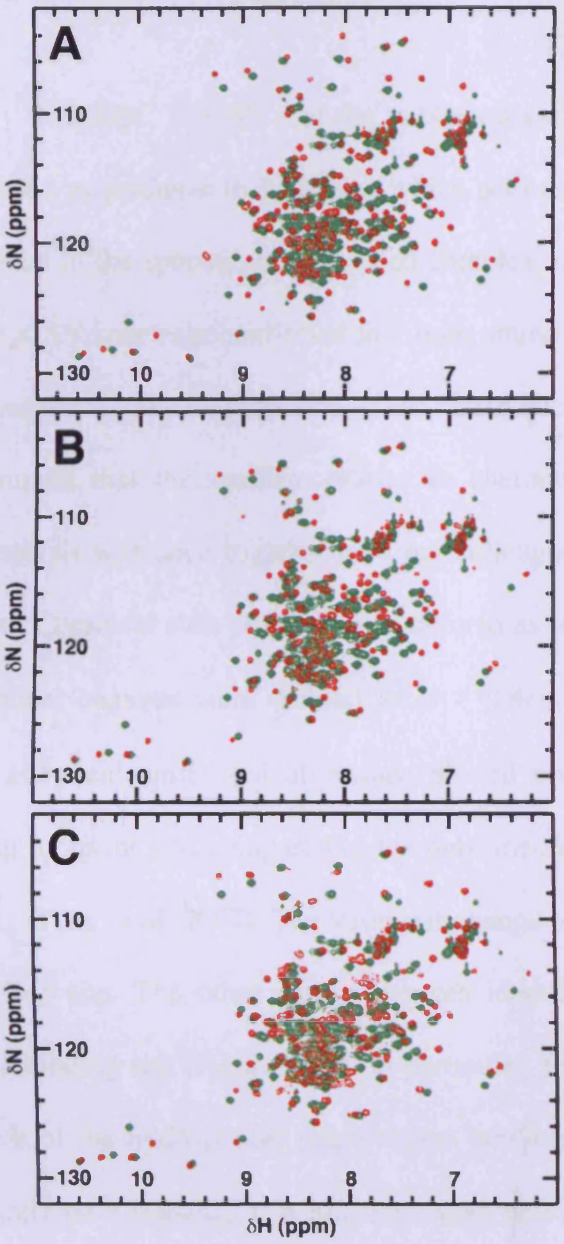

Figure 3.24: *^{1}H ^{15}N HSQC spectra of free Bcl-x_L 1-212 (Δ45-84) (green) and in complex (red) with A) Bak_{72-87}^{wt} peptide, B) dark-adapted alkylated Bak_{72-87}^{i+11} and C) Bak_{72-87}^{i+7} (Kneissl* et al. *2008).*

3.3.7.3 ^{1}H ^{15}N HSQC TOCSY NMR experiments

A combination of ^{1}H ^{15}N HSQC TOCSY and the published assignments for the Bcl-x_L/Bad complex was used as guidance to determine which peaks are homologous in the two spectra. If two peaks in the spectra of Bcl-x_L/Bad complex and Bcl-x_L /$Bak_{72\text{-}87}^{i+11}$ overlapped and the TOCSY spectrum confirmed that both amino acids are of a similar type then they were assumed to be identical. If no clear "assignment" could be made for a residue, it was assumed that the smallest change in chemical shift had occurred (Figure 3.25). This analysis was done together with my colleagues Dr. Joel Loveridge and Piotr Wysoczanski. Chemical shift changes were defined as stated in Equation 2.11 (see page 68). Significant changes were defined as $\omega > 0.4\omega_{max}$ (ω_{max} is the largest measured change in chemical shift) and all values plotted onto the model of the complex. The resulting footprint was compared to the published data for BH3 peptides in complex with Bcl-x_L (Feng *et al.* 2007). The strongest change observed corresponded to Phe 91 at the binding site. The other strong changes identified were also almost exclusively around the binding site (Figure 3.26). In particular, Phe 65, which has been shown to flip outwards of the hydrophobic pocket upon binding, shows a very strong change in chemical shift ($\omega = 0.94\omega_{max}$). A102, F57, Q85 and E58 also show strong changes in chemical shoft and are located at the binding site of the peptide. F106, T69, G94 and T132 showed strong changes in chemical but were located a bit further away from the interaction site. The moderate changes were mainly located in the α2, α3, α2-α3 loop and α4 regions as previously described for the binding of Bcl-x_L to various peptides (Feng *et al.* 2007) (Table A1). Overall, these results strongly indicate that $Bak_{72\text{-}87}^{i+11}$ targets the same cleft in Bcl-x_L as the wild-type peptide (Kneissl *et al.* 2008).

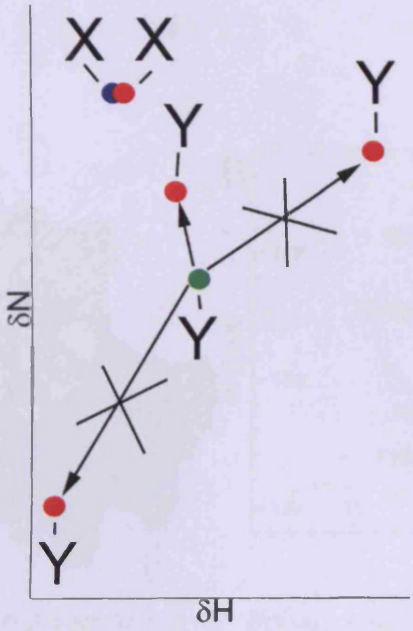

Figure 3.25: *Principle of the methods used to identify homologous peaks in the Bcl-x_L spectra. Green: Peak in the spectrum of free Bcl-x_L, blue: peak in the spectrum of Bcl-x_L/Bad and red: peaks in the Bcl-x_L /Bak_{72-87}^{i+11} spectrum. X and Y correspond to different types of amino acids identified from the TOCSY spectrum. If two peaks in the spectra of Bcl-x_L/Bad complex and Bcl-x_L/Bak_{72-87}^{i+11} overlapped and the TOCSY spectrum confirmed that both amino acids are of a similar type then they were assumed to be identical. If no clear "assignment" could be made for a residue, it was assumed that the smallest change in chemical shift had occured.*

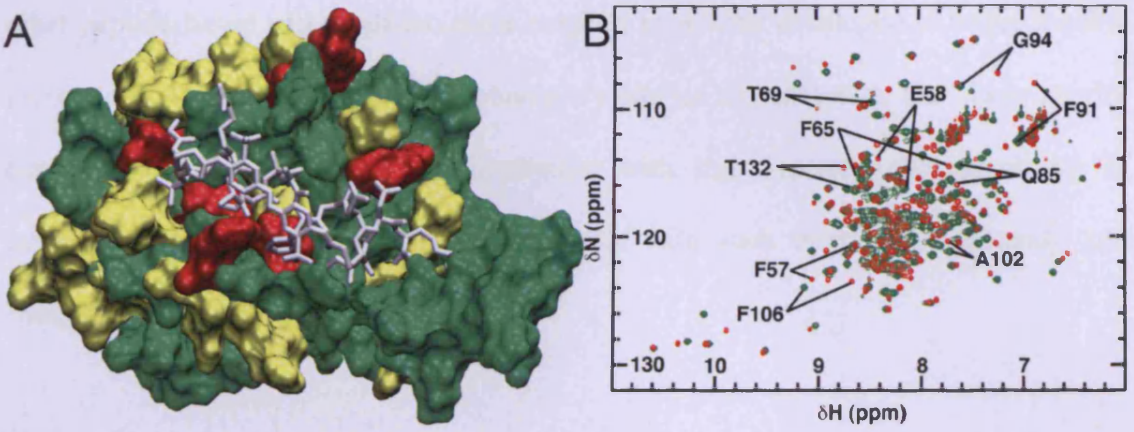

Figure 3.26: *A) Surface representation of Bcl-x_L showing residues that undergo changes in NH chemical shift upon binding to Bak_{72-87}^{i+11}. Minimum chemical shift changes were mapped onto the model of the Bcl-x_L/Bak_{72-87}^{i+11} complex. Red: $\omega > 0.4\omega_{max}$, yellow: $0.4\omega_{max} > \omega > 0.15\omega_{max}$, green: $\omega < 0.15\omega_{max}$. The modeled Bak_{72-87}^{i+11} peptide is shown as white sticks (Kneissl* et al. *2008). B) HSQC spectrum of free Bcl-x_L (green) and the Bcl-x_L/Bak_{72-87}^{i+11} complex (red). Identified strong changes in chemical shift are indicated.*

3.4 Conclusion

In summary, a family of biophotonic nanoswitches that could act as antagonists of Bcl-x_L were developed using an azobenzene-derived photo-activatable cross-linker to regulate the conformation of short peptides based on the BH3 regions of the Bcl-x_L-binding proteins Bak (Sattler *et al.* 1997) and Bid (Walensky *et al.* 2004). The binding mode of the biophotonic nanoswitches was determined by CD and NMR spectroscopy, which revealed that these peptides bind to the same cleft of Bcl-x_L identified as the target site of wild-type Bak and Bid. However, helix-stabilised peptides showed significantly greater affinities for Bcl-x_L than the unalkylated and wild-type peptides, whereas the helix-destabilised forms generally showed reduced affinity. The combined features of high affinity and high specificity together with their stable peptide

fold suggest that these and similar peptides might be used to probe and modulate a large variety of specific protein functions within the context of the cellular proteome. While other peptide-based and small molecule reagents have been developed to target specific protein-protein interactions, the biophotonic switches are unique in that their activity can be controlled externally by irradiation with light opening the possibility of interfering rapidly, reversibly and specifically with such interactions to study and modulate cellular function.

CHAPTER 4:

Photocontrol of protein-RNA interactions

4.1 Introduction

The human immunodeficiency virus (HIV) belongs to a retrovirus subfamily, the lentivirii. It targets CD4-bearing cells such as T-helper cells and is the cause of the acquired immunodeficiency syndrome (AIDS) (Vaishnav *et al.* 1991).

4.1.1 Structure of the virus particle

The HI virus is spherical and about 100 nm in size, it has two copies of a single stranded RNA genome, the particle is surrounded by a membrane (envelope), underneath the envelope lies the p17 structural protein matrix. Projecting from the envelope is the viral glycoprotein (gp120) which is connected *via* the gp41 protein (Gelderblom *et al.* 1987; Ozel *et al.* 1988; Gelderblom *et al.* 1989). The proximal bullet-shaped viral capsid is comprised of the structural protein p24 and encloses the RNA and the viral enzymes (integrase, reverse transcriptase and a protease) (Vaishnav *et al.* 1991) (Figure 4.1).

4.1.2 Genome organisation

The HIV genome consists of a 9 kb long single stranded RNA molecule. It efficiently utilises this relatively short sequence by making extensive use of overlapping reading frames, alternative splicing and translation of mRNAs with retained introns (Hope 1999). HIV has several major genes coding for structural proteins that are found in all retroviruses and several accessory genes that are HIV specific. The *gag* (group-specific antigen) gene encodes the protein that forms the basic virus structure (for example p17 and p24). The *pol* gene codes for a number of important viral enzymes such as reverse transcriptase, integrase and protease (PR). This protease is used to cleave the protein

products derived from pol and gag to give a number of important functional proteins. The envelope gene (env) codes for the precursor of gp120 and gp41. Those proteins are part of the viral envelope and necessary for attachment and fusion with target cells (Vaishnav *et al.* 1991). The other six HIV gene products have regulatory functions; for example, the 16 kDa protein TAT is crucial for the transcactivation of long terminal repeat (contains the promoter region) directed gene expression, rendering it essential for the production of further virions (Arya *et al.* 1985).

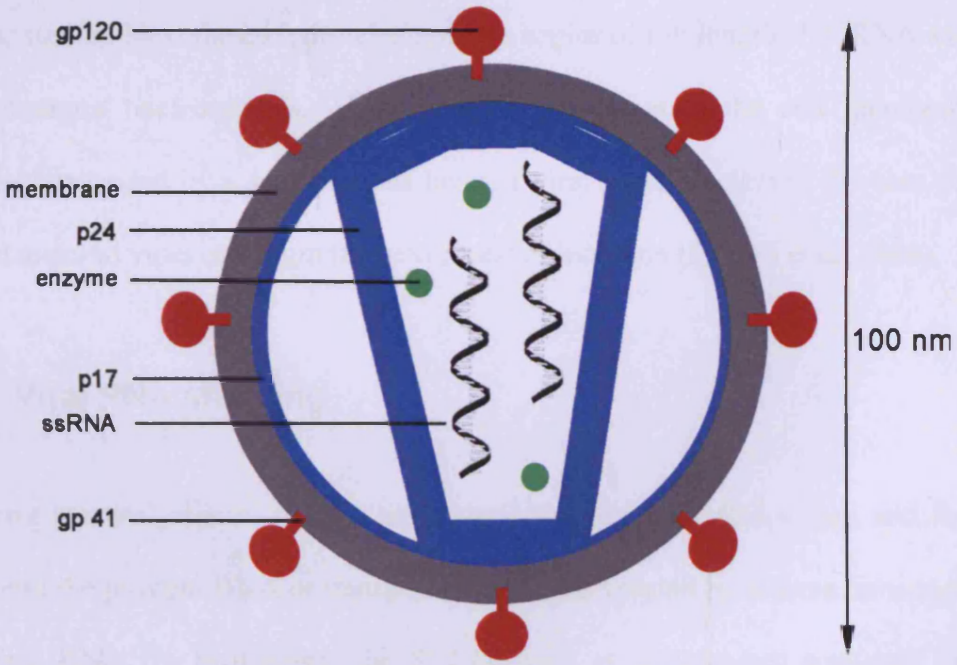

Figure 4.1: *Schematic representation of the HIV structure. Grey: viral envelope, red: coat proteins, blue: structural proteins, black: RNA and green: the viral enzymes integrase, reverse transcriptase and protease.*

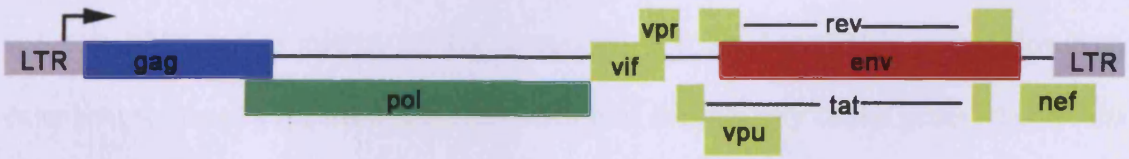

Figure 4.2: *Schematic representation of the HIV-1 genome organisation. Red: genes coding for coat proteins, blue: genes coding for structural proteins, yellow: genes coding for regulatory proteins and green: genes coding for viral enzymes.*

4.1.3 The HIV infection cycle

HIV initially interacts with the CD4 cellular receptors on the surface of a target cells *via* the envelope glycoproteins. Mediated by gp41, the lipid membranes fuse and the nucleocapsid goes into the cytoplasm. The viral genome is then transcribed into double-stranded DNA with the aid of the enzyme reverse transcriptase. This transcript enters the nucleus and is integrated into the cellular genome catalysed by the viral enzyme integrase. The resulting 'provirus' functions as a transcriptional template with the synthesised RNA undergoing further process followed by transportation to the cytosol and translation. Next the core proteins and two copies of full length HIV RNA assemble into immature nucleocapsids. These particles bud through the cell membrane and become surrounded by a membranous layer, a viral protease cleaves the core proteins and the matured virus can begin the next round of infection (Pollard *et al.* 1998).

4.1.4 Viral RNA shuttling

The long terminal repeats (LTRs) are several hundred nucleotides long and found at either end the proviral DNA or transposons. They are formed by reverse transcription of retroviral RNA. In proviruses, the 5'-LTR acts as a promoter sequence and the downstream long terminal repeat as a polyadenylation site. The transcription of HIV occurs from a single promoter within the 5'-LTR. The resulting transcript functions as genomic RNA and as mRNA for the expression of a number of HIV genes. However, extensive splicing is required in the expression of the majority of the genes; this results in a mixture of unspliced, single spliced and multiple spliced RNA products in the nucleus (Figure 4.3). Intron-containing pre-mRNAs are usually retained in the nucleus by the interaction of splicing factors. The incompletely spliced viral mRNAs therefore

contain a specific sequence known as the Rev response element. The Rev protein binds to the corresponding response element and activates the nuclear export of unspliced viral mRNA to the cytoplasm. The Rev protein, which is expressed in the early phase from the fully spliced mRNA, contains a nuclear localisation sequence (NLS) (Figure 4.5). This sequence overlaps with the RRE binding region therefore masking it upon binding. For the successful export of the Rev/RRE complex, a nuclear export sequence (NES) is required which is located at the *C*-terminal end of the protein. Rev levels rise in the late phase of the infection making binding and subsequent multimerisation a frequent event, this then leads to effective export of the longer mRNAs (Pollard *et al.* 1998).

4.1.5 The structure of the rev response element

The RRE is a 234 nucleotide structure that is found within the env intron within the unspliced HIV mRNAs. It consists of five stem regions (Figure 4.4). The specific sequence within the RRE that determines Rev responsiveness is very small compared to the size of the structure. Recognition is facilitated by a single high-affinity binding site. A combination of RRE mutagenesis experiments (Heaphy *et al.* 1990; Holland *et al.* 1990; Malim *et al.* 1990; Dayton *et al.* 1993), *in vitro* binding studies (Cook *et al.* 1991), chemical modification interference (Kjems *et al.* 1992; Tiley *et al.* 1992), and iterative *in vitro* genetic selection assays (Bartel *et al.* 1991) have mapped the interaction site to stems IIB and IID. NMR studies have subsequently elucidated the structure of a short Rev-based peptide bound to the stem IIB/IID region and identified important contacts between Rev and the RRE (Battiste *et al.* 1996).

Even though the RRE has only a single high-affinity site, a number of studies with full-length Rev and larger RRE fragments have shown that multiple Rev proteins bind to

one RNA molecule. The large size of the structure is probably necessary for the formation of the appropriate secondary structure and presentation of the high affinity binding site. Furthermore, the remaining stem loops serve as secondary Rev binding sites (Kjems *et al.* 1991; Pollard *et al.* 1998).

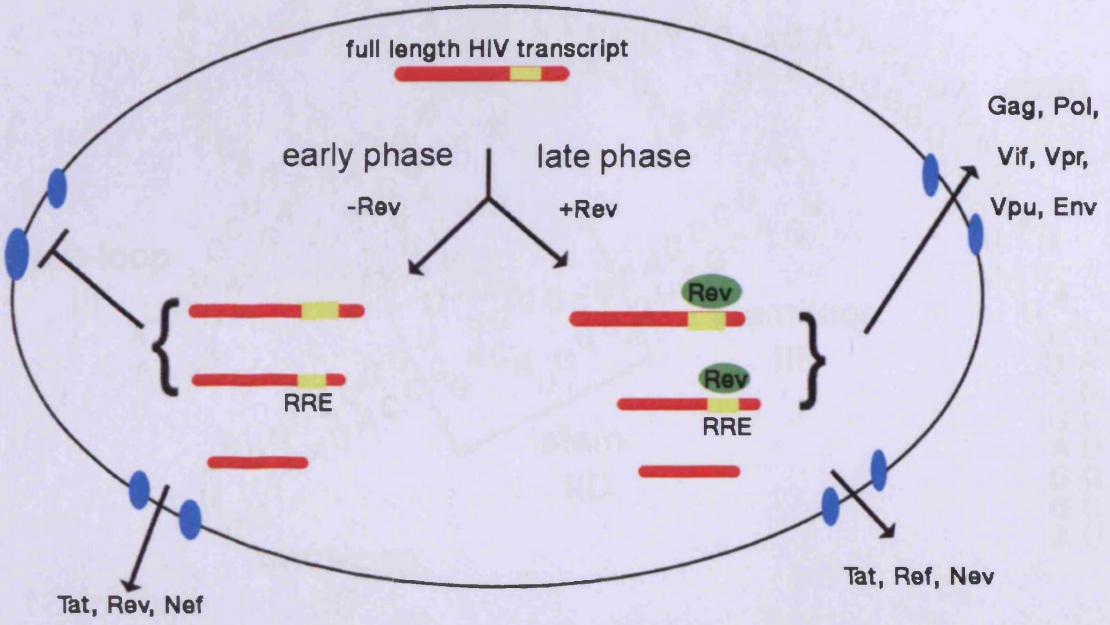

Figure 4.3: *Viral RNA shuttling. Red: mRNA, yellow: RRE and blue: nuclear pore complex (Pollard* et al. *1998).*

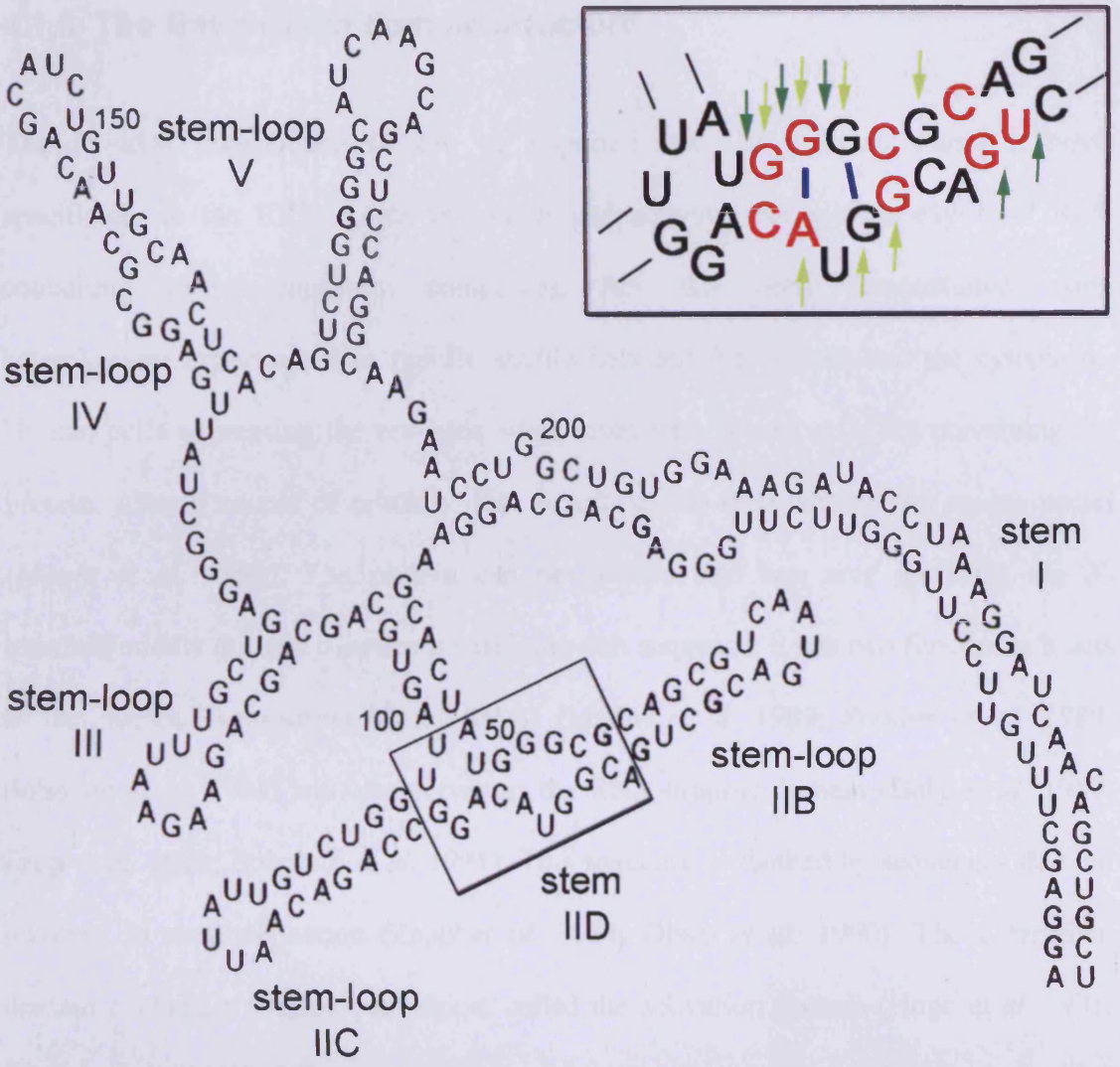

Figure 4.4: *The RRE 234 nucleotide domain structure. The primary Rev binding site is surrounded by a box and shown in greater detail in the inset. The standard Watson-Crick base pairs are represented with the bases drawn in close proximity. The two non-canonical base pairs (G47·A73 and G48·G71) are represented with blue lines between them. The red bases were invariant in iterative* in vitro *genetic selection experiments. The chemical modification of the purines marked with green arrows resulted in severely reduced Rev binding* in vitro *as did modification of the sugar-phosphate backbone at the positions indicated with yellow arrows (Pollard et al. 1998).*

4.1.6 The Rev protein domain structure

The 18 kDa phosphoprotein can be imported into the nucleus, where it binds specifically to the RRE, forms multimers and activates the nuclear export of RRE containing ribonucleoprotein complexes. Rev has been demonstrated using heterokaryon experiments to rapidly shuttle between the nucleus and the cytoplasm. Human cells expressing the rev gene were fused with mouse cells not containing the protein. After a couple of minutes Rev was then also detectable in the mouse nuclei (Meyer *et al.* 1994). The protein can be divided into two core domains; the *N*-terminal/middle domain contains an arginine-rich sequence, it has two functions; it acts as the nuclear localisation signal (NLS) (Malim *et al.* 1989; Perkins *et al.* 1989; Bohnlein *et al.* 1991) and also serves as the RNA-binding domain (Daly *et al.* 1989; Zapp *et al.* 1989; Bohnlein *et al.* 1991). This sequence is flanked by sequences that are involved in multimerisation (Zapp *et al.* 1989; Olsen *et al.* 1990). The *C*-terminal domain contains a leucine-rich region, called the activation domain (Hope *et al.* 1991; Malim *et al.* 1991b). It functions as the nuclear export signal (Figure 4.5). Both the NLS and NES work by accessing pathways for nuclear import or export. The Rev protein first binds monomerically to the high affinity site on the RRE (Cook *et al.* 1991; Malim *et al.* 1991a). This leads to localised melting of the RNA conformation (Tan *et al.* 1994; Renwick *et al.* 1995) and more Rev molecules can then multimerise and contact the RNA *via* a number of cooperative protein-protein and protein-RNA interactions (Daly *et al.* 1993). In total, eight or more Rev molecules can interact with one RRE sequence (Mann *et al.* 1994). The resulting complex is targeted for nuclear export by the activation domain (Pollard *et al.* 1998).

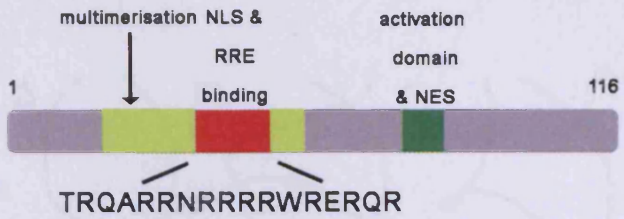

Figure 4.5: *The Rev protein domain structure (Pollard* et al. *1998).*

4.1.7 The Rev/RRE interaction

The Rev peptide binds to the RNA major groove in an α-helical conformation. The A-form RNA major grove is normally deep and too narrow to accommodate an α-helix, however, it may be widened by non-Watson-Crick interactions. The G48·G71 pair bends the RNA backbone into an S-shape conformation and facilitates the local opening of the major groove (Figure 4.6). The protein-RNA interaction interface is extensive, approximately four helix turns long (Battiste *et al.* 1996). The short Rev peptide is able to make numerous backbone and base-specific contacts without any additional protein contacts. This is in contrast to typical DNA-protein interactions where accessory protein structures contribute to high affinity binding by contacting the phosphate backbone (Grate *et al.* 1997). A number of arginine residues form base-specific contacts and the asparagine residue interacts with a G·A basepair. Arg35 and Arg39 make base-specific contacts on one side of the groove and Asn40 and Arg44 on the opposite side. Thr34 and several arginines (Arg38, Arg41, Arg42, Arg43, Arg46 and Arg48) contact the backbone (Figure 4.7). The Rev helix penetrates more deeply than most nucleic acid binding proteins as evident by the comparison to the GCN4 binding to the major groove which is typical for most DNA binding helices (Figure 4.6). It is situated about 0.3 nm deeper inside the groove than for example the GCN4 helix (Battiste *et al.* 1996; Grate *et al.* 1997).

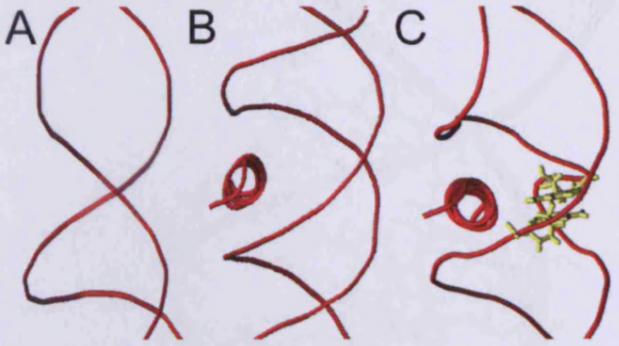

Figure 4.6: *Comparison of the major groove depth and width. The Rev peptide is buried much deeper within the A-form RNA major groove then most other peptides. A) Standard A-form RNA duplex. B) View perpendicular to the helix-axes of GCN4 (1YSA.pdb) (Ellenberger* et al. *1992) and C) View down the helix axes of Rev (1ETF.pdb) (Battiste* et al. *1996). The G48-G71 base pair is displayed in yellow.*

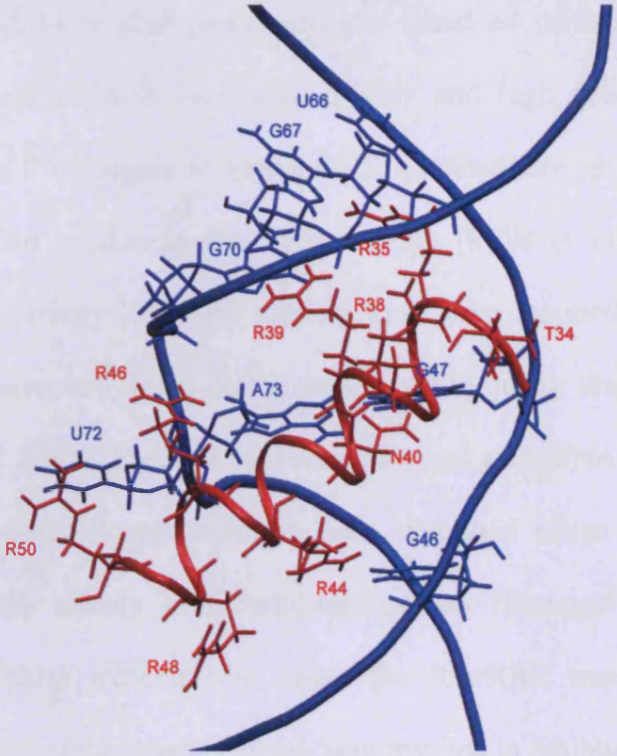

Figure 4.7: *NMR structure of the Rev/RRE interaction (1ETF.pdb) (Battiste* et al. *1996). Sidechains of amino acids that contribute to binding (greater than 3-fold loss of affinity upon mutation) are displayed in red and the bases that are contacted in the RNA are shown in blue.*

4.1.8 Compounds that target the Rev/RRE interaction

The Rev/RRE interaction is of great therapeutic interest due to its crucial involvement in the HIV life cycle. A number of strategies have been employed to target this complex. Cyclic β-hairpin mimetics that successfully mimic the helical conformation of the Rev peptide have been described recently. The measured K_D values were in the micro- to low nanomolar range. The best designed ligand R-27 bound with higher affinity to RRE than the Rev peptide and discriminated by approximately 50-fold between RRE and the related RNA sequence TAR. The binding mode of the mimetics was investigated by NMR spectroscopy and it was confirmed that they bind to the same position on the RRE as the Rev peptide (Moehle *et al.* 2007; Robinson 2008). A

macrolactam-bridged 14 residue peptidomimetic based on the sequence R_6QR_7, has been reported that binds with nanomolar affinity and high specificity to the Rev recognition element. This degree of specificity is obtained through the conformational restraint and the Gln residue in the right position (Mills *et al.* 2006). Pico- and nanomolar binding affinity Zn-finger proteins have been reported. They were either developed using a structure-based design strategy or by phage display (McColl *et al.* 1999; Friesen *et al.* 2001) (Figure 1.9). Peptide nucleic acid (PNA) modified peptides and nucleobase-conjugated peptides have been described which bind to the target sequence with similar affinity as the wild-type peptide (Kumagai *et al.* 2000; 2001; Takahashi *et al.* 2001). Attempts to target the Rev/RRE interaction with small molecules such as unfused aromatic cations have resulted in inhibitors with IC_{50} values in the high nanomolar or low micromolar range and good specificity (Xiao *et al.* 2001) (Figure 4.8). The design was established using a lead compound identified by an initial screen. The structure of this molecule was systematically varied using different proximal heterocycles and substituents. The contribution of each unit to activity could be determined from gel-shift assays in this way. The fact that DB340 binds close to the internal loop region of RRE and competes for binding with Rev was established by NMR spectroscopy.

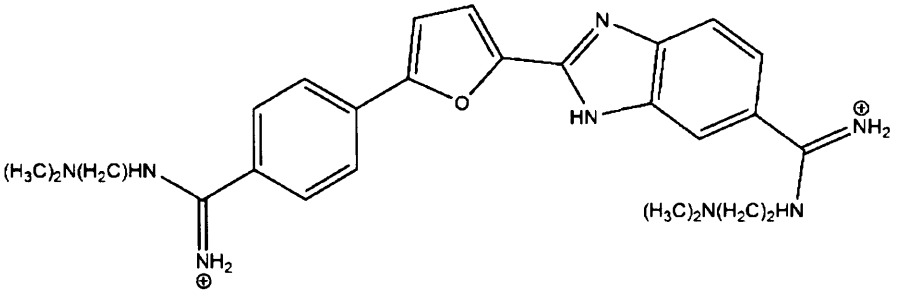

Figure 4.8: *Structure of DB340, a small molecule inhibitor of the Rev/RRE interaction.*

4.2 Aim of the project

While several potent small molecule and peptide-based inhibitors of the Rev/RRE complex have been developed recently, none of these have the potential to program changes in discrete and critical intracellular protein-RNA interactions through external stimuli and in a reversible manner. This could enable the development of novel tools for the study of cellular pathways involved in RNA metabolism or the generation of light-activatable therapeutics.

The aim of the project was therefore the development of photocontrollable peptides that target RNA-protein interactions. The Rev/RRE interaction of HIV-1 was selected as a model system since it is well characterised and an important therapeutic target. The plan was to develop Rev-based peptides with an azobenzene cross-linker in different spacings and to characterise these functionally by using UV/Vis spectroscopy and fluorescence-based binding assays and disruption assays and to characterise the structural change upon irradiation by CD spectroscopy.

4.3 Results and discussion

4.3.1 Design of the Rev peptides

The 18 amino acid peptide design was based on the NMR structure of the Rev/RRE complex (Battiste *et al.* 1996). The program MOE was used to create models of the cross-linked peptides in complex with the RNA so that the suitability of different designs could be evaluated (Figure 4.9). Since the Rev peptide is surrounded to 270° by RNA the right spacing of the cysteines was especially important (Battiste *et al.* 1996). Amino acids that can be replaced without significant loss of affinity were used preferentially for incorporating the cysteine residues. Residues on the same face as the cross-linker that could potentially interfere with it were changed to alanine. *i, i+7* and *i, i+11* designs were established in this way so that either inactivation or activation of the complex disruption could be accomplished by irradiation. The sequences of the two BPNs are shown in Table 4.1

Table 4.1: *Rev peptide sequences. Amino acid substitutions are given in blue.*

Peptide	33	50
$Rev_{33\text{-}50}^{wt}$	DTRQARRNRRRRWRERQR	
$Rev_{33\text{-}50}^{i+11}$	DTRQACRNRARRARERCR	
$Rev_{33\text{-}50}^{i+7}$	DTRQACRNAARRCRERQR	

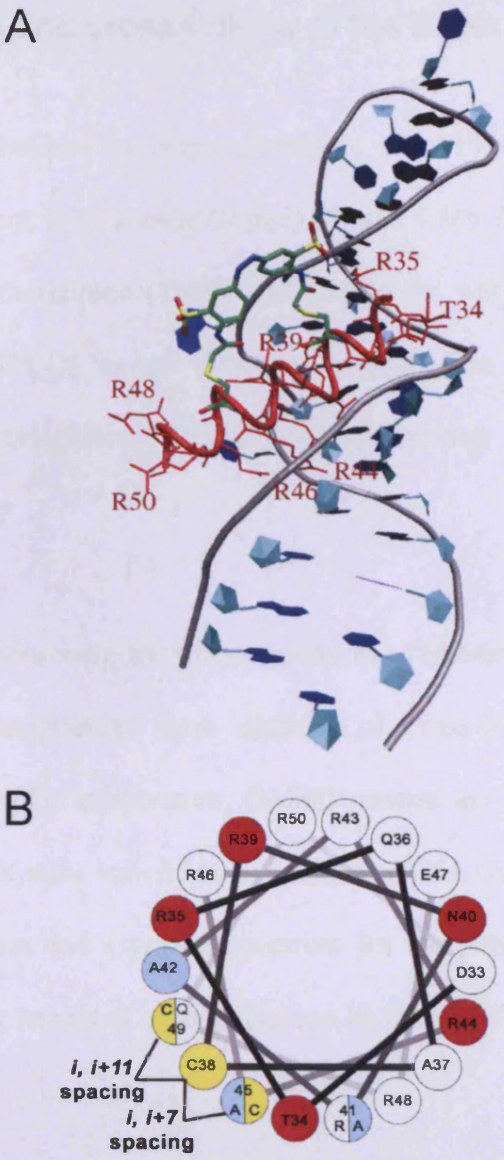

Figure 4.9: *Model of an activated BPN in complex with RRE (based on 1ETF.pdb (Battiste* et al. *1996)). A) Rev_{33-50}^{i+7} and B) Helical wheel representation of both BPNs. Red: residues shown to result in >10-fold loss of binding affinity upon replacement to an alanine, yellow: cysteine residues and cyan: residues replaced by alanine to avoid steric clash.*

4.3.2 Synthesis and cross-linking of the BPNs

Peptides were synthesised by Fmoc chemistry and SPPS; purification was achieved using HPLC (gradient: 0-60% over 60 min) (Figure 4.10). *N*-terminal modification with carboxytetramethylrhodamine (TMR) was carried out while the peptide was bound to the resin using DIPCDI as the coupling reagent. The cross-linking reaction with 3,3'-bis(sulfo)-4,4'-bis(chloroacetamido)azobenzene was performed as described in Chapter 3.

A variety of conditions were tested to alkylate the TMR-labelled peptides. However, in all cases rapid precipitation upon addition of cross-linker was observed. Buffer parameters such as pH, temperature, DMSO content and the concentration of cross-linker in each aliquot were varied but no product could be obtained. Figure 4.10 shows a typical chromatogram and a typical spectrum for the purified peptides. The retention times and molecular weight of all peptides can be found in Table 4.2.

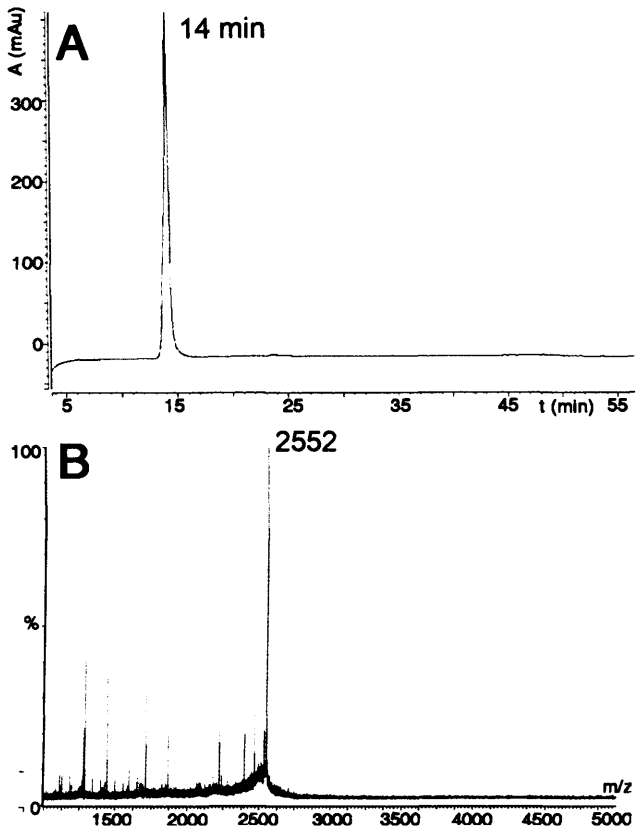

Figure 4.10: A) *Typical HPLC trace and B) typical mass spectrum of a purified BPN ($Rev_{33\text{-}50}^{wt}$).*

Table 4.2: *Molecular weight of the Rev peptides (X = alkylated with the azobenzene cross-linker). Major MS peak corresponds to the species observed in the mass spectrum. The molecular weight calculated from that is given in the column to the right. Theoretical average MW corresponds to the anticipated mass of each molecule.*

Peptide	Ion	Major MS peak	MW (g mol^{-1})	Theoretical MW (g mol^{-1})
$Rev_{33\text{-}50}^{wt}$	$[M+H]^+$	2,552	2,251	2,552
TMR-$Rev_{33\text{-}50}^{wt}$	$[M+H]^+$	2,970	2,969	2,966
$Rev_{33\text{-}50}^{i+7}$	$[M+H]^+$	2,245	2,244	2,245
$Rev_{33\text{-}50}^{i+7}$X	$[M+H]^+$	2,698	2,697	2,696
TMR-$Rev_{33\text{-}50}^{i+7}$	$[M+H]^+$	2,663	2,662	2,658
$Rev_{33\text{-}50}^{i+11}$	$[M+H]^+$	2,274	2,273	2,274
$Rev_{33\text{-}50}^{i+11}$X	$[M+H]^+$	2,725	2,724	2,724
TMR-$Rev_{33\text{-}50}^{i+11}$	$[M+H]^+$	2,690	2,689	2,688

4.3.3 UV/Vis characterisation

The isomerisation of the peptides was followed by UV/Vis spectroscopy at different temperatures as previously reported for the BH3 domain BPNs. This was used to characterise the thermal isomerisation of irradiated $Rev_{33\text{-}50}^{i+7}$and $Rev_{33\text{-}50}^{i+11}$. The absorption spectrum of the dark-adapted BPNs (with the azobenzene cross-linker in the thermally stable *trans*-configuration) was characterised by the same maximum as described in Chapter 3.3.5.1 (Figure 4.11). Since the presence of more than one isosbestic point was observed in the spectrum, the rate was determined by assuming first order kinetics for the reaction (Figure 4.12). Irradiated $Rev_{33\text{-}50}^{i+11}$ reverted to the dark-adapted state in a non-photochemical process with a half-life of 118 min (Table 4.5) (Figure 4.12). This was similar to the half-life of the previously reported HDH-3 (150 min) (Guerrero *et al.* 2005b) but significantly longer than for $Bak_{78\text{-}87}^{i+11}$. The UV/Vis spectra of dark-adapted and light-induced $Rev_{33\text{-}50}^{i+7}$ was similar to those observed for $Rev_{33\text{-}50}^{i+11}$ and the thermal reversion from the irradiated state occurred with a similar half-life of 154 min at 15 °C so the spacing did not strongly influence the reversion rate in this system (Table 4.5) (Figure 4.12). Comparison of this reversion rate to the data for $Bak_{72\text{-}87}^{i+7}$ ($t_{½}$ = 174 min) (Table 3.8) and PhotoMyoD ($t_{½}$ = 193 min at 15 °C) (Guerrero *et al.* 2005a) where the cross-linkers were also in the *i, i*+7 configuration indicated that the rate of thermal reversion is relatively sequence independent for this spacing.

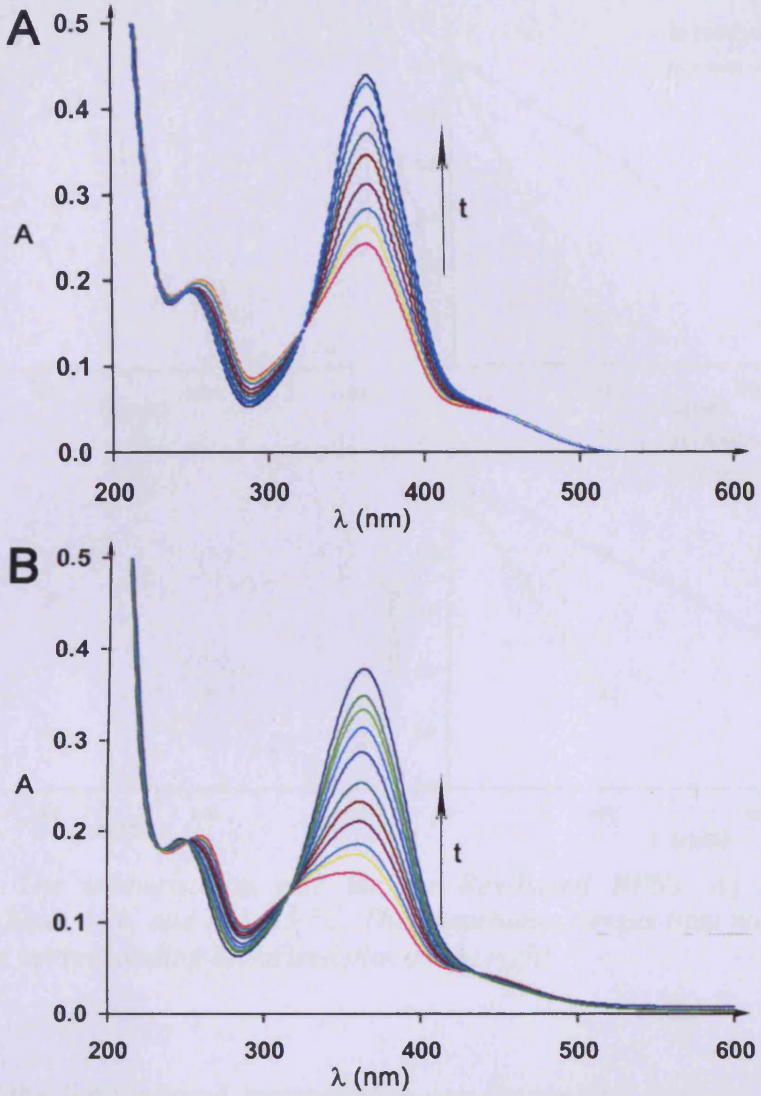

Figure 4.11: *UV/Vis spectra in the dark (top dark blue line), immediately after irradiation (pink) and at different times after irradiation A) $Rev_{33\text{-}50}^{i+11}$ and B) $Rev_{33\text{-}50}^{i+7}$.*

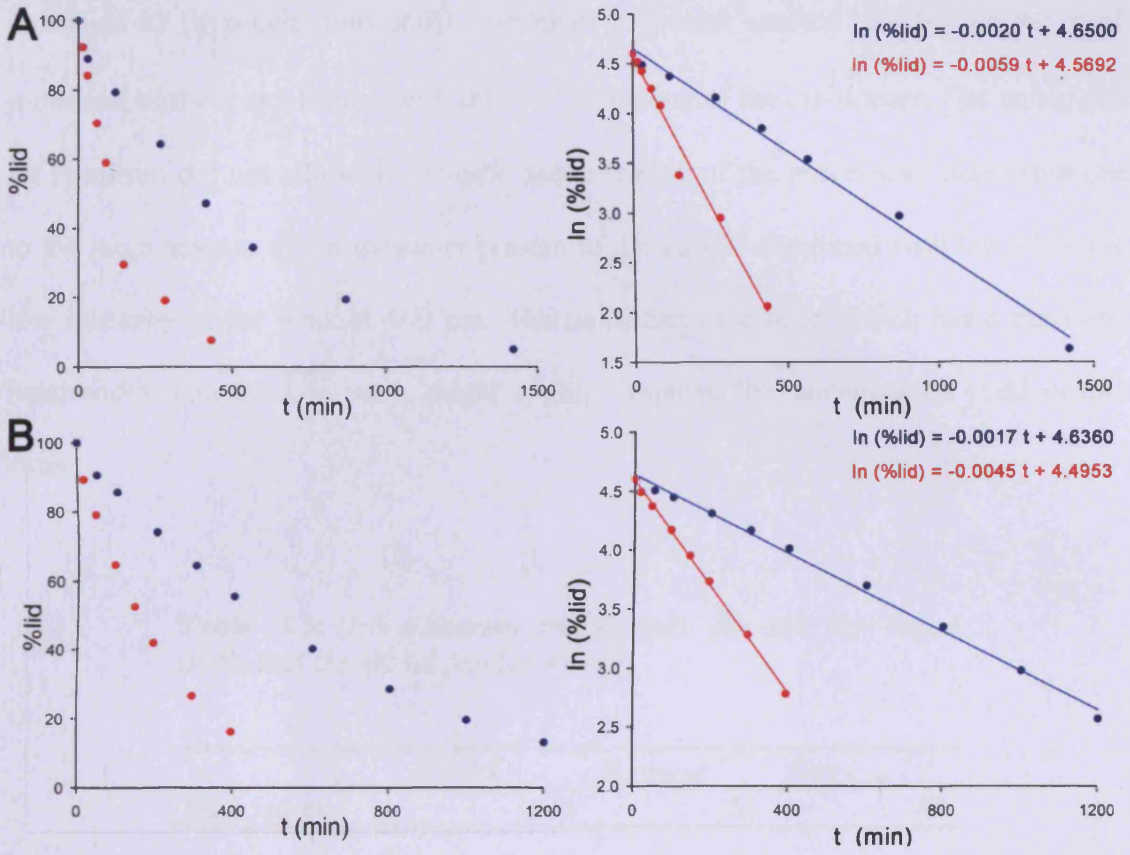

Figure 4.12: *The isomerisation rate for the Rev-based BPNs. A) $Rev_{33\text{-}50}^{i+11}$ and B) $Rev_{33\text{-}50}^{i+7}$; blue: 5 °C and red: 15 °C. The absorbance versus time plot is shown on the left and the corresponding linearised plot on the right.*

The extent of the light-induced isomerisation was determined from the absorbance at 363 nm, using the difference between the extinction coefficients for the *cis* and *trans* azobenzene cross-linker (Zhang *et al.* 2003). 48% and 61% of the irradiated material was found to be in the *cis*-configuration for alkylated $Rev_{33\text{-}50}^{i+11}$ and $Rev_{33\text{-}50}^{i+7}$ respectively (Table 4.3). The value for $Rev_{33\text{-}50}^{i+11}$ is significantly lower than typically observed in the photoisomerisation of azobenzenes (Guerrero *et al.* 2005b; Renner *et al.* 2006). The model peptide FK-11 for example gives 85% *cis* isomer upon irradiation (Zhang *et al.* 2003). After 4 min of irradiation there was no further change in the spectrum. A possible cause for this deviation could be a blue-shift of the n-π* transition absorbance maximum of the *cis*-isomer (usually around 440 nm for the azobenzene

cross-linker) (hypsochromic shift), resulting in greater spectral overlap of the π-π* transition of the *trans*-isomer with the n-π* transition of the *cis*-isomer. The calculated *cis* spectrum did not allow an accurate determination of the absorbance maximum due to the large amount of *trans*-isomer present in the sample combined with the relatively low intensity of the peak at 440 nm. The utilisation of a laser, which has a narrower band-width than the UV lamp, might slightly improve the isomerisation yield in this case.

Table 4.3: *Isomerisation percentages for the Rev-based BPNs and the model peptide FK-11.*

	FK-11	Rev_{33-50}^{i+7}	Rev_{33-50}^{i+11}
%cis isomer	85	61	48

4.3.4 Structural characterisation by CD spectroscopy

CD spectroscopy indicated that there are no significant differences in the conformation of Rev_{33-50}^{wt} and the uncross-linked Rev_{33-50} peptides. All of them show a spectrum of a mostly random coil conformation with minima around 200 nm. However, Rev_{33-50}^{i+11} is slightly more structured than the other two peptides with a mean residue ellipticity at 222 nm $[\Theta]_{r,\,222}$ of -6,455 deg cm^2 dmol^{-1} (20% helix content) (Figure 4.11) (Table 4.4). For the *trans*-configuration of this peptide in the cross-linked form, the CD spectrum revealed very substantial helix formation with a $[\Theta]_{r,\,222}$ of -19,627 deg cm^2 dmol^{-1} (Figure 4.13). This value is lower than that found for dad Bak_{72-87}^{i+11} (Table 3.6), but similar to the previous observations regarding HDH-3 (Guerrero *et al.* 2005b). The mean residue ellipticity at 208 nm was lower than at 222 nm, suggesting contributions

to the CD spectrum from the cross-linker as previously described (Flint *et al.* 2002) and as mentioned in Chapter 3.3.5.2 Irradiation with 360 nm light led to a significant increase in $[\Theta]_{r, 222}$ to -9,583 deg cm^2 dmol^{-1}, indicating a reduction in the amount of the peptide that adopts an α-helical structure as expected from the literature (Kumita *et al.* 2000; Kumita *et al.* 2003; Zhang *et al.* 2003; Guerrero *et al.* 2005a; Guerrero *et al.* 2005b; Woolley *et al.* 2006). However, even in this state, the amount of α-helical character was 31%, which is probably due to the presence in the irradiated state of $Rev_{33\text{-}50}^{i+11}$ of approximately 52% of the *trans*-configured peptide (Table 4.3). Since the isomerisation yield was relatively low for this peptide, the spectrum of the *cis*-form was calculated to fully evaluate the structural change upon irradiation (Figure 4.13). The spectrum of the *cis*-form shows almost no structure indicating that the helical conformation is fully destabilised in this isomer. As expected, the spectrum of $Rev_{33\text{-}50}^{i+7}$ in the dark displays little helical character with $[\Theta]_{r,222}$-values of -1,203 deg cm^2 dmol^{-1}. Upon irradiation, this value decreased 4-fold to -4,404 deg cm^2 dmol^{-1}. Since the percentage of *cis*-isomer obtained in this case is only 61% (Table 4.3), the full *cis*-spectrum was calculated from the data, giving a curve with minima at 222 nm, 208 nm and 195 nm as typical for α-helices (Figure 4.13). The *cis-trans* isomerisation rate for the cross-linked peptides was determined from the change in mean residue ellipticity at 222 nm and the obtained data compared to the results for the rate determined from the UV studies. The previously observed deviation for the isomerisation of *i, i+11* peptides (Chapter 3 and Guerrero *et al.*, PhD thesis 2005) at low temperature was also observed in this case but to a lesser extent (about 2-fold at 5 °C) (Table 4.5). The small difference at 15 °C for $Rev_{33\text{-}50}^{i+7}$ is unlikely to be significant since the structural change at this temperature is less pronounced and the calculation therefore of lower accuracy (Figure 4.14).

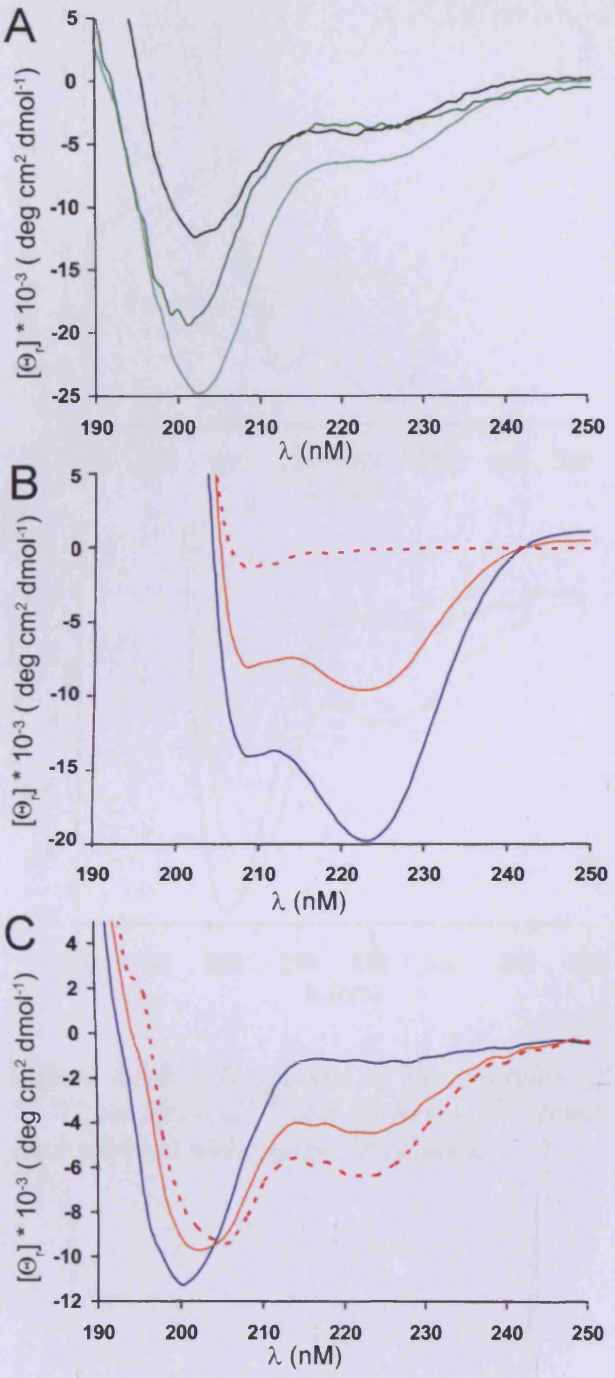

Figure 4.13: *CD spectra of the peptides at 5 °C. A) Unalkylated peptides, B)* $Rev_{33\text{-}50}^{i+11}$ *and C)* $Rev_{33\text{-}50}^{i+7}$*; black:* $Rev_{33\text{-}50}^{wt}$*, light green: uncross-linked* $Rev_{33\text{-}50}^{i+11}$*, dark green: uncross-linked* $Rev_{33\text{-}50}^{i+7}$*, blue: dark-adapted, orange: irradiated and red: 100%* cis *form (calculated from the spectra of the two states and the* cis/trans *ratio of the light-induced state which was determined from UV measurements).*

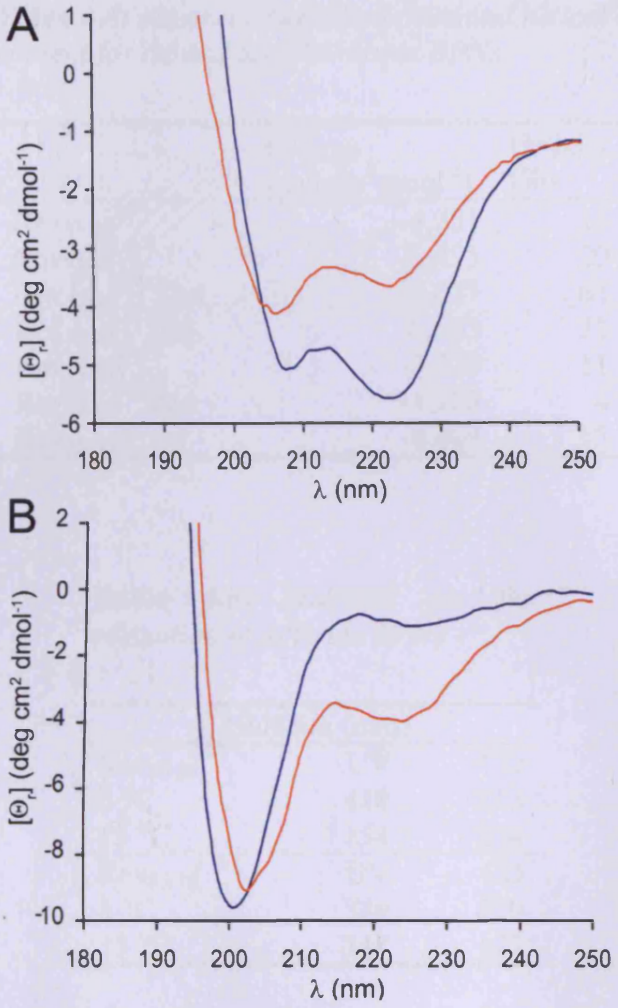

Figure 4.14: *CD spectra of the peptides at 15 °C .A) $Rev_{33\text{-}50}^{i+11}$ and B) $Rev_{33\text{-}50}^{i+7}$; blue: dark-adapted and orange: irradiated.*

Table 4.4: *Mean residue ellipticities and helical content for lid and dad Rev-based BPNs.*

	$[\Theta]_{r,222}$ (deg cm^2 dmol^{-1})	Helicity (%)
Rev_{33-50}^{wt}	-4,321	14
Rev_{33-50}^{i+11}	-6,455	20
Rev_{33-50}^{i+11} dad	-19,627	63
Rev_{33-50}^{i+11} lid	-9,583	31
Rev_{33-50}^{i+7}	-3,379	11
Rev_{33-50}^{i+7} dad	-1,203	4
Rev_{33-50}^{i+7} lid	-4,404	15

Table 4.5: *Half-life for the relaxation of different BPNs.*

Half-life (min)		
Rev_{33-50}^{i+7}	UV	CD
5 °C	418	413
15 °C	154	274
Rev_{33-50}^{i+11}	UV	CD
5 °C	339	629
15 °C	118	132

4.3.5 Binding assays

Fluorescence anisotropy measurements (Heyduk *et al.* 1996) were performed to determine the affinities of Rev_{33-50}^{i+11} and Rev_{33-50}^{i+7} in their uncross-linked, dark-adapted and light-induced states. Neither addition of dad Rev_{33-50}^{i+11} nor addition of wild-type peptide to a solution of fluorescently labelled RRE RNA resulted in an increase in the fluorescence anisotropy. This is probably due to the small size of the ligand compared to the larger RRE RNA, making this assay unsuitable for the application.

A FRET-based binding assay was optimised instead; TMR-labelled peptide was titrated into a solution of FAM-labelled RNA leading to a saturatable decrease in FAM fluorescence intensity. The data obtained was fitted to the Langmuir isotherm (Equation 2.8 on page 64). For both the wild-type peptide complex and the unalkylated $Rev_{33\text{-}50}^{i+11}$, the best fits were obtained for 1:1 binding (n = 1) as was expected from previous results with the wild-type peptide (Mills *et al.* 2006). These fits yielded the dissociation constants in Table 4.6. The obtained K_D value for the wild-type peptide was 7 ± 2 nM which is in agreement with previously reported data (K_D values between 2 nM and 70 nM) (Tan *et al.* 1993; Takahashi *et al.* 1999; Kumagai *et al.* 2000; Takahashi *et al.* 2001; Mills *et al.* 2006). The dissociation constant for the R38C substituted peptide was reduced by one order of magnitude (69 ± 27 nM) as expected from previous mutagenesis experiments (Battiste *et al.* 1996) (Figure 4.7). Since the other BPN displayed a very similar CD spectrum (Figure 4.13) and contained the same R38C substitution, it was decided not to determine the affinity in this case. The affinities of the cross-linked peptides could not be determined due to the problems with alkylating the TMR-derivatives.

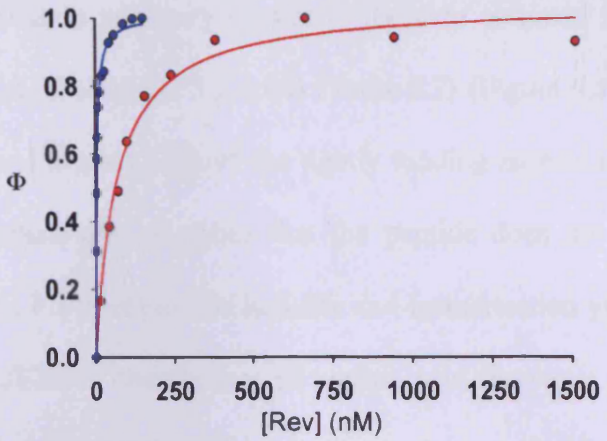

Figure 4.15: *Typical binding curves for $Rev_{33\text{-}50}^{wt}$ (blue) and $Rev_{33\text{-}50}^{i+11}$ (red).*

Table 4.6: *Dissociation constants for the wild-type peptide and one of the uncross-linked peptides.*

Peptide	K_D
$Rev_{33\text{-}50}^{wt}$	7 ± 2
$Rev_{33\text{-}50}^{i+11}$ (unalkylated)	69 ± 27

4.3.6 Rev/RRE disruption assay

The ability of the BPNs to disrupt the Rev/RRE interaction *in vitro* was analysed using a FRET based assay. The cross-linked BPNs (with no attached fluorophore) were titrated into a solution of TMR-wild-type peptide and FAM-labelled RNA, leading to a saturatable decrease in fluorescence intensity of the TMR-fluorophore (the assay conditions having been optimised using the wild-type peptide (K_i = 3 ± 1 nM and Hill slope = 1.1 ± 0.2). IC_{50} values and K_i values were determined from the curves using Equation 2.9 and Equation 2.10 (see page 65), respectively. The K_i value for the dark-adapted state of $Rev_{33\text{-}50}^{i+11}$ was 0.7 ± 0.2 nM (Hill slope 0.87 ± 0.02). This is two orders of magnitude lower than the K_D value obtained for the unalkylated peptide and one order of magnitude lower than the wild-type K_D value (Table 4.6). The apparent K_i

for the light-induced state was very similar to the data obtained for the dark-adapted form (0.9 ± 0.3 nM, Hill slope 0.53 ± 0.04) (Table 4.7) (Figure 4.16). This is probably due to the presence of around 52% of the tightly binding isomer in the mixture, since the structural characterisation suggests that the peptide does not adopt the required helical conformation. Furthermore the half-life and isomerisation yield for the *cis*-form have only been obtained in the absence of nucleic acid. Previous studies have shown that the presence of nucleic acid target sequence can have a significant influence on the reversion rate and therefore in this case a reduction of the amount of *cis*-isomer present is likely (Guerrero *et al.*).

The inhibitory constant for light-induced $Rev_{33\text{-}50}^{i+7}$ was in the picomomolar range (K_i = 0.3 ± 0.3 nM, Hill slope 0.65 ± 0.03), indicating that this BPN binds one order of magnitude more tightly to the target sequence than the wild-type peptide and that the pre-organisation of the peptide conformation for binding was successful. In the dark-adapted state, there is significant loss of activity resulting in a K_i value of 61 ± 29 nM. The Hill slope in this case was only 0.41 ± 0.03 (for one site competitive binding it is around 1.0) suggesting that the mechanism of inhibition is not competitive and this peptide conformer has a different mode of action than the lid-form.

The inhibition constants of the complexes of these BPNs rivalled these of the best RRE-targeting peptides and small molecules reported so far (Friesen *et al.* 2001; Xiao *et al.* 2001). However, unlike compounds in which the α-helical conformation is fixed, the activity of the $Rev_{33\text{-}50}^{i+7}$ biophotonic nanoswitch described here can be switched between high and low affinity RRE binding states with external light pulses. It has been demonstrated that the binding specificity of the Rev peptide depends on helix content

therefore $Rev_{33\text{-}50}^{i+11}$ might have the potential to very accurately discriminate between related RNA sequences due to its extensive conformational pre-organisation (Tan *et al.* 1993).

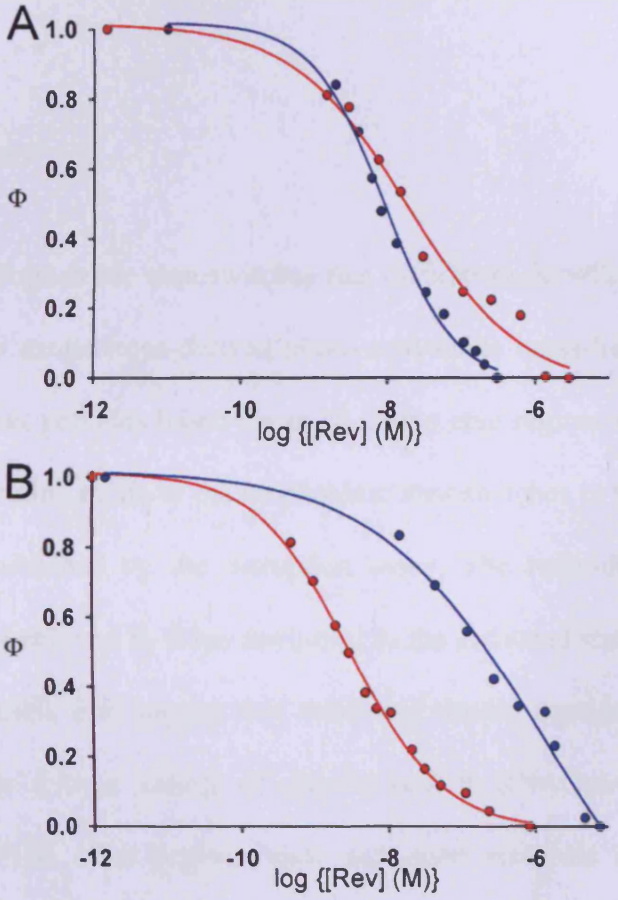

Figure 4.16: *Typical disruption curves for A) $Rev_{33\text{-}50}^{i+11}$ and B) $Rev_{33\text{-}50}^{i+7}$. The blue line corresponds to the dark-adapted state and the red line to the irradiated state.*

Table 4.7: *IC_{50} and K_i values obtained from competition experiments for the Rev-based BPNs.*

	IC_{50} (nM)	Hill slope	K_i (nM)
$Rev_{33\text{-}50}^{i+11}$ dad	8 ± 2	0.87 ± 0.02	0.7 ± 0.2
$Rev_{33\text{-}50}^{i+11}$ lid	11 ± 4	0.53± 0.04	0.9 ± 0.3
$Rev_{33\text{-}50}^{i+7}$ dad	717 ± 345	0.41 ± 0.03	61 ± 29
$Rev_{33\text{-}50}^{i+7}$ lid	3 ± 3	0.65 ± 0.03	0.3 ± 0.3

4.4 Conclusion

In summary, two biophotonic nanoswitches that disrupt the Rev/RRE interaction were developed using an azobenzene-derived photo-activatable cross-linker to regulate the conformation of short peptides based on an 18 amino acid regions of the RRE-binding protein Rev. The binding mode of the biophotonic nanoswitches in the activated state is competitive, as established by the disruption assay. The helix-destabilised form of $Rev_{33\text{-}50}^{i+7}$ showed a reduced K_i value compared to the activated state. The high affinity together with the stable fold suggest that these and similar peptides might be used to probe and modulate a large variety of specific protein RNA interactions within the cellular context. While other peptide-based and small molecule reagents have been developed to target specific protein-RNA interactions, the biophotonic nanoswitches are unique in that their activity can be controlled externally by irradiation with light, opening the possibility of interfering rapidly, reversibly and specifically with such interactions to study and modulate cellular function.

CHAPTER 5:

Towards cell membrane penetrating BPNs

5.1 Introduction

The plasma membrane is a lipid bilayer containing proteins and glycoproteins. Hydrophilic compounds cannot cross the lipid membrane unless specific mechanisms are in place to facilitate their transport, small ions can cross *via* specific channels, and other hydrophilic compounds are transported through shuttle proteins. For larger proteins uptake is endocytotic and the cargo is initially retained in vesicles. Subsequent steps are required in this case to release the compounds into the cytoplasm (Joliot *et al.* 2004).

A series of small domains termed protein transduction domains (PTDs) have been demonstrated to efficiently cross biological membranes and reach compartments such as the cytoplasm and the nucleus. This was initially described for HIV TAT and the homeodomain of the *Drosophila melanogaster* transcription factor Antennapedia but has since expanded to include other natural and non-natural peptides (Frankel *et al.* 1988; Joliot *et al.* 1991; Derossi *et al.* 1994; Oehlke *et al.* 1998; Morris *et al.* 2001; Sawada *et al.* 2003). In biological context, these proteins have a messenger function since they regulate the transcription of specific genes in the target cells. For example, the homeoprotein expression differs regionally so it probably conveys positional information between cells (Levine *et al.* 1983). It has been demonstrated by mutation and deletion analysis that in fact small domains within the full-length protein are responsible for the activity.

Subsequently, a short 11 amino acid domain of the TAT protein has been shown to deliver biologically active 120 kDa β-galactosidase into various tissues (Schwarze *et al.* 1999). The 18 amino acid peptide Penetratin (derived form helix 3 of Antennapedia) has been used to target anti-apoptotic proteins to the brain. This has been shown to protect the cells from ischemic injury (caused by a restriction of blood flow to certain areas of tissue) (Cao *et al.* 2002). This transduction strategy is not limited to unmodified proteins and peptides but also enables the internalisation of other compounds, such as nucleic acids, peptide nucleic acid or modified proteins (Hall *et al.* 1996; Pooga *et al.* 1998; Joliot *et al.* 2004).

Three different models for the transduction mechanism have been proposed and studies have suggested that the individually followed uptake pathway depends on the peptide, cell-type as well as on the cargo (Derossi *et al.* 1996; Dom *et al.* 2003; Vives 2003; Joliot *et al.* 2004). The first mechanism starts with endocytotic uptake of the peptide followed by vesicle disruption and passage of the peptide and cargo into the cytoplasm. The second model involves the perpendicular insertion of the amphiphatic peptide domains into the lipid bilayer. The hydrophobic residues orient towards the lipids and the hydrophilic helix faces multimerise and form a channel. This would then allow the cargo to pass through. Thirdly, the peptides can interact electrostatically with the polar groups of lipids in the membrane. This leads to the formation of inverted micelles, engulfing the peptide and the cargo. The reopening of the micelle on the other side results in the transfer to the cytoplasm (Futaki 2002; Joliot *et al.* 2004; Futaki *et al.* 2007).

5.2 Aim of the project

The optical control of DNA binding by PhotoMyoD and the Bcl-x_L binding of the BH3-domain BPNs has been shown *in vitro*. But neither the light activation of transcription (by PhotoMyoD or an artificial transcription factor based on HDH-3) nor the photocontrol of apoptotic processes by the BH3-domain BPNs has been demonstrated yet (Guerrero *et al.* 2005a; Kneissl *et al.* 2008). Although the strategy for stabilising peptide secondary structure with an azobenzene cross-linker has proven useful *in vitro*, the *in vivo* application is limited by the inherent cell impermeability of most large peptides (> 600 Da) (Egleton *et al.* 1997; van de Waterbeemd *et al.* 1998). While microinjection can be useful for the analysis of a small number of cells, it is unsuitable for most applications using larger areas of tissue. Therefore, cell and nuclear membrane impermeability is a major obstacle for the use of this system *in vivo*. The aim of this project was the development of a membrane penetrative version of the photocontrollable transcriptional activator PhotoMyoD and of the BH3-domain BPNs, this could then enable future *in vivo* experiments and applications such as tools for tissue engineering or photocontrollable cancer therapeutics.

5.3 Development of a membrane penetrating PhotoMyoD

5.3.1 Previous work on PhotoMyoD

As mentioned in Chapter 1, the regulation of specific DNA-protein complex formation is important for processes such as transcription. MyoD is a basic helix loop helix transcription factor. These proteins bind DNA as homo- or heterodimers. The bHLH domain is a 68 amino acid residue motif. It can be divided into two parts, the HLH

motif and an N-terminal α-helix. The HLH element is responsible for dimerisation and the *N*-terminal basic α-helix binds to the major groove of the DNA (Lassar *et al.* 1989; Murre *et al.* 1989a).

MyoD is expressed in numerous cell types such as fibroblasts and myoblasts. It activates the transcription of myogenesis inducing genes (Olson 1990). MyoD recognises the E-box sequence (CANNTG), it forms heterodimers with the ubiquitous factors E12 and E47 to perform its function *in vivo* (Murre *et al.* 1989a; Murre *et al.* 1989b; Tapscott *et al.* 1993; Maleki *et al.* 1997). E12 and E47 alone can bind the E-box site but are unable to induce myogenesis. PhotoMyoD was designed in accordance with examinations of the crystal structure of MyoD in complex with its cognate DNA (MDY1.pdb) (Ma *et al.* 1994) and by analysing the sequence conservation between MyoD and related proteins. One double cysteine mutant was selected in which the cross-linker could be introduced on the opposite side of the basic helix without mutating any crucial residues (Guerrero *et al.* 2005a).

The introduction of an azobenzene cross-linker into the DNA recognition helix of the transcription factor MyoD resulted in a DNA binding protein, the activity of which could be photocontrolled (Figure 5.1). The light-induced form demonstrated significant stability of the recognition helix relative to the dark-adapted state as demonstrated by CD spectroscopy. Light activation resulted in an increase of the DNA binding specificity of more than two orders of magnitude. Such photo-activatable DNA binding proteins could be important building blocks for reagents to control developmental processes and lead to new therapeutics (Guerrero *et al.* 2005a). However, PhotoMyoD has not been shown yet to function as a transcriptional activator.

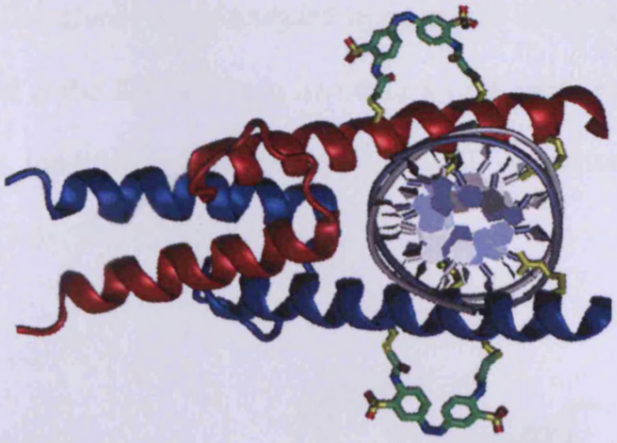

Figure 5.1: *Model of the DNA complex of the alkylated PhotoMyoD with the azobenzene-based cross-linker in its* cis*-configuration (Figure taken from Guerrero* et al.*), based on the crystal structure of MyoD-bHLH in complex with DNA (Ma* et al. *1994).*

5.3.2 Design and cloning of different PhotoMyoD constructs

Two different designs were established using either the TAT or the penetratin domain on the *N*- or *C*-terminus. A His-tagged version was also generated to compare different purification options.

5.3.2.1 Design and cloning of TAT PhotoMyoD

The previously established design for PhotoMyoD (Guerrero *et al.* 2005a) was modified with an *N*-terminal TAT-domain (Figure 5.2). The construction of the appropriate DNA sequence was accomplished in three steps; a pET19b vector was modified by excising the region between the *Nco*I and *Nde*I restriction sites, which codes for the His-tag and replacing it with a sequence coding for TAT (Table 5.1). This plasmid (pET TAT) and the photoMyoD pJGetita construct were cut with *Nde*I and *Bam*HI and the resulting two

fragments ligated. The clones were analysed using a *Pst*I diagnostic digest. The new plasmid was mutated at the *Bam*HI site to introduce a stop codon in the right frame and the success of the modification judged by a *Bam*HI restriction digest and DNA sequencing (Figure 5.3) (Table 5.2).

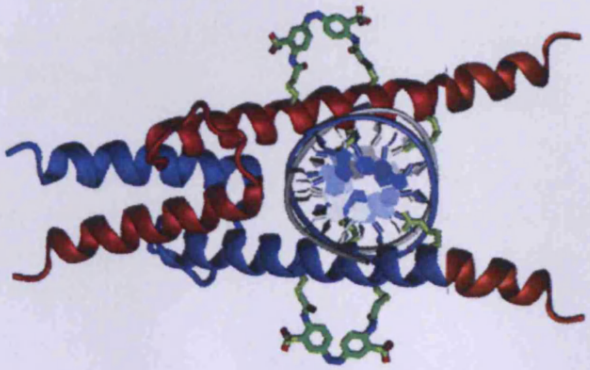

Figure 5.2: *Model of the TAT PhotomyoD protein. The bHLH domains are shown in red/blue and the N-terminal TAT domain in orange.*

Table 5.1: *Oligonucleotides used to create the pET TAT vector.*

Oligonucleotide	Sequence
TAT fwd	5'-CATGGCGTATGGCCGTAAAAAACGTCGTCAGCGTCGT CGTGGCCA-3'
TAT rev	5'-TATGGCCACGACGACGCTGACGACGTTTTTTACGGCC ATACG C-3'

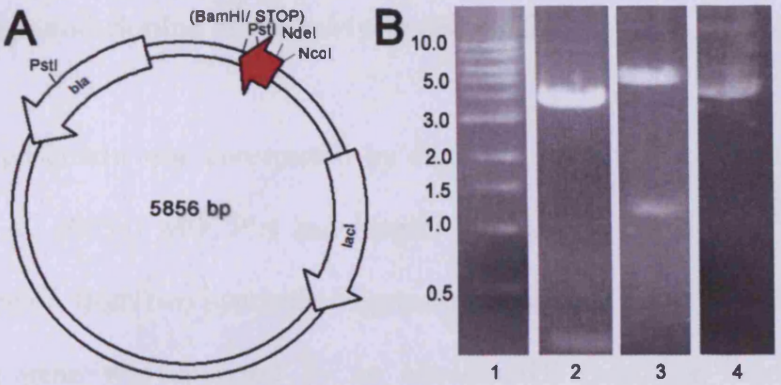

Figure 5.3: *Cloning of TAT PhotoMyoD. A) Vector map of TAT PhotoMyoD. The TAT PhotoMyoD open reading frame is shown in red. B) Ethidium bromide stained agarose gel of TAT PhotoMyoD. Lane 1: marker (fragment size is displayed in kbps), lane 2:* Nde*I and* Bam*HI MyoD pJGetita vector digest, lane 3:* Pst*I digest of the TAT PhotoMyoD vector and lane 4:* Bam*HI digest after site directed mutagenesis (the plasmid has remained uncut).*

Table 5.2: *Primer sequences for site directed mutagenesis. The two mismatching nucleotides are underlined.*

Oligonucleotide	Sequence
TAT PhotoMyoD fwd	5'-CAGGCTCTGCTGCGGTAACCGGCTGCTAACAAAG-3'
TAT PhotoMyoD rev	5'-CTTTGTTAGCAGCCGGTTACCGCAGCAGAGCCTG-3'

5.3.2.2 Design and cloning of PhotoMyoD penetratin

PhotoMyoD penetratin was constructed by digesting the photoMyoD pJGetita vector (Guerrero *et al.* 2005a) with *Pst*I and *Bam*HI followed by the assembly of the new *C*-terminal region from two synthetic oligonucleotides (Table 5.3). The correct size of the resulting gene was analysed by an *NdeI/Bam*HI restriction digest and DNA sequencing (Figure 5.4).

An alternative construct encoding for an additional *N*-terminal His-tag was obtained by subcloning photoMyoD penetratin into a pET19b vector using the *Nde*I and *Bam*HI restriction sites, verified by restriction digest and DNA sequencing (Figure 5.5).

Table 5.3: *Oligonucleotide sequences used in the construction of the penetratin insert.*

Oligonucleotide	Sequence
penetratin fwd	5'GGCTCTGCTGCGGGGCCGTCAGATTAAAATTTGGTTT CAGAACCGTCGTATGAAATGGAAAAAATAATAAG-3'
penetratin rev	5'GATCCTTATTATTTTTTCCATTTCATACGACGGTTCTG AAACCAATTTTAATCTGACGGCCCCGCAGCAGAGCCTG CA-3'

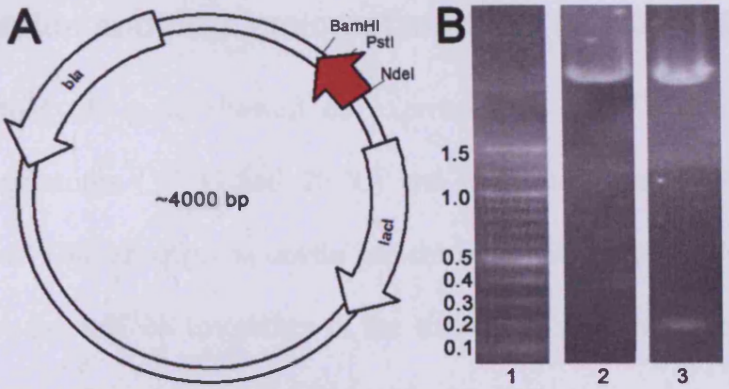

Figure 5.4: *Cloning of photoMyoD penetratin. A) Plasmid map of photoMyoD penetratin in a pJGetita vector. B) Ethidium bromide stained agarose gel of photoMyoD penetratin. Lane 1: Marker (fragment size is displayed in kbp), lane 2:* BamHI/PstI *digest of photoMyoD/pJGetita and lane 3:* NdeI/BamHI *digest of photoMyoD penetratin/pJGetita.*

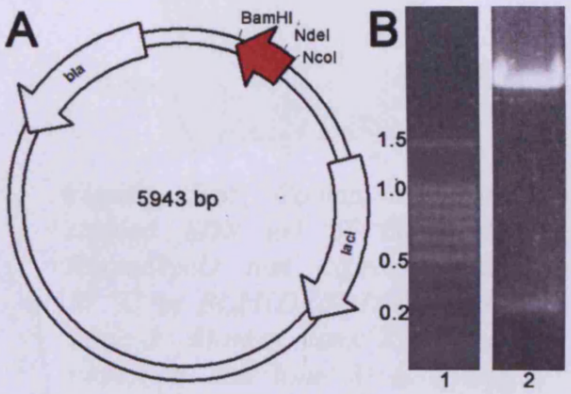

Figure 5.5: *Cloning of His-tagged PhotoMyoD penetratin. A) Vector map. Shown in red is the His-PhotoMyoD penetratin open reading frame. B) Ethidium bromide stained agarose gel of the* NdeI/BamHI *digested plasmid. Lane 1: marker (fragment size is annotated in kbp) and lane 2: digested vector.*

5.3.3 Expression and purification of modified PhotoMyoD

The TAT PhotoMyoD gene showed no expression in 2× YT medium. Different incubation temperatures (37 °C and 20 °C) and cells were tested (BL21(DE3) and BL21(DE3)pLysS) but attempts to obtain protein were unsuccessful (Figure 5.6). This could be due to the mRNA instability of the transcript or degradation of the protein itself; subsequent work was focused on PhotoMyoD penetratin.

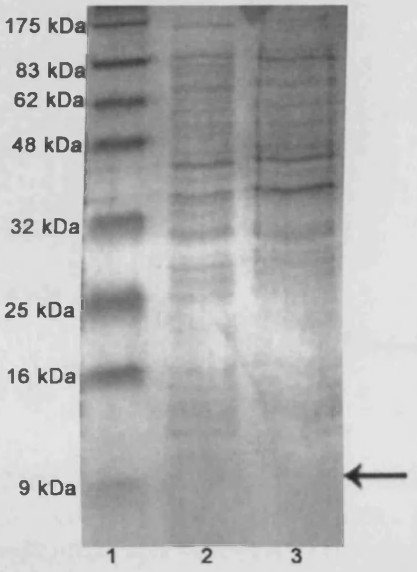

Figure 5.6: *Coomassie blue stained SDS gel of the TAT PhotoMyoD test expression at 37 °C in BL21(DE3)pLysS cells. Lane 1: Marker, lane 2: before induction and lane 3: 6 hours after induction. The arrow indicates the absence of the band that would correspond to the size of TAT PhotoMyoD.*

The expression of the gene coding for PhotoMyoD penetratin in 2× YT medium was successful. Purification by CM cation exchange chromatography, as previously described (Guerrero *et al.* 2005a), resulted in substantial loss of protein since most of the desired protein was in the flow-through of the column (Figure 5.7). Therefore size exclusion chromatography was used instead and resulted in almost pure protein. The

remaining impurities were removed by passing the solution through a 30,000 Da cut off membrane (Figure 5.8). The pure protein was then analysed by mass spectrometry. The obtained value (m/z = 9,153) was in agreement with the expected mass of 9,085 g mol^{-1} for the protein without the initiating methionine (Figure 5.9).

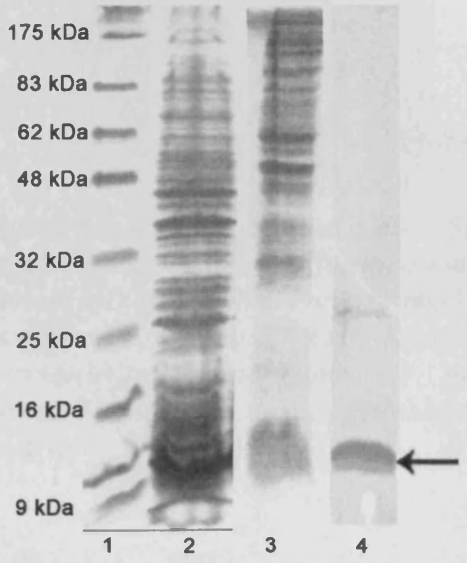

Figure 5.7: *Coomassie blue stained SDS gel of the expression and purification of PhotoMyoD penetratin. Lane 1: molecular weight marker, lane 2: crude PhotoMyoD penetratin, lane 3: flow through of the CM column chromatography and lane 4: eluted protein from the CM column. The arrow indicates PhotoMyoD penetratin.*

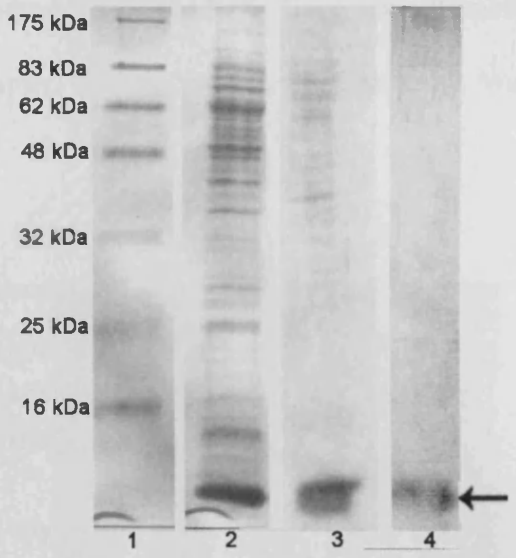

Figure 5.8: *Coomassie blue stained SDS gel of the expression and purification of PhotoMyoD penetratin. Lane 1: marker, lane 2: crude, lane 3: after size exclusion chromatography and lane 4: pure protein. The arrow indicates PhotoMyoD penetratin.*

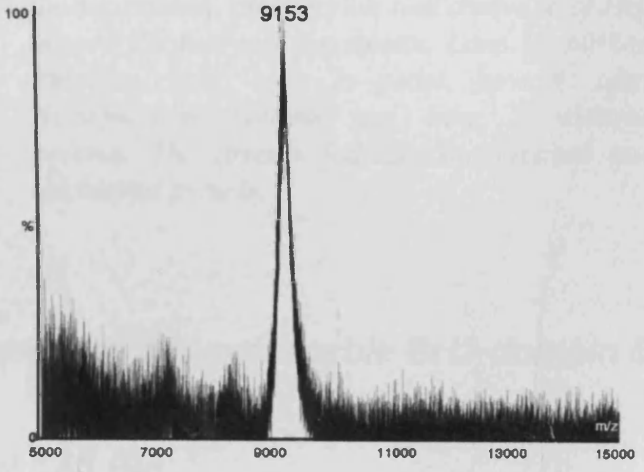

Figure 5.9: *MALDI-TOF mass spectrum of PhotoMyoD penetratin.*

Expression of the His-tagged protein resulted in the formation of inclusion bodies. The protein was extracted from the pellet with 6 M guanidinium hydrochloride, purified by Ni-sepharose chromatography and dialysed into 2 M urea containing buffer; it was then digested with enterokinase under the same conditions to remove the tag. The digest

resulted in the formation of side product. Since the alternative purification by size, exclusion chromatography was successful, this strategy was not followed further (Figure 5.10).

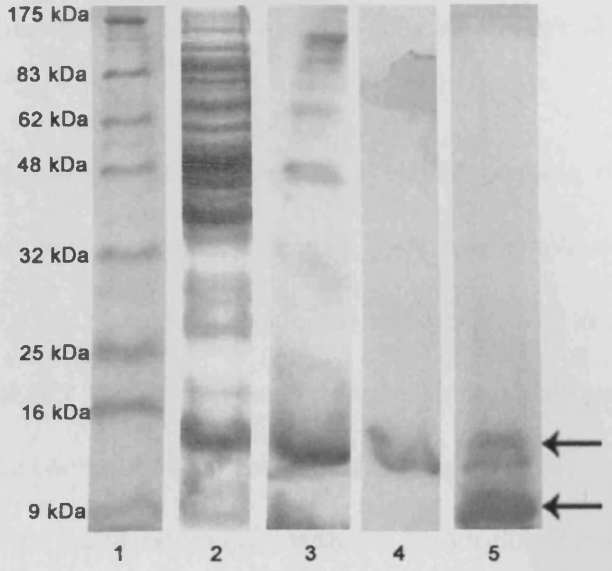

Figure 5.10: *Coomassie blue stained SDS gel of the expression, purification and cleavage of His-tagged PhotoMyoD penetratin. Lane 1: marker, lane 2: crude, lane 3: pellet, lane 4: after Ni-Sepharose column and lane 5: cleaved protein. The arrows indicate the cleaved and uncleaved protein.*

5.4 Development of cell permeable BH3-domain BPN

5.4.1 Design of TAT Bid

Development of the BH3-domain based BPNs is discussed in detail in Chapter 3. For future *in vivo* experiments it was decided that the addition of a cell membrane penetrating domain to the $Bid_{91\text{-}111}^{i+4}$ peptide since it shows a strong difference between the K_D values in the two states and a similarly constrained stapled Bid peptide has already been applied successfully in *in vivo* experiments (Walensky *et al.* 2004). The

11-amino acid protein transduction domain from the human immunodeficiency virus TAT protein was chosen since it has been proven to successfully deliver peptides and even biologically active proteins, up to 120 kDa into mammalian cells (Frankel *et al.* 1988; Schwarze *et al.* 1999; Becker-Hapak *et al.* 2001; Joliot *et al.* 2004). An additional glycine residue was introduced to act as a spacer between the two domains.

Solid phase synthesis of the peptide repeatedly failed because of the length of the peptide (33 amino acids) so expression in *E. coli* was employed as an alternative strategy. Due to the small size, this peptide had to be expressed as a fusion protein and cleaved off subsequently with cyanogen bromide, since small peptides are prone to degradation inside the bacterial cell. Ketosteroid isomerase (KSI) was used as the fusion partner because it forms inclusion bodies inside the bacterial cell from which the desired protein can be easily obtained. The cleavage resulted in an additional homoserine lactone at the *C*-terminus. The mechanism of the CnBr mediated cleavage is depicted in Scheme 5.1.

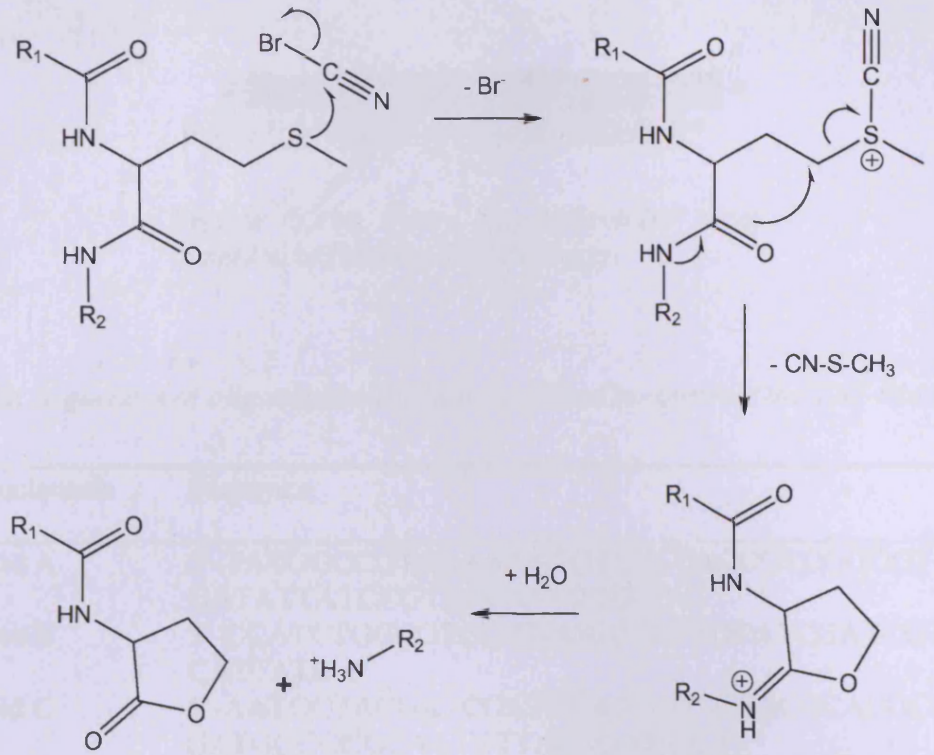

Scheme 5.1: *Mechanism of the cyanogen bromide mediated Met-X cleavage.*

The designed TAT Bid peptide has the following sequence (TAT is shown in red and $Bid_{91\text{-}111}^{i+4}$ in blue):

YGRKKRRQRRRGDIIRNIARHLACVGDCIDRSIZ Z = Homoserine

5.4.2 Cloning of TAT Bid

The unique *Alw*NI restriction site of the pET31b vector was utilised to introduce the DNA sequence encoding for TAT Bid by means of phosphorylating, annealing and ligating four overlapping oligonucleotides into the vector (Figure 5.11) (Table 5.4). The presence of the insert was confirmed by *Nde*I/*Xho*I restriction digest and DNA sequencing (Figure 5.12).

Figure 5.11: *Four oligonucleotides were annealed to form the TAT Bid insert.*

Table 5.4: *Sequences of oligonucleotides that were used to construct the TAT Bid insert.*

Oligonucleotide	Sequence
TAT Bid A	5'-TATGGCCGTAAAAAACGTCGCCAGCGTCGGCGTGGC GATATTATCCGTAACATTGCGCG-3'
TAT Bid B	5'-CCATCTGGCGTGCGTGGGCGATTGCATCGATCGTAG CATTATG-3'
TAT Bid C	5'-AATGCTACGATCGATGCAATCGCCCACGCACGCCA GATGGCGCGCAATGTTACGGATAA-3'
TAT Bid D	5'-TATCGCCACGGCCACGCTGGCGACGTTTTTTACGGC CATACAT-3'

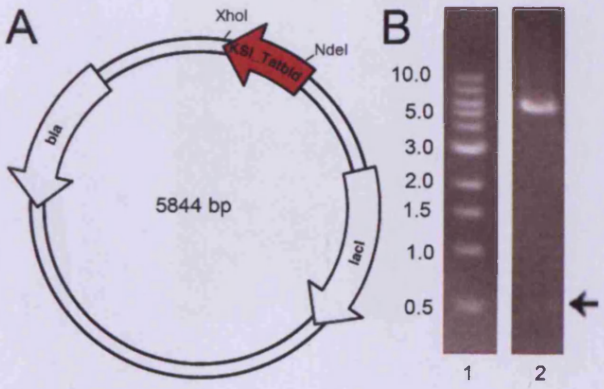

Figure 5.12: *A) Map of the pET31b TAT Bid vector B) Restriction digest of the pET31b TAT Bid vector. Lane 1: DNA ladder (fragment size is indicated in kilobasepairs), lane 2:* NdeI/XhoI *digest of the vector (the small 500bp fragment is indicated by an arrow).*

5.4.3 Expression and purification of TAT Bid KSI fusion protein

After expression in BL21(DE3)pLysS cells and 2× YT medium, the insoluble protein was obtained in the pellet (Figure 5.13). The pure fusion protein was cleaved with cyanogen bromide (Figure 5.13) and the solvent removed by evaporation. The free peptide was extracted from the pellet with PBS buffer. Subsequent purification by reverse phase HPLC yielded pure product. Analysis by MALDI-TOF mass spectroscopy confirmed that the peptide was of the expected mass. The addition of base resulted in opening of the lactone ring and the peptide was cross-linked and purified by HPLC (Figure 5.14).

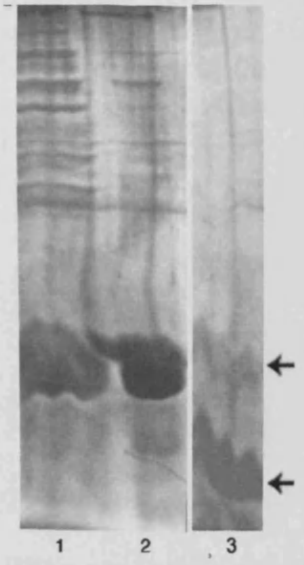

Figure 5.13: *SDS polyacrylamide gel of TAT Bid KSI after staining with Coomassie blue. Lanes are 1: crude TAT Bid KSI; 2: pellet; 3: after cyanogen bromide cleavage. The arrows indicate the protein before and after cleavage.*

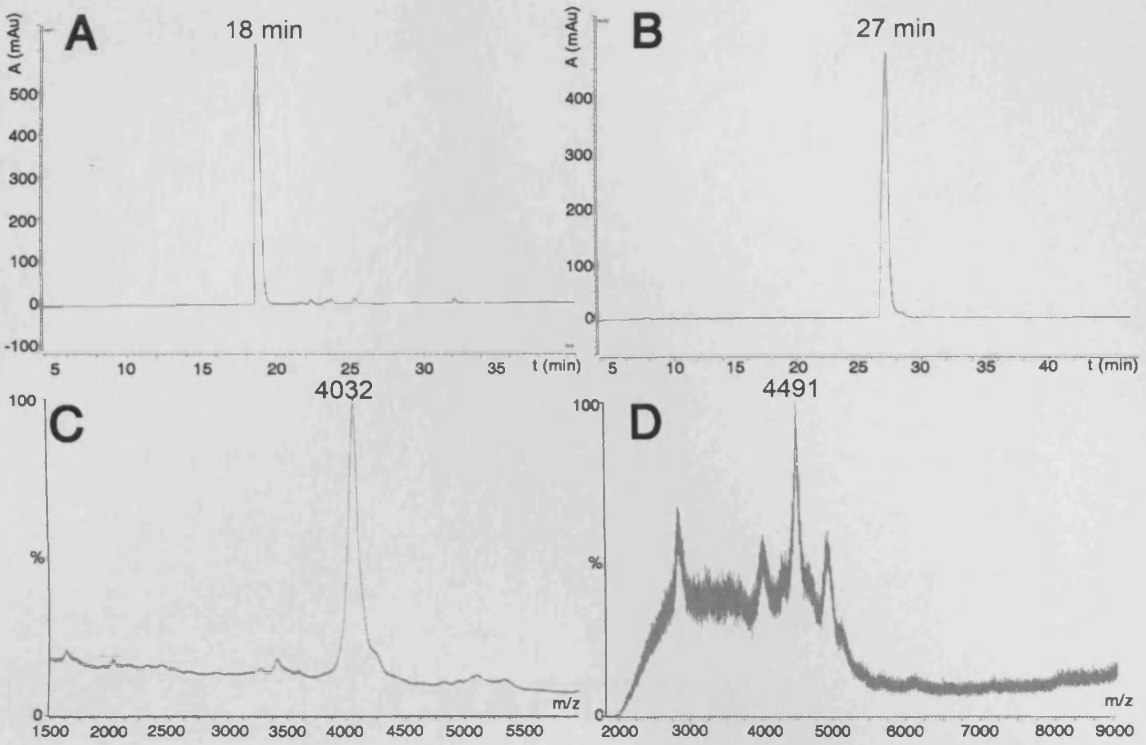

Figure 5.14: *A) HPLC trace of purified TAT Bid (Gradient: 0-100% over 60min), B) HPLC trace of purified cross-linked TAT Bid (Gradient: 0-60% over 60 min) C) Mass spectrum of purified TAT Bid (lactone form, expected molecular weight is 4,036 g mol^{-1}) D) Mass spectrum of cross-linked TAT Bid (homoserine form, expected molecular weight is 4,486 g/mol).*

5.5 Conclusion

A BPN based on $Bid_{91\text{-}111}^{i+4}$ with an additional TAT domain to promote cell permeability was expressed, purified and cross-linked. It could be utilised to establish whether the BH3-domain based BPNs can induce apoptotic processes inside a cell upon an optical signal. A number of different DNA constructs have been generated, tested and an expression and purification strategy to obtain a modified PhotoMyoD protein with a *C*-terminal penetratin domain has been established. This is likely to facilitate future *in vivo* experiments and applications, such as demonstrating the light-activated induction of myogenesis by PhotoMyoD.

CHAPTER 6:

General conclusions and future work

Biomolecular interactions are crucial to all living processes. Interference with these interactions in a specific and reversible manner is therefore of great scientific and therapeutic interest. The work described in this thesis demonstrates the utilisation of a photochromic compound bound to two cysteine residues within an α-helix motif to control protein-protein and protein-RNA interactions. Three sets of cysteine spacings, *i, i+4, i, i+7* and *i, i+11*, for which helix stabilisation is possible, were investigated. Isomerisation of the azobenzene moiety from the *trans*- to the *cis*-configuration was accomplished by irradiating the samples with 360 nm light. UV/Vis absorption spectroscopy was used to follow the thermal relaxation. Structural characterisation of *cis* and *trans* isomers of the BPNs was carried out using CD spectroscopy. As anticipated, either induced helicity or helix disruption was observed upon irradiation depending on the cysteine spacing (although in some cases the effect was only pronounced in the presence of TFE as a cosolvent). Furthermore, the helix-destabilised conformations resembled those of their uncross-linked counterparts or showed less helical content. This indicates that these photoswitches can be employed to activate the stable conformation upon a signal. In order to investigate the effect of photocontrol on the RNA- and protein-binding properties of the BPNs, fluorescence based assays were performed. Protein binding experiments with Bcl-x_L and BH3-based peptides, revealed a difference in affinity of up to one order of magnitude for the lid and dad states. The interaction in the stabilised states was highly specific as determined from binding experiments with HDM2. The Rev-based peptides successfully disrupted the target interaction in the activated state by competitive inhibition, as determined from the disruption assays. NMR spectroscopic experiments demonstrated that $Bak_{72\text{-}87}^{i+11}$ in the dark-adapted form targets the same cleft on Bcl-x_L as the wild-type Bak peptide.

$Bid_{91\text{-}111}{}^{i+4}$ and PhotoMyoD were modified with a peptide transduction motif since the cell membrane impermeability of these compounds is a major obstacle for application of these photoresponsive systems *in vivo*. The new, potentially membrane crossing, peptides could serve as therapeutic agents and be employed to investigate whether these photoresponsive miniature proteins can actually induce apoptosis and activate transcription respectively. Furthermore, they could be developed into useful tools for cell biology. An *in vitro* cytochrome C release assay would also be a good initial experiment to prove that the BH3-derived peptides in their activated states induce apoptotic processes.

The Rev-based BPNs can be characterised further, it would be of interest to obtain the K_D values for the different states by using a gel-shift assay. The specificity for the RRE target could be investigated and the effect of the RNA target sequence on the conformation of the BPNs and the half-life of the *cis*-state determined. Additional studies to complement this work and gain a deeper understanding of the photoregulation of protein-protein and protein-nucleic acid binding would be beneficial. Since the *trans* to *cis* isomerisation obtained for this azobenzene system was never close to 100%, it would be interesting to test alternative strategies to increase the quantum yield of isomerisation, for example, by using lasers for the switching reactions. Alternatively, isosteric derivatives could be characterised to obtain data which would be similar to the expected data for the *cis*-form of azobenzene cross-linked peptides. A *cis*-stilbene version of the linker is currently being synthesised in our laboratory for this purpose. Lasers could also be used in overcoming a major obstacle related to these azobenzene-based systems by avoiding the use of harmful UV radiation and using red light instead in a two-photon excitation approach. Furthermore, it would be interesting to obtain a

crystal or NMR solution structure of one of these systems to study the accurate conformation and binding mode of the biophotonic nanoswitches, giving new insights into the understanding of biomolecular interactions and to the development of other BPNs. The NMR structure of the $Bak_{72\text{-}87}^{i+11}$/Bcl-$x_L$ complex is therefore being solved at the moment. Since the CD spectrum has been demonstrated to be strongly influenced, at least in some cases, by the azobenzene moiety, alternative strategies such as IR or NMR spectroscopy could be used to determine the helical content in future studies to obtain more accurate results. The deviation of the reversion rates observed for UV and CD measurements should be studied in more detail; this could be accomplished by monitoring both processes simultaneously by NMR spectroscopy. Bcl-x_L contains a deep binding pocket relative to most protein binding interfaces. It would therefore be useful to apply the approach described here to more challenging protein-protein interaction interfaces such as the interaction between CBP KIX and the kinase-inducible activation domain of CREB in order to underpin the general applicability of this strategy. Since only a fraction of biomolecular interactions rely on α-helices, a similar approach could be applied to control other elements of secondary structure such as 3_{10}-helices. Finally, it would be interesting to extent the approach described in this work for protein-protein and protein-nucleic acid interactions to the photocontrol of other functions such as the modulation of the catalytic activity of enzymes.

Appendix

Amino acid sequence of Bcl-x_L (1-212)

M G H H H H H H H H H H S S G H I D D D D K H M S Q S N R E
L V V D F L S Y K L S Q K G Y S W S Q F S D V E E N R T E A
P E G T E S E M E T P S A I N G N P S W H L A D S P A V N G
A T G H S S S L D A R E V I P M A A V K Q A L R E A G D E F
E L R Y R R A F S D L T S Q L H I T P G T A Y Q S F E Q V V
N E L F R D G V N W G R I V A F F S F G G A L C V E S V D K
E M Q V L V S R I A A W M A T Y L N D H L E P W I Q E N G G
W D T F V E L Y G N N

Amino acid sequence of Bcl-x_L (Δ45-84)

M S Q S N R E L V V D F L S Y K L S Q K G Y S W S Q F S D V
E E N R T E A P E G T E S E A V K Q A L R E A G D E F E L R
Y R R A F S D L T S Q L H I T P G T A Y Q S F E Q V V N E L
F R D G V N W G R I V A F F S F G G A L C V E S V D K E M Q
V L V S R I A A W M A T Y L N D H L E P W I Q E N G G W D T
F V E L Y G N N A A A E S R K G Q E R L E H H H H H H L E H
H H H H H

Amino acid sequence of PhotoMyoD penetratin

M A D R R K A A T C R E R R R L C K V N E A F E T L K R S T
S S N P N Q R L P K V E I L R N A T R Y I E G L Q A L L R G
R Q I K I W F Q N R R M K W K K

Amino acid sequence of His-tagged PhotoMyoD penetratin

M G H H H H H P H H H S S G H I D D D D K H M A D R R K A A
T C R E R R R L C K V N E A F E T L K R S T S S N P N Q R L
P K V E I L R N A T R Y I E G L Q A L L R G R Q I K I W F Q
N R R M K W K K

Amino acid sequence of the TAT Bid KSI fusion protein

M H T P E H I T A V V Q R F V A A L N A G D L D G I V A L F
A D D A T V E D P V G S E P R S G T A A I R E F Y A N S L K
L P L A V E L T Q E V R A V A N E A A F A F T V S F E Y Q G
R K T V V A P I D H F R F N G A G K V V S I R A L F G E K N
I H A C Q M Y G R K K R R Q R R R G D I I R N I A R H L A C
V G D C I D R S I M L L E H H H H H H

Table A1: *Isotope-weighted chemical shift changes (ω) in the HSQC spectrum of Bcl-x_L on addition of dark-adapted $Bak_{72\text{-}87}^{i+11}$ (Kneissl* et al. *2008) (ω_{max} correspond to the strongest change in chemical shift observed in the spectra).*

Residue	δ (ppm)		ω	ω/ω_{max}
	Free Bcl-x_L	Bcl-x_L/$Bak_{72\text{-}87}^{i+11}$		
3Gln	8.42	8.44	0.056	0.059
	121.56	121.82		
5Asn	8.66	8.70	0.131	0.140
	120.92	121.55		
6Arg	8.06	8.07	0.205	0.218
	121.00	119.98		
7Glu	7.97	7.99	0.052	0.056
	117.17	117.42		
8Leu	7.80	7.87	0.116	0.124
	119.58	120.03		
9Val	7.75	7.62	0.139	0.148
	117.14	117.28		
10Val	8.34	8.40	0.114	0.121
	116.67	117.14		
11Asp	8.06	8.07	0.152	0.162
	121.00	120.24		
12Phe	8.32	8.23	0.166	0.177
	119.61	120.29		
13Leu	8.90	8.91	0.016	0.017
	116.22	116.27		
14Ser	8.51	8.55	0.051	0.054
	113.62	113.74		
15Tyr	8.26	8.31	0.082	0.087
	124.36	124.70		
17Leu	8.74	8.76	0.024	0.026
	117.94	117.85		
18Ser	8.39	8.43	0.041	0.043
	117.15	117.12		
19Gln	7.68	7.64	0.044	0.047
	122.24	122.17		

Residue	δ (ppm)		ω	ω/ω_{max}
	Free Bcl-x_L	Bcl-x_L/Bak_{72-87}^{i+11}		
20Lys	7.26	7.26	0.052	0.056
	115.84	116.10		
21Gly	7.61	7.58	0.040	0.043
	104.97	104.84		
22Tyr	7.89	7.83	0.065	0.069
	119.23	119.07		
23Ser	8.57	8.62	0.088	0.094
	114.76	114.44		
24Trp	9.03	9.08	0.077	0.082
	126.90	127.18		
24Trp(Nε)	10.07	10.10	0.029	0.031
	128.32	128.32		
25Ser	8.24	8.29	0.210	0.224
	111.53	110.51		
26Gln	7.47	7.47	0.043	0.046
	118.86	118.65		
27Phe	7.34	7.21	0.196	0.210
	115.91	115.14		
28Ser	7.32	7.15	0.199	0.212
	113.45	112.99		
29Asp	8.37	8.27	0.111	0.119
	122.11	122.39		
30Val	7.96	7.96	0.030	0.032
	118.68	118.53		
31Glu	8.51	8.54	0.062	0.067
	123.91	124.18		
32Glu	8.44	8.46	0.103	0.110
	121.56	122.07		
33Asn	8.50	8.52	0.039	0.042
	119.03	119.20		
34Arg	8.33	8.35	0.028	0.030
	121.48	121.56		
35Thr	8.28	8.29	0.023	0.025
	115.32	115.42		
36Glu	8.40	8.41	0.021	0.022
	122.52	122.61		

Residue	δ (ppm)		ω	ω/ω_{max}
	Free Bcl-x_L	Bcl-x_L/Bak_{72-87}^{i+11}		
37Ala	8.31	8.31	0.004	0.004
	125.62	125.63		
39Glu	8.63	8.64	0.028	0.030
	120.51	120.65		
40Gly	8.52	8.53	0.004	0.004
	109.70	109.72		
41Thr	8.25	8.21	0.043	0.045
	112.51	112.40		
42Glu	8.87	8.88	0.016	0.017
	122.61	122.66		
43Ser	8.49	8.46	0.040	0.043
	114.88	114.77		
44Glu	8.31	8.19	0.124	0.132
	122.47	122.57		
45Ala	8.22	8.18	0.068	0.073
	118.21	118.51		
46Val	7.55	7.50	0.073	0.078
	120.28	120.53		
47Lys	7.46	7.45	0.011	0.012
	117.36	117.32		
48Gln	8.17	8.17	0.020	0.021
	115.82	115.72		
49Ala	8.06	7.87	0.209	0.223
	121.00	121.42		
50Leu	8.51	8.48	0.052	0.056
	120.04	119.81		
51Arg	8.18	8.21	0.124	0.132
	118.28	117.67		
52Glu	7.91	8.00	0.108	0.115
	115.87	116.15		
53Ala	8.91	8.91	0.128	0.136
	122.68	123.32		
54Gly	9.19	9.23	0.252	0.269
	108.04	106.79		
55Asp	8.23	8.34	0.119	0.127
	122.21	122.24		

Residue	δ (ppm)		ω	ω/ω_{max}
	Free Bcl-x_L	Bcl-x_L/Bak_{72-87}^{i+11}		
56Glu	8.27	8.27	0.068	0.073
	120.30	119.96		
57Phe	8.65	9.07	0.660	0.704
	120.73	123.27		
58Glu	8.15	8.40	0.517	0.551
	116.19	113.92		
59Leu	7.53	7.58	0.221	0.236
	116.69	117.76		
60Arg	8.04	8.06	0.037	0.039
	117.00	117.16		
61Tyr	7.96	7.96	0.051	0.055
	118.68	118.42		
62Arg	7.42	7.11	0.334	0.356
	119.33	119.95		
63Arg	8.55	8.69	0.239	0.255
	118.61	117.62		
64Ala	7.80	7.79	0.034	0.036
	119.83	119.68		
65Phe	8.56	7.70	0.885	0.944
	115.49	114.47		
66Ser	8.04	8.24	0.297	0.317
	117.56	116.46		
67Asp	8.38	8.47	0.140	0.150
	120.47	120.99		
68Leu	8.06	7.88	0.216	0.231
	121.00	120.43		
69Thr	8.45	9.00	0.551	0.588
	109.51	109.97		
70Ser	7.80	7.76	0.092	0.098
	116.33	115.92		
71Gln	7.92	7.75	0.177	0.189
	118.67	118.42		
72Leu	7.75	7.58	0.253	0.269
	119.23	118.29		
73His	8.26	8.22	0.064	0.068
	119.14	119.38		

Residue	δ (ppm)		ω	ω/ω_{max}
	Free Bcl-x_L	Bcl-x_L/Bak_{72-87}^{i+11}		
74Ile	8.39	8.72	0.334	0.356
	121.70	122.11		
79Ala	7.91	7.84	0.077	0.082
	125.13	124.92		
80Tyr	8.56	8.84	0.320	0.341
	119.80	120.53		
81Gln	8.17	8.51	0.333	0.355
	114.75	114.68		
82Ser	7.63	7.38	0.401	0.427
	112.35	113.91		
84Glu	8.56	8.65	0.143	0.152
	119.80	119.25		
85Gln	7.59	7.62	0.295	0.315
	114.46	115.93		
86Val	7.15	7.17	0.027	0.029
	118.01	117.89		
87Val	7.96	7.97	0.099	0.106
	118.68	119.17		
88Asn	8.45	8.22	0.349	0.372
	116.88	115.60		
89Glu	7.37	7.36	0.053	0.057
	118.26	118.00		
90Leu	7.61	7.63	0.046	0.050
	120.42	120.21		
91Phe	7.03	6.86	0.938	1.000
	112.65	108.03		
92Arg	7.24	7.31	0.115	0.122
	123.35	122.90		
93Asp	8.44	8.71	0.460	0.491
	118.13	116.27		
94Gly	7.58	7.22	0.412	0.440
	108.25	107.25		
95Val	8.27	8.27	0.003	0.003
	120.30	120.31		
96Asn	6.39	6.25	0.250	0.267
	115.49	114.45		

Residue	δ (ppm)		ω	ω/ω_{max}
	Free Bcl-x_L	Bcl-x_L/Bak_{72-87}^{i+11}		
97Trp	8.56	8.62	0.383	0.409
	118.03	116.13		
97Trp(Nε)	10.27	10.37	0.095	0.102
	128.16	128.30		
98Gly	8.61	8.64	0.090	0.096
	105.98	106.39		
99Arg	8.23	8.12	0.132	0.141
	121.11	121.49		
100Ile	7.61	7.81	0.202	0.215
	120.42	120.68		
101Val	8.38	8.35	0.060	0.064
	120.47	120.73		
102Ala	7.71	7.72	0.151	0.161
	121.13	120.38		
103Phe	8.11	8.23	0.145	0.154
	119.09	119.53		
104Phe	8.06	8.06	0.192	0.204
	121.00	120.04		
105Ser	8.51	8.41	0.283	0.301
	114.16	112.84		
106Phe	9.14	8.67	0.482	0.514
	123.93	123.48		
107Gly	8.06	8.05	0.029	0.031
	105.86	106.01		
108Gly	8.90	8.91	0.121	0.129
	107.14	106.54		
109Ala	8.34	8.20	0.157	0.167
	124.30	123.94		
110Leu	8.31	8.38	0.133	0.142
	118.68	118.12		
111Cys	8.22	8.22	0.027	0.029
	118.81	118.68		
112Val	8.22	8.10	0.130	0.139
	118.18	118.43		
113Glu	8.18	8.25	0.122	0.130
	118.82	118.32		

Residue	δ (ppm)		ω	ω/ω_{max}
	Free Bcl-x_L	Bcl-x_L/Bak_{72-87}^{i+11}		
114Ser	7.77	7.84	0.077	0.082
	113.28	113.24		
115Val	7.42	7.25	0.167	0.178
	120.57	120.53		
116Asp	8.39	8.36	0.156	0.166
	121.70	122.46		
117Lys	7.69	7.84	0.175	0.186
	115.57	115.17		
118Glu	7.96	7.85	0.180	0.192
	113.64	112.92		
119Met	8.53	8.68	0.178	0.190
	118.71	118.25		
120Gln	8.80	8.92	0.138	0.147
	119.09	118.79		
121Val	7.96	7.94	0.200	0.213
	116.68	117.67		
122Leu	7.89	8.00	0.303	0.324
	116.86	115.46		
123Val	7.61	7.45	0.257	0.275
	120.42	119.41		
124Ser	8.40	8.57	0.212	0.226
	110.51	109.91		
125Arg	6.69	6.54	0.328	0.350
	122.80	121.34		
126Ile	8.12	8.12	0.091	0.098
	118.12	117.66		
127Ala	7.75	7.69	0.080	0.085
	119.23	118.98		
128Ala	7.61	7.34	0.281	0.300
	120.42	120.16		
129Trp	9.07	8.92	0.143	0.152
	121.08	121.06		
129Trp(Nε)	10.12	9.90	0.332	0.354
	126.02	127.27		
130Met	9.01	9.04	0.093	0.099
	116.88	117.32		

Residue	δ (ppm)		ω	ω/ω_{max}
	Free Bcl-x_L	Bcl-x_L/Bak_{72-87}^{i+11}		
131Ala	8.27	8.28	0.031	0.034
	120.30	120.16		
132Thr	8.63	8.74	0.377	0.402
	116.37	114.56		
133Tyr	8.50	8.90	0.410	0.437
	123.38	122.96		
134Leu	8.83	8.71	0.124	0.133
	118.92	118.71		
135Asn	8.43	8.48	0.221	0.236
	116.96	115.88		
136Asp	8.56	8.55	0.048	0.051
	115.27	115.03		
137His	8.12	7.92	0.316	0.337
	111.82	113.04		
138Leu	7.29	7.22	0.106	0.113
	116.75	117.16		
139Glu	8.72	8.68	0.056	0.060
	121.36	121.18		
141Trp	7.19	7.12	0.089	0.095
	117.69	117.40		
141Trp(Nε)	9.52	9.54	0.040	0.043
	128.84	129.00		
142Ile	8.52	8.56	0.044	0.047
	122.08	122.18		
144Glu	7.62	7.54	0.131	0.140
	118.82	118.29		
145Asn	7.20	7.15	0.082	0.087
	116.36	116.71		
146Gly	7.45	7.46	0.020	0.021
	104.61	104.65		
147Gly	8.58	8.58	0.009	0.010
	108.16	108.21		
148Trp	8.71	8.70	0.016	0.017
	117.95	118.01		
148Trp(Nε)	10.60	10.61	0.010	0.011
	128.67	128.63		

Residue	δ (ppm)		ω	ω/ω_{max}
	Free Bcl-x_L	Bcl-x_L/Bak_{72-87}^{i+11}		
149Asp	8.90	8.87	0.043	0.046
	117.59	117.41		
150Thr	7.62	7.58	0.055	0.059
	116.58	116.43		
151Phe	6.63	6.60	0.055	0.059
	121.96	121.76		
152Val	7.89	7.78	0.162	0.173
	117.03	116.40		
153Glu	7.51	7.43	0.098	0.105
	119.68	119.38		
154Leu	7.68	7.65	0.180	0.192
	116.88	117.77		
155Tyr	8.17	8.20	0.103	0.110
	114.75	115.25		
156Gly	8.13	8.28	0.183	0.195
	108.04	108.53		
157Asn	8.45	8.58	0.180	0.192
	117.99	117.36		
158Asn	8.45	8.61	0.160	0.171
	118.68	118.73		
159Ala	8.22	8.15	0.068	0.073
	122.96	122.97		
160Ala	8.16	8.27	0.118	0.126
	121.24	121.09		
161Ala	8.05	8.00	0.053	0.057
	121.93	121.84		
162Glu	8.33	8.31	0.032	0.035
	118.02	118.12		
163Ser	8.12	8.14	0.031	0.033
	114.73	114.85		
164Arg	8.05	8.04	0.046	0.049
	121.37	121.59		
165Lys	8.11	8.14	0.053	0.057
	120.51	120.71		
166Gly	8.44	8.45	0.021	0.022
	108.85	108.92		

Residue	δ (ppm)		ω	ω/ω_{max}
	Free Bcl-x_L	Bcl-x_L/Bak_{72-87}^{i+11}		
167Gln	8.14	8.14	0.010	0.010
	119.14	119.19		
168Glu	8.53	8.55	0.030	0.032
	121.03	121.15		
169Arg	8.28	8.29	0.053	0.056
	120.56	120.82		
170Leu	8.19	8.10	0.126	0.134
	122.27	122.67		

References

Adams, J. M. and S. Cory (2007). "The Bcl-2 apoptotic switch in cancer development and therapy." Oncogene **26**(9): 1324-37.

Aemissegger, A. and D. Hilvert (2007). "Synthesis and application of an azobenzene amino acid as a light-switchable turn element in polypeptides." Nat Protoc **2**(1): 161-7.

Allemann, R. K. (1999). DNA: "Protein Interaction Thermodynamics". Encyclopedia of Molecular Biology. T. E. Creighton. New York, NY, Wiley: 745-55.

Andersen, M. H., D. Schrama, P. Thor Straten and J. C. Becker (2006). "Cytotoxic T cells." J Invest Dermatol **126**(1): 32-41.

Arya, S. K., C. Guo, S. F. Josephs and F. Wong-Staal (1985). "Trans-activator gene of human T-lymphotropic virus type III (HTLV-III)." Science **229**(4708): 69-73.

Ashkenazi, A. and V. M. Dixit (1998). "Death receptors: signaling and modulation." Science **281**: 1305-8.

Bahadur, R. P., P. Chakrabarti, F. Rodier and J. Janin (2004). "A dissection of specific and non-specific protein-protein interfaces." J Mol Biol **336**(4): 943-55.

Bahadur, R. P., M. Zacharias and J. Janin (2008). "Dissecting protein-RNA recognition sites." Nucleic Acids Res **36**(8): 2705-16.

Bakhshi, A., J. P. Jensen, P. Goldman, J. J. Wright, O. W. McBride, A. L. Epstein and S. J. Korsmeyer (1985). "Cloning the chromosomal breakpoint of t(14;18) human lymphomas: clustering around JH on chromosome 14 and near a transcriptional unit on 18." Cell **41**(3): 899-906.

Banghart, M., K. Borges, E. Isacoff, D. Trauner and R. H. Kramer (2004). "Light-activated ion channels for remote control of neuronal firing." Nat Neurosci **7**(12): 1381-6.

Barlow, D. J. and J. M. Thornton (1988). "Helix geometry in proteins." J Mol Biol **201**: 601-19.

Bartel, D. P., M. L. Zapp, M. R. Green and J. W. Szostak (1991). "HIV-1 Rev regulation involves recognition of non-Watson-Crick base pairs in viral RNA." Cell **67**(3): 529-36.

Battiste, J. L., H. Mao, N. S. Rao, R. Tan, D. R. Muhandiram, L. E. Kay, A. D. Frankel and J. R. Williamson (1996). "Alpha helix-RNA major groove recognition in an HIV-1 rev peptide-RRE RNA complex." Science **273**(5281): 1547-51.

Becker-Hapak, M., S. S. McAllister and S. F. Dowdy (2001). "TAT-mediated protein transduction into mammalian cells." Methods **24**(3): 247-56.

Behrendt, R., C. Renner, M. Schenk, F. Wang, J. Wachtveitl, D. Oesterhelt and L. Moroder (1999a). "Photomodulation of the Conformation of Cyclic Peptides with Azobenzene Moieties in the Peptide Backbone." Angew Chem Int Ed Engl **38**(18): 2771-4.

Behrendt, R., M. Schenk, H. J. Musiol and L. Moroder (1999b). "Photomodulation of conformational states. Synthesis of cyclic peptides with backbone-azobenzene moieties." J Pept Sci **5**(11): 519-29.

Bernal, F., A. F. Tyler, S. J. Korsmeyer, L. D. Walensky and G. L. Verdine (2007). "Reactivation of the p53 tumor suppressor pathway by a stapled p53 peptide." J Am Chem Soc **129**(9): 2456-7.

Bewley, C. A., A. M. Gronenborn and G. M. Clore (1998). "Minor groove-binding architectural proteins: structure, function, and DNA recognition." Annu Rev Biophys Biomol Struct **27**: 105-31.

Bohnlein, E., J. Berger and J. Hauber (1991). "Functional mapping of the human immunodeficiency virus type 1 Rev RNA binding domain: new insights into the domain structure of Rev and Rex." J Virol **65**(12): 7051-5.

Boise, L. H., M. Gonzalez-Garcia, C. E. Postema, L. Ding, T. Lindsten, L. A. Turka, X. Mao, G. Nunez and C. B. Thompson (1993). "bcl-x, a bcl-2-related gene that functions as a dominant regulator of apoptotic cell death." Cell **74**(4): 597-608.

Boulegue, C., M. Loweneck, C. Renner and L. Moroder (2007). "Redox potential of azobenzene as an amino acid residue in peptides." Chembiochem **8**(6): 591-4.

Boyd, J. M., G. J. Gallo, B. Elangovan, A. B. Houghton, S. Malstrom, B. J. Avery, R. G. Ebb, T. Subramanian, T. Chittenden, R. J. Lutz and et al. (1995). "Bik, a novel death-inducing protein shares a distinct sequence motif with Bcl-2 family proteins and interacts with viral and cellular survival-promoting proteins." Oncogene **11**(9): 1921-8.

Bratton, S. B., M. MacFarlane, K. Cain and G. M. Cohen (2000). "Protein complexes activate distinct caspase cascades in death receptor and stress-induced apoptosis." Exp Cell Res **256**(1): 27-33.

Burns, D. C., F. Zhang and G. A. Woolley (2007). "Synthesis of 3,3'-bis(sulfonato)-4,4'-bis(chloroacetamido)azobenzene and cysteine cross-linking for photo-control of protein conformation and activity." Nat Protoc **2**(2): 251-8.

Caamano, A. M., M. E. Vazquez, J. Martinez-Costas, L. Castedo and J. L. Mascarenas (2000). "A Light-Modulated Sequence-Specific DNA-Binding Peptide " Angew Chem Int Ed Engl **39**(17): 3104-7.

Cabezas, E. and A. C. Satterthwait (1999). "The Hydrogen Bond Mimic Approach: Solid-Phase Synthesis of a Peptide Stabilized as an a-Helix with a Hydrazone Link." J Am Chem Soc **121**(16): 3862-75.

Cai, J., D. C. Wallace, B. Zhivotovsky and D. P. Jones (2000). "Separation of cytochrome c-dependent caspase activation from thiol-disulfide redox change in cells lacking mitochondrial DNA." Free Radic Biol Med **29**(3-4): 334-42.

Cao, G., W. Pei, H. Ge, Q. Liang, Y. Luo, F. R. Sharp, A. Lu, R. Ran, S. H. Graham and J. Chen (2002). "In Vivo Delivery of a Bcl-xL Fusion Protein Containing the TAT Protein Transduction Domain Protects against Ischemic Brain Injury and Neuronal Apoptosis." J Neurosci **22**(13): 5423-31.

Cattani-Scholz, A., C. Renner, D. Oesterhelt and L. Moroder (2001). "Photoresponsive dendritic azobenzene peptides." Chembiochem **2**(7-8): 542-9.

Chakrabartty, A., T. Kortemme and R. L. Baldwin (1994). "Helix propensities of the amino acids measured in alanine-based peptides without helix-stabilizing side-chain interactions." Protein Sci **3**(5): 843-52.

Chin, J. W. and A. Schepartz (2001). "Design and Evolution of a Miniature Bcl-2 Binding Protein." Angew Chem Int Ed Engl **40**(20): 3806-9.

Chipuk, J. E., L. Bouchier-Hayes, T. Kuwana, D. D. Newmeyer and D. R. Green (2005). "PUMA couples the nuclear and cytoplasmic proapoptotic function of p53." Science **309**(5741): 1732-5.

Chittenden, T., E. A. Harrington, R. O'Connor, C. Flemington, R. J. Lutz, G. I. Evan and B. C. Guild (1995). "Induction of apoptosis by the Bcl-2 homologue Bak." Nature **374**(6524): 733-6.

Chou, P. Y. and G. D. Fasman (1978). "Empirical predictions of protein conformation." Annu Rev Biochem **47**: 251-76.

Clackson, T. and J. A. Wells (1995). "A hot spot of binding energy in a hormone-receptor interface." Science **267**(5196): 383-6.

Cleary, M. L., S. D. Smith and J. Sklar (1986). "Cloning and structural analysis of cDNAs for bcl-2 and a hybrid bcl-2/immunoglobulin transcript resulting from the t(14;18) translocation." Cell **47**(1): 19-28.

Cook, K. S., G. J. Fisk, J. Hauber, N. Usman, T. J. Daly and J. R. Rusche (1991). "Characterization of HIV-1 REV protein: binding stoichiometry and minimal RNA substrate." Nucleic Acids Res **19**(7): 1577-83.

Cory, S., D. C. Huang and J. M. Adams (2003). "The Bcl-2 family: roles in cell survival and oncogenesis." Oncogene **22**(53): 8590-607.

Crecca, C. R. and A. E. Roitberg (2006). "Theoretical study of the isomerization mechanism of azobenzene and disubstituted azobenzene derivatives." J Phys Chem A **110**(26): 8188-203.

Creighton, T. E. (1993). Proteins: "Structures and Molecular Properties". New York, W. H. Freeman and Company.

Cureton, C. H. (2003). "Understanding Acyl Chymotrypsin Vibrational Spectra Using Molecular Modelling." School of Biosciences University of Birmingham PhD thesis.

Cusick, M. E., N. Klitgord, M. Vidal and D. E. Hill (2005). "Interactome: gateway into systems biology." Hum Mol Genet **14 Spec No. 2**: R171-81.

Dall'Acqua, W., E. R. Goldman, E. Eisenstein and R. A. Mariuzza (1996). "A mutational analysis of the binding of two different proteins to the same antibody." Biochemistry **35**(30): 9667-76.

Daly, T. J., K. S. Cook, G. S. Gray, T. E. Maione and J. R. Rusche (1989). "Specific binding of HIV-1 recombinant Rev protein to the Rev-responsive element in vitro." Nature **342**(6251): 816-9.

Daly, T. J., R. C. Doten, P. Rennert, M. Auer, H. Jaksche, A. Donner, G. Fisk and J. R. Rusche (1993). "Biochemical characterization of binding of multiple HIV-1 Rev monomeric proteins to the Rev responsive element." Biochemistry **32**(39): 10497-505.

Davies, D. R. (1964). "A Correlation between Amino Acid Composition and Protein Structure." J Mol Biol **9**: 605-9.

Dayton, E. T., D. A. Konings, S. Y. Lim, R. K. Hsu, L. Butini, G. Pantaleo and A. I. Dayton (1993). "The RRE of human immunodeficiency virus type 1 contributes to cell-type-specific viral tropism." J Virol **67**(5): 2871-8.

Delaglio, F., S. Grzesiek, G. W. Vuister, G. Zhu, J. Pfeifer and A. Bax (1995). "NMRPipe: a multidimensional spectral processing system based on UNIX pipes." J Biomol NMR **6**(3): 277-93.

Derossi, D., S. Calvet, A. Trembleau, A. Brunissen, G. Chassaing and A. Prochiantz (1996). "Cell internalization of the third helix of the Antennapedia homeodomain is receptor-independent." J Biol Chem **271**(30): 18188-93.

Derossi, D., A. H. Joliot, G. Chassaing and A. Prochiantz (1994). "The third helix of the Antennapedia homeodomain translocates through biological membranes." J Biol Chem **269**(14): 10444-50.

Desrosiers, D. C. and Z. Y. Peng (2005). "A binding free energy hot spot in the ankyrin repeat protein GABPbeta mediated protein-protein interaction." J Mol Biol **354**(2): 375-84.

Dime, D. S. (2002). "Methanethiosulfonate Reagants: Application to the Study of Protein Topology and Ion Channels", Toronto Research Chemicals Inc, available at www.trc-canada.com.

Doig, A. J., A. Chakrabartty, T. M. Klingler and R. L. Baldwin (1994). "Determination of free energies of N-capping in alpha-helices by modification of the Lifson-Roig helix-coil therapy to include N- and C-capping." Biochemistry **33**(11): 3396-403.

Dom, G., C. Shaw-Jackson, C. Matis, O. Bouffioux, J. J. Picard, A. Prochiantz, M. P. Mingeot-Leclercq, R. Brasseur and R. Rezsohazy (2003). "Cellular uptake of Antennapedia Penetratin peptides is a two-step process in which phase transfer precedes a tryptophan-dependent translocation." Nucleic Acids Res **31**(2): 556-61.

Dong, S. L., M. Loweneck, T. E. Schrader, W. J. Schreier, W. Zinth, L. Moroder and C. Renner (2006). "A photocontrolled beta-hairpin peptide." Chemistry **12**(4): 1114-20.

Draper, D. E. (1995). "Protein-RNA recognition." Annu Rev Biochem **64**: 593-620.

Egleton, R. D. and T. P. Davis (1997). "Bioavailability and transport of peptides and peptide drugs into the brain." Peptides **18**(9): 1431-9.

Eisenberg, D., W. Wilcox, S. M. Eshita, P. M. Pryciak, S. P. Ho and W. F. DeGrado (1986). "The design, synthesis, and crystallization of an alpha-helical peptide." Proteins **1**(1): 16-22.

Ellenberger, T. E., C. J. Brandl, K. Struhl and S. C. Harrison (1992). "The GCN4 basic region leucine zipper binds DNA as a dimer of uninterrupted alpha helices: crystal structure of the protein-DNA complex." Cell **71**(7): 1223-37.

Ernst, J. T., J. Becerril, H. S. Park, H. Yin and A. D. Hamilton (2003). "Design and application of an alpha-helix-mimetic scaffold based on an oligoamide-foldamer strategy: antagonism of the Bak BH3/Bcl-xL complex." Angew Chem Int Ed Engl **42**(5): 535-9.

Feng, W., S. Huang, H. Wu and M. Zhang (2007). "Molecular basis of Bcl-xL's target recognition versatility revealed by the structure of Bcl-xL in complex with the BH3 domain of Beclin-1." J Mol Biol **372**(1): 223-35.

Fields, S. and O. Song (1989). "A novel genetic system to detect protein-protein interactions." Nature **340**(6230): 245-6.

Finnegan, N. M., J. F. Curtin, G. Prevost, B. Morgan and T. G. Cotter (2001). "Induction of apoptosis in prostate carcinoma cells by BH3 peptides which inhibit Bak/Bcl-2 interactions." Br J Cancer **85**(1): 115-21.

Flint, D. G., J. R. Kumita, O. S. Smart and G. A. Woolley (2002). "Using an azobenzene cross-linker to either increase or decrease peptide helix content upon trans-to-cis photoisomerization." Chem Biol **9**(3): 391-7.

Frankel, A. D. and C. O. Pabo (1988). "Cellular uptake of the tat protein from human immunodeficiency virus." Cell **55**(6): 1189-93.

Friesen, W. J. and M. K. Darby (2001). "Specific RNA binding by a single C2H2 zinc finger." J Biol Chem **276**(3): 1968-73.

Fujimoto, K., M. Kajino and M. Inouye (2007). "Development of a Series of Cross-Linking Agents that Effectively Stabilize alpha-Helical Structures in Various Short Peptides." Chemistry **14**(3): 857-63.

Fujimoto, K., N. Oimoto, K. Katsuno and M. Inouye (2004). "Effective stabilisation of alpha-helical structures in short peptides with acetylenic cross-linking agents." Chem Commun (11): 1280-1.

Futaki, S. (2002). "Arginine-rich peptides: potential for intracellular delivery of macromolecules and the mystery of the translocation mechanisms." Int J Pharm **245**(1-2): 1-7.

Futaki, S., I. Nakase, A. Tadokoro, T. Takeuchi and A. T. Jones (2007). "Arginine-rich peptides and their internalization mechanisms." Biochem Soc Trans **35**(Pt 4): 784-7.

Gelderblom, H. R., E. H. Hausmann, M. Ozel, G. Pauli and M. A. Koch (1987). "Fine structure of human immunodeficiency virus (HIV) and immunolocalization of structural proteins." Virology **156**(1): 171-6.

Gelderblom, H. R., M. Ozel and G. Pauli (1989). "Morphogenesis and morphology of HIV. Structure-function relations." Arch Virol **106**(1-2): 1-13.

Gemperli, A. C., S. E. Rutledge, A. Maranda and A. Schepartz (2005). "Paralog-selective ligands for bcl-2 proteins." J Am Chem Soc **127**(6): 1596-7.

Ghadiri, M. R. and C. Choi (1990). "Secondary structure nucleation in peptides. Transition metal ion stabilized alpha-helices." J Am Chem Soc **112**(4): 1630.

Gibson, L., S. P. Holmgreen, D. C. Huang, O. Bernard, N. G. Copeland, N. A. Jenkins, G. R. Sutherland, E. Baker, J. M. Adams and S. Cory (1996). "bcl-w, a novel member of the bcl-2 family, promotes cell survival." Oncogene **13**(4): 665-75.

Gorostiza, P. and E. Y. Isacoff (2008). "Optical switches for remote and noninvasive control of cell signaling." Science **322**(5900): 395-9.

Gorostiza, P., M. Volgraf, R. Numano, S. Szobota, D. Trauner and E. Y. Isacoff (2007). "Mechanisms of photoswitch conjugation and light activation of an ionotropic glutamate receptor." Proc Natl Acad Sci USA **104**(26): 10865-70.

Grad, J. M., X. R. Zeng and L. H. Boise (2000). "Regulation of Bcl-xL: a little bit of this and a little bit of STAT." Curr Opin Oncol **12**(6): 543-9.

Grate, D. and C. Wilson (1997). "Role REVersal: understanding how RRE RNA binds its peptide ligand." Structure **5**(1): 7-11.

Green, D. R. and J. C. Reed (1998). "Mitochondria and apoptosis." Science **281**(5381): 1309-12.

Greenhalgh, D. G. (1998). "The role of apoptosis in wound healing." Int J Biochem Cell Biol **30**(9): 1019-30.

Guerrero, L., O. S. Smart, C. J. Weston, D. C. Burns, G. A. Woolley and R. K. Allemann (2005a). "Photochemical regulation of DNA-binding specificity of MyoD." Angew Chem Int Ed Engl **44**(47): 7778-82.

Guerrero, L., O. S. Smart, G. A. Woolley and R. K. Allemann (2005b). "Photocontrol of DNA Binding Specificity of a Miniature Engrailed Homeodomain." J Am Chem Soc **127**(44): 15624-9.

Guzzo, A. V. (1965). "The influence of amino-acid sequence on protein structure." Biophys J **5**(6): 809-22.

Halgren, T. A. (1996). "Merck molecular forcefield. I. Basis, Form, Scope, Parametrization and Performance." J Comp Chem **17**: 490-519.

Hall, H., E. J. Williams, S. E. Moore, F. S. Walsh, A. Prochiantz and P. Doherty (1996). "Inhibition of FGF-stimulated phosphatidylinositol hydrolysis and neurite outgrowth by a cell-membrane permeable phosphopeptide." Curr Biol **6**(5): 580-7.

Hard, T. and T. Lundback (1996). "Thermodynamics of sequence-specific protein-DNA interactions." Biophys Chem **62**(1-3): 121-39.

Heaphy, S., C. Dingwall, I. Ernberg, M. J. Gait, S. M. Green, J. Karn, A. D. Lowe, M. Singh and M. A. Skinner (1990). "HIV-1 regulator of virion expression (Rev) protein binds to an RNA stem-loop structure located within the Rev response element region." Cell **60**(4): 685-93.

Heus, H. A. and A. Pardi (1991). "Structural features that give rise to the unusual stability of RNA hairpins containing GNRA loops." Science **253**(5016): 191-4.

Heyduk, T., Y. Ma, H. Tang and R. H. Ebright (1996). "Fluorescence anisotropy: rapid, quantitative assay for protein-DNA and protein-protein interaction." Methods Enzymol **274**: 492-503.

Hockenbery, D. M., Z. N. Oltvai, X. M. Yin, C. L. Milliman and S. J. Korsmeyer (1993). "Bcl-2 functions in an antioxidant pathway to prevent apoptosis." Cell **75**(2): 241-51.

Holland, S. M., N. Ahmad, R. K. Maitra, P. Wingfield and S. Venkatesan (1990). "Human immunodeficiency virus rev protein recognizes a target sequence in rev-responsive element RNA within the context of RNA secondary structure." J Virol **64**(12): 5966-75.

Hope, T. J. (1999). "The ins and outs of HIV Rev." Arch Biochem Biophys **365**(2): 186-91.

Hope, T. J., B. L. Bond, D. McDonald, N. P. Klein and T. G. Parslow (1991). "Effector domains of human immunodeficiency virus type 1 Rev and human T-cell leukemia virus type I Rex are functionally interchangeable and share an essential peptide motif." J Virol **65**(11): 6001-7.

Horvitz, H. R. (1999). "Genetic control of programmed cell death in the nematode Caenorhabditis elegans." Cancer Res **59**(7 Suppl): 1701s-6s.

Humphrey, W., A. Dalke and K. Schulten (1996). "VMD - Visual Molecular Dynamics." J Molec Graphics **14**: 33-8.

Jackson, D. V., S. K. King, J. Chmielewski, S. Singh and P. G. Schultz (1991). "General Approach to the Synthesis of Short α-helical Peptides." J Am Chem Soc **113**: 9391-2.

Jiang, X. and X. Wang (2004). "Cytochrome C-mediated apoptosis." Annu Rev Biochem **73**: 87-106.

Joerger, A. C. and A. R. Fersht (2007). "Structure-function-rescue: the diverse nature of common p53 cancer mutants." Oncogene **26**(15): 2226-42.

Johnsson, K., R. K. Allemann, H. Widmer and S. A. Benner (1993). "Synthesis, structure and activity of artificial, rationally designed catalytic polypeptides." Nature **365**(6446): 530-2.

Joliot, A., C. Pernelle, H. Deagostini-Bazin and A. Prochiantz (1991). "Antennapedia homeobox peptide regulates neural morphogenesis." Proc Natl Acad Sci USA **88**(5): 1864-8.

Joliot, A. and A. Prochiantz (2004). "Transduction peptides: from technology to physiology." Nat Cell Biol **6**(3): 189-96.

Jones, S., P. van Heyningen, H. M. Berman and J. M. Thornton (1999). "Protein-DNA interactions: A structural analysis." J Mol Biol **287**(5): 877-96.

Juo, Z., T. Chiu, P. Leiberman, Baikalov I, A. Berk and R. Dickerson (1996). "How proteins recognize the TATA box." J Mol Biol **261**(2): 239-54.

Jurt, S., A. Aemissegger, P. Guntert, O. Zerbe and D. Hilvert (2006). "A photoswitchable miniprotein based on the sequence of avian pancreatic polypeptide." Angew Chem Int Ed Engl **45**(38): 6297-300.

Kallenbach, N. R. and E. J. Spek (1998). "Modified amino acids as probes of helix stability." Methods Enzymol **295**: 26-41.

Kaufmann, T., L. Tai, P. G. Ekert, D. C. Huang, F. Norris, R. K. Lindemann, R. W. Johnstone, V. M. Dixit and A. Strasser (2007). "The BH3-only protein bid is

dispensable for DNA damage- and replicative stress-induced apoptosis or cell-cycle arrest." Cell **129**(2): 423-33.

Kenyon, G. L. and T. W. Bruice (1977). "Novel sulfhydryl reagents." Methods Enzymol **47**: 407-30.

Kerr, J. F., A. H. Wyllie and A. R. Currie (1972). "Apoptosis: a basic biological phenomenon with wide-ranging implications in tissue kinetics." Br J Cancer **26**(4): 239-57.

Kischkel, F. C., S. Hellbardt, I. Behrmann, M. Germer, M. Pawlita, P. H. Krammer and M. E. Peter (1995). "Cytotoxicity-dependent APO-1 (Fas/CD95)-associated proteins form a death-inducing signaling complex (DISC) with the receptor." Embo J **14**(22): 5579-88.

Kjems, J., M. Brown, D. D. Chang and P. A. Sharp (1991). "Structural analysis of the interaction between the human immunodeficiency virus Rev protein and the Rev response element." Proc Natl Acad Sci USA **88**(3): 683-7.

Kjems, J., B. J. Calnan, A. D. Frankel and P. A. Sharp (1992). "Specific binding of a basic peptide from HIV-1 Rev." EMBO J **11**(3): 1119-29.

Kline, M. P., S. V. Rajkumar, M. M. Timm, T. K. Kimlinger, J. L. Haug, J. A. Lust, P. R. Greipp and S. Kumar (2007). "ABT-737, an inhibitor of Bcl-2 family proteins, is a potent inducer of apoptosis in multiple myeloma cells." Leukemia **21**(7): 1549-60.

Kneissl, S., E. J. Loveridge, C. Williams, M. P. Crump and R. K. Allemann (2008). "Photocontrollable peptide-based switches target the anti-apoptotic protein Bcl-xL." Chembiochem **9**(18): 3046-54.

Kocer, A., M. Walko, W. Meijberg and B. L. Feringa (2005). "A light-actuated nanovalve derived from a channel protein." Science **309**(5735): 755-8.

Kong D, Park EJ, Stephen AG, Calvani M, Cardellina JH, Monks A, Fisher RJ, Shoemaker RH, Melillo G. (2005) "Echinomycin, a small-molecule inhibitor of hypoxia-inducible factor-1 DNA-binding activity" Cancer Res. 1;65(19):9047-55.

Kritzer, J. A., R. Zutshi, M. Cheah, F. A. Ran, R. Webman, T. M. Wongjirad and A. Schepartz (2006). "Miniature protein inhibitors of the p53-hDM2 interaction." Chembiochem **7**(1): 29-31.

Kumagai, I., T. Takahashi, K. Hamasaki, A. Ueno and H. Mihara (2000). "Construction of HIV Rev peptides containing peptide nucleic acid that bind HIV RRE IIB RNA." Bioorg Med Chem Lett **10**(4): 377-9.

Kumagai, I., T. Takahashi, K. Hamasaki, A. Ueno and H. Mihara (2001). "HIV Rev peptides conjugated with peptide nucleic acids and their efficient binding to RRE RNA." Bioorg Med Chem Lett **11**(9): 1169-72.

Kumita, J. R., D. G. Flint, G. A. Woolley and O. S. Smart (2003). "Achieving photo-control of protein conformation and activity: producing a photo-controlled leucine zipper." Faraday Discuss **122**: 89-103; discussion 71-90.

Kumita, J. R., O. S. Smart and G. A. Woolley (2000). "Photo-control of helix content in a short peptide." Proc Natl Acad Sci USA **97**(8): 3803-8.

Kusebauch, U., S. A. Cadamuro, H. J. Musiol, L. Moroder and C. Renner (2007). "Photocontrol of the collagen triple helix: synthesis and conformational characterization of bis-cysteinyl collagenous peptides with an azobenzene clamp." Chemistry **13**(10): 2966-73.

Kussie, P. H., S. Gorina, V. Marechal, B. Elenbaas, J. Moreau, A. J. Levine and N. P. Pavletich (1996). "Structure of the MDM2 oncoprotein bound to the p53 tumor suppressor transactivation domain." Science **274**(5289): 948-53.

Kutzki, O., H. S. Park, J. T. Ernst, B. P. Orner, H. Yin and A. D. Hamilton (2002). "Development of a potent Bcl-x(L) antagonist based on alpha-helix mimicry." J Am Chem Soc **124**(40): 11838-9.

Lassar, A. B., J. N. Buskin, D. Lockshon, R. L. Davis, S. Apone, S. D. Hauschka and H. Weintraub (1989). "Myod Is a Sequence-Specific DNA-Binding Protein Requiring a Region of *myc* Homology to Bind to the Muscle Creatine-Kinase Enhancer." Cell **58**(5): 823-31.

Lejeune, D., N. Delsaux, B. Charloteaux, A. Thomas and R. Brasseur (2005). "Protein-nucleic acid recognition: statistical analysis of atomic interactions and influence of DNA structure." Proteins **61**(2): 258-71.

Letai, A. (2005). "Pharmacological manipulation of Bcl-2 family members to control cell death." J Clin Invest **115**(10): 2648-55.

Levine, M., E. Hafen, R. L. Garber and W. J. Gehring (1983). "Spatial distribution of Antennapedia transcripts during Drosophila development." EMBO J **2**(11): 2037-46.

Li, H., H. Zhu, C. J. Xu and J. Yuan (1998). "Cleavage of BID by caspase 8 mediates the mitochondrial damage in the Fas pathway of apoptosis." Cell **94**(4): 491-501.

Lingel, A. and M. Sattler (2005). "Novel modes of protein-RNA recognition in the RNAi pathway." Curr Opin Struct Biol **15**(1): 107-15.

Liu, D. K., J.; Yu, C.; Zhang, Z.; Woolley, G. (1997). "Site-specific incorporation of photoisomerizable azobenzene groups into ribonuclease S" Bioorg Med Chem Lett **7**: 2677-80.

Liu, M., H. Asanuma and M. Komiyama (2006). "Azobenzene-tethered T7 promoter for efficient photoregulation of transcription." J Am Chem Soc **128**(3): 1009-15.

Lockshin, R. A. and J. Beaulaton (1974). "Programmed cell death." Life Sci **15**(9): 1549-65.

Lockshin, R. A. and C. M. Williams (1965). "Programmed Cell Death-I. Cytology of Degeneration in the Intersegmental Muscles of the Pernyi Silkmoth." J Insect Physiol **11**: 123-33.

Lopez, M. M., D. H. Chin, R. L. Baldwin and G. I. Makhatadze (2002). "The enthalpy of the alanine peptide helix measured by isothermal titration calorimetry using metal-binding to induce helix formation." Proc Natl Acad Sci USA **99**(3): 1298-302.

Lyu, P. C., J. C. Sherman, A. Chen and N. R. Kallenbach (1991). "Alpha-helix stabilization by natural and unnatural amino acids with alkyl side chains." Proc Natl Acad Sci USA **88**(12): 5317-20.

Ma, P. C. M., M. A. Rould, H. Weintraub and C. O. Pabo (1994). "Crystal structure of MyoD bHLH domain-DNA complex: Perspectives on DNA Recognition and Implications for Transcriptional Activation." Cell **77**: 451-9.

Majno, G. and I. Joris (1995). "Apoptosis, oncosis, and necrosis. An overview of cell death." Am J Pathol **146**(1): 3-15.

Maleki, S. J., C. A. Royer and B. K. Hurlburt (1997). "MyoD-E12 heterodimers and MyoD-MyoD homodimers are equally stable." Biochemistry **36**(22): 6762-7.

Malim, M. H., S. Bohnlein, J. Hauber and B. R. Cullen (1989). "Functional dissection of the HIV-1 Rev trans-activator derivation of a trans-dominant repressor of Rev function." Cell **58**(1): 205-14.

Malim, M. H. and B. R. Cullen (1991a). "HIV-1 structural gene expression requires the binding of multiple Rev monomers to the viral RRE: implications for HIV-1 latency." Cell **65**(2): 241-8.

Malim, M. H., D. F. McCarn, L. S. Tiley and B. R. Cullen (1991b). "Mutational definition of the human immunodeficiency virus type 1 Rev activation domain." J Virol **65**(8): 4248-54.

Malim, M. H., L. S. Tiley, D. F. McCarn, J. R. Rusche, J. Hauber and B. R. Cullen (1990). "HIV-1 structural gene expression requires binding of the Rev trans-activator to its RNA target sequence." Cell **60**(4): 675-83.

Mann, D. A., I. Mikaelian, R. W. Zemmel, S. M. Green, A. D. Lowe, T. Kimura, M. Singh, P. J. Butler, M. J. Gait and J. Karn (1994). "A molecular rheostat. Co-operative rev binding to stem I of the rev-response element modulates human immunodeficiency virus type-1 late gene expression." J Mol Biol **241**(2): 193-207.

Marqusee, S. and R. L. Baldwin (1987). "Helix stabilization by Glu- Lys+ salt bridges in short peptides of de novo design." Proc Natl Acad Sci USA **84**(24): 8898-902.

Martins, J. C., F. J. Van de Ven and F. A. Borremans (1995). "Determination of the three-dimensional solution structure of scyllatoxin by 1H nuclear magnetic resonance." J Mol Biol **253**(4): 590-603.

Mayne, L., S. W. Englander, R. Y. Qiu, J., Y. Gong, E. J. Spek and N. R. Kallenbach (1998). "Stabilizing Effect of a Multiple Salt Bridge in a Prenucleated Peptide." J Am Chem Soc **1220**(41): 10643-5.

McColl, D. J., C. D. Honchell and A. D. Frankel (1999). "Structure-based design of an RNA-binding zinc finger." Proc Natl Acad Sci USA **96**(17): 9521-6.

Meng, Y., W. Tang, Y. Dai, X. Wu, M. Liu, Q. Ji, M. Ji, K. Pienta, T. Lawrence and L. Xu (2008). "Natural BH3 mimetic (-)-gossypol chemosensitizes human prostate cancer via Bcl-xL inhibition accompanied by increase of Puma and Noxa." Mol Cancer Ther **7**(7): 2192-202.

Merrifield, R. B. (1963). "Solid Phase Peptide Synthesis. I. The Synthesis of a Tetrapeptide " J Am Chem Soc **85**: 2149-54.

Meyer, B. E. and M. H. Malim (1994). "The HIV-1 Rev trans-activator shuttles between the nucleus and the cytoplasm." Genes Dev **8**(13): 1538-47.

Mills, N. L., M. D. Daugherty, A. D. Frankel and R. K. Guy (2006). "An alpha-helical peptidomimetic inhibitor of the HIV-1 Rev-RRE interaction." J Am Chem Soc **128**(11): 3496-7.

Mishra, S. H., C. M. Shelley, D. J. Barrow, Jr., M. K. Darby and M. W. Germann (2006). "Solution structures and characterization of human immunodeficiency virus Rev responsive element IIB RNA targeting zinc finger proteins." Biopol **83**(4): 352-64.

Moehle, K., Z. Athanassiou, K. Patora, A. Davidson, G. Varani and J. A. Robinson (2007). "Design of beta-hairpin peptidomimetics that inhibit binding of alpha-helical HIV-1 Rev protein to the rev response element RNA." Angew Chem Int Ed Engl **46**(47): 9101-4.

Mohammad, R. M., A. S. Goustin, A. Aboukameel, B. Chen, S. Banerjee, G. Wang, Z. Nikolovska-Coleska, S. Wang and A. Al-Katib (2007). "Preclinical studies of TW-37, a new nonpeptidic small-molecule inhibitor of Bcl-2, in diffuse large cell lymphoma xenograft model reveal drug action on both Bcl-2 and Mcl-1." Clin Cancer Res **13**(7): 2226-35.

Moras, D. and A. Poterszman (1996). "Getting into the major groove. Protein-RNA interactions." Curr Biol **6**(5): 530-2.

Morris, M. C., J. Depollier, J. Mery, F. Heitz and G. Divita (2001). "A peptide carrier for the delivery of biologically active proteins into mammalian cells." Nat Biotechnol **19**(12): 1173-6.

Murre, C., P. S. McCaw and D. Baltimore (1989a). "A new DNA binding and dimerization motif in immunoglobulin enhancer binding, daughterless, MyoD, and myc proteins." Cell **56**(5): 777-83.

Murre, C., P. S. McCaw, H. Vaessin, M. Caudy, L. Y. Jan, Y. N. Jan, C. V. Cabrera, J. N. Buskin, S. D. Hauschka, A. B. Lassar and et al. (1989b). "Interactions between heterologous helix-loop-helix proteins generate complexes that bind specifically to a common DNA sequence." Cell **58**(3): 537-44.

Nakano, K. and K. H. Vousden (2001). "PUMA, a novel proapoptotic gene, is induced by p53." Mol Cell **7**(3): 683-94.

Neely, W. B. and C. F. Thompson (1959). "Kinetic study of dextransurase based on the Langmuir adsorption isotherm." Nature **184**: 64.

Nijhawan, D., N. Honarpour and X. Wang (2000). "Apoptosis in neural development and disease." Annu Rev Neurosci **23**: 73-87.

Nooren, I. M. and J. M. Thornton (2003). "Structural characterisation and functional significance of transient protein-protein interactions." J Mol Biol **325**(5): 991-1018.

Oda, E., R. Ohki, H. Murasawa, J. Nemoto, T. Shibue, T. Yamashita, T. Tokino, T. Taniguchi and N. Tanaka (2000). "Noxa, a BH3-only member of the Bcl-2 family and candidate mediator of p53-induced apoptosis." Science **288**(5468): 1053-8.

Oehlke, J., A. Scheller, B. Wiesner, E. Krause, M. Beyermann, E. Klauschenz, M. Melzig and M. Bienert (1998). "Cellular uptake of an alpha-helical amphipathic model peptide with the potential to deliver polar compounds into the cell interior non-endocytically." Biochim Biophys Acta **1414**(1-2): 127-39.

Olsen, H. S., A. W. Cochrane, P. J. Dillon, C. M. Nalin and C. A. Rosen (1990). "Interaction of the human immunodeficiency virus type 1 Rev protein with a structured region in env mRNA is dependent on multimer formation mediated through a basic stretch of amino acids." Genes Dev **4**(8): 1357-64.

Olson, E. N. (1990). "Myod Family - a Paradigm for Development - Comment." Genes Dev **4**(9): 1454-61.

Oltersdorf, T., S. W. Elmore, A. R. Shoemaker, R. C. Armstrong, D. J. Augeri, B. A. Belli, M. Bruncko, T. L. Deckwerth, J. Dinges, P. J. Hajduk, M. K. Joseph, S. Kitada, S. J. Korsmeyer, A. R. Kunzer, A. Letai, C. Li, M. J. Mitten, D. G. Nettesheim, S. Ng, P. M. Nimmer, J. M. O'Connor, A. Oleksijew, A. M. Petros, J. C. Reed, W. Shen, S. K. Tahir, C. B. Thompson, K. J. Tomaselli, B. Wang, M. D. Wendt, H. Zhang, S. W. Fesik and S. H. Rosenberg (2005). "An inhibitor of Bcl-2 family proteins induces regression of solid tumours." Nature **435**(7042): 677-81.

Opferman, J. T. and S. J. Korsmeyer (2003). "Apoptosis in the development and maintenance of the immune system." Nat Immunol **4**(5): 410-5.

Osapay, G. and J. W. Taylor (1992). "Multicyclic polypeptide model compounds. Synthesis and conformational properties of a highly α-helical uncosapeptide constrained by three side-chain to side-chain lactam bridges." J Am Chem Soc **114**(18): 6966-73.

Ozel, M., G. Pauli and H. R. Gelderblom (1988). "The organization of the envelope projections on the surface of HIV." Arch Virol **100**(3-4): 255-66.

Pabo, C. O. and L. Nekludova (2000). "Geometric analysis and comparison of protein-DNA interfaces: why is there no simple code for recognition?" J Mol Biol **301**(3): 597-624.

Pardo, J., A. Bosque, R. Brehm, R. Wallich, J. Naval, A. Mullbacher, A. Anel and M. M. Simon (2004). "Apoptotic pathways are selectively activated by granzyme A and/or granzyme B in CTL-mediated target cell lysis." J Cell Biol **167**(3): 457-68.

Park, C. M., M. Bruncko, J. Adickes, J. Bauch, H. Ding, A. Kunzer, K. C. Marsh, P. Nimmer, A. R. Shoemaker, X. Song, S. K. Tahir, C. Tse, X. Wang, M. D. Wendt, X. Yang, H. Zhang, S. W. Fesik, S. H. Rosenberg and S. W. Elmore (2008). "Discovery of an Orally Bioavailable Small Molecule Inhibitor of Prosurvival B-Cell Lymphoma 2 Proteins." J Med Chem **51** (21): 6902-15.

Pease, J. H., R. W. Storrs and D. E. Wemmer (1990). "Folding and activity of hybrid sequence, disulfide-stabilized peptides." Proc Natl Acad Sci USA **87**(15): 5643-7.

Perkins, A., A. W. Cochrane, S. M. Ruben and C. A. Rosen (1989). "Structural and functional characterization of the human immunodeficiency virus rev protein." J Acquir Immune Defic Syndr **2**(3): 256-63.

Peter, M. E. and P. H. Krammer (1998). "Mechanism of CD95 (APO-1/Fas)- mediated apoptosis." Curr Opin Immunol **10**: 545-51.

Petros, A. M., D. G. Nettesheim, Y. Wang, E. T. Olejniczak, R. P. Meadows, J. Mack, K. Swift, E. D. Matayoshi, H. Zhang, C. B. Thompson and S. W. Fesik (2000). "Rationale for Bcl-xL/Bad peptide complex formation from structure, mutagenesis, and biophysical studies." Protein Sci **9**(12): 2528-34.

Pollard, V. W. and M. H. Malim (1998). "The HIV-1 Rev protein." Annu Rev Microbiol **52**: 491-532.

Pooga, M., U. Soomets, M. Hallbrink, A. Valkna, K. Saar, K. Rezaei, U. Kahl, J. X. Hao, X. J. Xu, Z. Wiesenfeld-Hallin, T. Hokfelt, T. Bartfai and U. Langel (1998). "Cell penetrating PNA constructs regulate galanin receptor levels and modify pain transmission in vivo." Nat Biotechnol **16**(9): 857-61.

Presta, L. G. and G. D. Rose (1988). "Helix signals in proteins." Science **240**(4859): 1632-41.

Puthalakath, H., L. A. O'Reilly, P. Gunn, L. Lee, P. N. Kelly, N. D. Huntington, P. D. Hughes, E. M. Michalak, J. McKimm-Breschkin, N. Motoyama, T. Gotoh, S. Akira, P. Bouillet and A. Strasser (2007). "ER stress triggers apoptosis by activating BH3-only protein Bim." Cell **129**(7): 1337-49.

Rajashankar, K. R., S. Ramakumar, R. M. Jain and V. S. Chauhan (1995). "First Observation of an α-helix in α,ß-Dehydrooligopeptides: Crystal Structure of Boc-Val-ΔPhe-Ala-Leu-Gyl-OMe." J Am Chem Soc **117**: 10129-30.

Rau, H. (1990). "Photoisomerisation of azobenzenes." FL: pp 119.

Reichmann, D., O. Rahat, S. Albeck, R. Meged, O. Dym and G. Schreiber (2005). "The modular architecture of protein-protein binding interfaces." Proc Natl Acad Sci USA **102**(1): 57-62.

Reichmann, D., O. Rahat, M. Cohen, H. Neuvirth and G. Schreiber (2007). "The molecular architecture of protein-protein binding sites." Curr Opin Struct Biol **17**(1): 67-76.

Renehan, A. G., S. P. Bach and C. S. Potten (2001). "The relevance of apoptosis for cellular homeostasis and tumorigenesis in the intestine." Can J Gastroenterol **15**(3): 166-76.

Renner, C., R. Behrendt, N. Heim and L. Moroder (2002). "Photomodulation of conformational states. III. Water-soluble bis-cysteinyl-peptides with (4-aminomethyl) phenylazobenzoic acid as backbone constituent." Biopol **63**(6): 382-93.

Renner, C., R. Behrendt, S. Sporlein, J. Wachtveitl and L. Moroder (2000a). "Photomodulation of conformational states. I. Mono- and bicyclic peptides with (4-amino)phenylazobenzoic acid as backbone constituent." Biopol **54**(7): 489-500.

Renner, C., J. Cramer, R. Behrendt and L. Moroder (2000b). "Photomodulation of conformational states. II. Mono- and bicyclic peptides with (4-aminomethyl)phenylazobenzoic acid as backbone constituent." Biopol **54**(7): 501-14.

Renner, C., U. Kusebauch, M. Loweneck, A. G. Milbradt and L. Moroder (2005). "Azobenzene as photoresponsive conformational switch in cyclic peptides." J Pept Res **65**(1): 4-14.

Renner, C. and L. Moroder (2006). "Azobenzene as conformational switch in model peptides." Chembiochem **7**(6): 868-78.

Renwick, S. B., A. D. Critchley, C. J. Adams, S. M. Kelly, N. C. Price and P. G. Stockley (1995). "Probing the details of the HIV-1 Rev-Rev-responsive element

interaction: effects of modified nucleotides on protein affinity and conformational changes during complex formation." Biochem J **308 (Pt 2)**: 447-53.

Rich, T., R. L. Allen and A. H. Wyllie (2000). "Defying death after DNA damage." Nature **407**(6805): 777-83.

Richardson, J. S. and D. C. Richardson (1988). "Amino acid preferences for specific locations at the ends of alpha helices." Science **240**(4859): 1648-52.

Riedl, S. J. and G. S. Salvesen (2007). "The apoptosome: signalling platform of cell death." Nat Rev Mol Cell Biol **8**(5): 405-13.

Riedl, S. J. and Y. Shi (2004). "Molecular mechanisms of caspase regulation during apoptosis." Nat Rev Mol Cell Biol **5**(11): 897-907.

Robinson, J. A. (2008). "beta-Hairpin Peptidomimetics: Design, Structures and Biological Activities." Acc Chem Res **41** (10): 1278-88.

Sadowsky, J. D., M. A. Schmitt, H. S. Lee, N. Umezawa, S. Wang, Y. Tomita and S. H. Gellman (2005). "Chimeric (alpha/beta + alpha)-peptide ligands for the BH3-recognition cleft of Bcl-XL: critical role of the molecular scaffold in protein surface recognition." J Am Chem Soc **127**(34): 11966-8.

Salvesen, G. S. and S. J. Riedl (2008). "Caspase mechanisms." Adv Exp Med Biol **615**: 13-23.

Sambrook, J., E. F. Fritsch and T. Maniatis (1989). Molecular Cloning: A Laboratory Manual. New York, Cold Spring Harbor Laoratory Press.

Sattler, M., H. Liang, D. Nettesheim, R. P. Meadows, J. E. Harlan, M. Eberstadt, H. S. Yoon, S. B. Shuker, B. S. Chang, A. J. Minn, C. B. Thompson and S. W. Fesik (1997). "Structure of Bcl-xL-Bak peptide complex: recognition between regulators of apoptosis." Science **275**(5302): 983-6.

Satzger, H., Root, C., Braun, M. (2004). "Excited-State Dynamics of trans- and cis-Azobenzene after UV Excitation in the $\pi\pi^*$ Band" J. Phys. Chem. **108** (30): 6265–6271

Sawada, M., P. Hayes and S. Matsuyama (2003). "Cytoprotective membrane-permeable peptides designed from the Bax-binding domain of Ku70." Nat Cell Biol **5**(4): 352-7.

Scaffidi, C., I. Schmitz, J. Zha, S. J. Korsmeyer, P. H. Krammer and M. E. Peter (1999). "Differential modulation of apoptosis sensitivity in CD95 type I and type II cells." J Biol Chem **274**(32): 22532-8.

Schafmeister, C. E., J. Po and G. L. Verdine (2000). "An all-hydrocarbon cross-linking system for enhancing the helicity and metabolic stability of peptides." J Am Chem Soc **122**(24): 5891-2.

Scholtz, A. and R. L. Baldwin (1992). "The Mechanism of alpha-Helix Formation by Peptides." Annu Rev Biophysics and Biomolecular Structure **21**: 25-47.

Scholtz, J. M., S. Marqusee, R. L. Baldwin, E. J. York, J. M. Stewart, M. Santoro and D. W. Bolen (1991). "Calorimetric determination of the enthalpy change for the alpha-helix to coil transition of an alanine peptide in water." Proc Natl Acad Sci USA **88**(7): 2854-8.

Schulze, F. W., H. J. Petrick, H. K. Cammenga and H. Klinge (1977). "Thermodynamic Properties of Structural Analogs Benzo [C] Cinnoline, Trans-Azobenzene, and Cis-Azobenzene." Z Phys Chem Neue Fol **107**(1): 1-19.

Schutt, M., S. S. Krupka, A. G. Milbradt, S. Deindl, E. K. Sinner, D. Oesterhelt, C. Renner and L. Moroder (2003). "Photocontrol of cell adhesion processes: model studies with cyclic azobenzene-RGD peptides." Chem Biol **10**(6): 487-90.

Schwarze, S. R., A. Ho, A. Vocero-Akbani and S. F. Dowdy (1999). "In vivo protein transduction: delivery of a biologically active protein into the mouse." Science **285**(5433): 1569-72.

Shi, H. and P. B. Moore (2000). "The crystal structure of yeast phenylalanine tRNA at 1.93 A resolution: a classic structure revisited." RNA **6**(8): 1091-105.

Spolar, R. S. and M. T. Record, Jr. (1994). "Coupling of local folding to site-specific binding of proteins to DNA." Science **263**(5148): 777-84.

Storrs, R. W., D. Truckses and D. E. Wemmer (1992). "Helix propagation in trifluoroethanol solutions." Biopol **32**(12): 1695-702.

Strasser, A., L. O'Connor and V. M. Dixit (2000). "Apoptosis signaling." Annu Rev Biochem **69**: 217-45.

Studier, F. and B. Moffatt (1986). "Use of bacteriophage T7 RNA polymerase to direct selective high-level expression of cloned genes." J Mol Biol **189**(1): 113-30.

Stumpf, M. P., T. Thorne, E. de Silva, R. Stewart, H. J. An, M. Lappe and C. Wiuf (2008). "Estimating the size of the human interactome." Proc Natl Acad Sci USA **105**(19): 6959-64.

Susin, S. A., H. K. Lorenzo, N. Zamzami, I. Marzo, B. E. Snow, G. M. Brothers, J. Mangion, E. Jacotot, P. Costantini, M. Loeffler, N. Larochette, D. R. Goodlett, R. Aebersold, D. P. Siderovski, J. M. Penninger and G. Kroemer (1999). "Molecular characterization of mitochondrial apoptosis-inducing factor." Nature **397**(6718): 441-6.

Takahashi, T., K. Hamasaki, A. Ueno and H. Mihara (2001). "Construction of peptides with nucleobase amino acids: design and synthesis of the nucleobase-conjugated peptides derived from HIV-1 Rev and their binding properties to HIV-1 RRE RNA." Bioorg Med Chem **9**(4): 991-1000.

Takahashi, T., I. Kumagai, K. Hamasaki, A. Ueno and H. Mihara (1999). "Design of artificial pepetides that recognize the HIV RRE IIB RNA." Nucleic Acids Symp Ser (42): 271-2.

Tan, R., L. Chen, J. A. Buettner, D. Hudson and A. D. Frankel (1993). "RNA recognition by an isolated alpha helix." Cell **73**(5): 1031-40.

Tan, R. and A. D. Frankel (1994). "Costabilization of peptide and RNA structure in an HIV Rev peptide-RRE complex." Biochemistry **33**(48): 14579-85.

Tapscott, S. J., M. J. Thayer and H. Weintraub (1993). "Deficiency in rhabdomyosarcomas of a factor required for MyoD activity and myogenesis." Science **259**(5100): 1450-3.

Taylor, S. E., T. J. Rutherford and R. K. Allemann (2001). "Design, synthesis and characterisation of a peptide with oxaloacetate decarboxylase activity." Bioorg Med Chem Lett **11**(19): 2631-5.

Taylor, S. E., T. J. Rutherford and R. K. Allemann (2002). "Design of a folded, conformationally stable oxaloacetate decarboxylase." Journal of the Chemical Society-Perkin Transactions **2**: 751-5.

Thornberry, N. A. and Y. Lazebnik (1998). "Caspases: Enemies within." Science **281**: 1312-16.

Tiley, L. S., M. H. Malim, H. K. Tewary, P. G. Stockley and B. R. Cullen (1992). "Identification of a high-affinity RNA-binding site for the human immunodeficiency virus type 1 Rev protein." Proc Natl Acad Sci USA **89**(2): 758-62.

Toogood, P. L. (2002). "Inhibition of protein-protein association by small molecules: approaches and progress." J Med Chem **45**(8): 1543-58.

Trapani, J. A. and M. J. Smyth (2002). "Functional significance of the perforin/granzyme cell death pathway." Nat Rev Immunol **2**(10): 735-47.

Trump, B. F., I. K. Berezesky, S. H. Chang and P. C. Phelps (1997). "The pathways of cell death: oncosis, apoptosis, and necrosis." Toxicol Pathol **25**(1): 82-8.

Tsujimoto, Y., J. Cossman, E. Jaffe and C. M. Croce (1985). "Involvement of the bcl-2 gene in human follicular lymphoma." Science **228**(4706): 1440-3.

Tsujimoto, Y., L. R. Finger, J. Yunis, P. C. Nowell and C. M. Croce (1984). "Cloning of the chromosome breakpoint of neoplastic B cells with the t(14;18) chromosome translocation." Science **226**(4678): 1097-9.

Tucker-Kellogg, L., M. A. Rould, K. A. Chambers, S. E. Ades, R. T. Sauer and C. O. Pabo (1997). "Engrailed (Gln50-->Lys) homeodomain-DNA complex at 1.9 A

resolution: structural basis for enhanced affinity and altered specificity." Structure **5**(8): 1047-54.

Vaishnav, Y. N. and F. Wong-Staal (1991). "The biochemistry of AIDS." Annu Rev Biochem **60**: 577-630.

van de Waterbeemd, H., G. Camenisch, G. Folkers, J. R. Chretien and O. A. Raevsky (1998). "Estimation of blood-brain barrier crossing of drugs using molecular size and shape, and H-bonding descriptors." J Drug Target **6**(2): 151-65.

Varani, G., C. Cheong and I. Tinoco, Jr. (1991). "Structure of an unusually stable RNA hairpin." Biochemistry **30**(13): 3280-9.

Vilar, S., G. Cozza and S. Moro (2008). "Medicinal chemistry and the molecular operating environment (MOE): application of QSAR and molecular docking to drug discovery." Curr Top Med Chem **8**(18): 1555-72.

Vita, C., E. Drakopoulou, J. Vizzavona, S. Rochette, L. Martin, A. Menez, C. Roumestand, Y. S. Yang, L. Ylisastigui, A. Benjouad and J. C. Gluckman (1999). "Rational engineering of a miniprotein that reproduces the core of the CD4 site interacting with HIV-1 envelope glycoprotein." Proc Natl Acad Sci USA **96**(23): 13091-6.

Vives, E. (2003). "Cellular uptake of the TAT peptide." J Mol Recognit **16**: 265-71.

Volgraf, M., P. Gorostiza, R. Numano, R. H. Kramer, E. Y. Isacoff and D. Trauner (2006). "Allosteric control of an ionotropic glutamate receptor with an optical switch." Nat Chem Biol **2**(1): 47-52.

Vranken, W. F., W. Boucher, T. J. Stevens, R. H. Fogh, A. Pajon, M. Llinas, E. L. Ulrich, J. L. Markley, J. Ionides and E. D. Laue (2005). "The CCPN data model for NMR spectroscopy: development of a software pipeline." Proteins **59**(4): 687-96.

Walensky, L. D. (2006). "BCL-2 in the crosshairs: tipping the balance of life and death." Cell Death Differ **13**(8): 1339-50.

Walensky, L. D., A. L. Kung, I. Escher, T. J. Malia, S. Barbuto, R. D. Wright, G. Wagner, G. L. Verdine and S. J. Korsmeyer (2004). "Activation of apoptosis in vivo by a hydrocarbon-stapled BH3 helix." Science **305**(5689): 1466-70.

Wang, G., Z. Nikolovska-Coleska, C. Y. Yang, R. Wang, G. Tang, J. Guo, S. Shangary, S. Qiu, W. Gao, D. Yang, J. Meagher, J. Stuckey, K. Krajewski, S. Jiang, P. P. Roller, H. O. Abaan, Y. Tomita and S. Wang (2006). "Structure-based design of potent small-molecule inhibitors of anti-apoptotic Bcl-2 proteins." J Med Chem **49**(21): 6139-42.

Wang, K., X. M. Yin, D. T. Chao, C. L. Milliman and S. J. Korsmeyer (1996). "BID: a novel BH3 domain-only death agonist." Genes Dev **10**(22): 2859-69.

Wang, X. (2001). "The expanding role of mitochondria in apoptosis." Genes Dev **15**(22): 2922-33.

Wang, Z., W. Song, A. Aboukameel, M. Mohammad, G. Wang, S. Banerjee, D. Kong, S. Wang, F. H. Sarkar and R. M. Mohammad (2008). "TW-37, a small-molecule inhibitor of Bcl-2, inhibits cell growth and invasion in pancreatic cancer." Int J Cancer **123**(4): 958-66.

Weeks, K. M. and D. M. Crothers (1993). "Major groove accessibility of RNA." Science **261**(5128): 1574-7.

Weston, C. J., C. H. Cureton, M. J. Calvert, O. S. Smart and R. K. Allemann (2004). "A stable miniature protein with oxaloacetate decarboxylase activity." Chembiochem **5**(8): 1075-80.

Williamson, J. R. (2000). "Induced fit in RNA-protein recognition." Nat Struct Biol **7**(10): 834-7.

Woolley, G. A., A. S. Jaikaran, M. Berezovski, J. P. Calarco, S. N. Krylov, O. S. Smart and J. R. Kumita (2006). "Reversible Photocontrol of DNA Binding by a Designed GCN4-bZIP Protein." Biochemistry **45**(19): 6075-84.

Xiao, G., A. Kumar, K. Li, C. T. Rigl, M. Bajic, T. M. Davis, D. W. Boykin and W. D. Wilson (2001). "Inhibition of the HIV-1 rev-RRE complex formation by unfused aromatic cations." Bioorg Med Chem **9**(5): 1097-113.

Yang, B., D. Liu and Z. Huang (2004). "Synthesis and helical structure of lactam bridged BH3 peptides derived from pro-apoptotic Bcl-2 family proteins." Bioorg Med Chem Lett **14**(6): 1403-6.

Yin, H. and A. D. Hamilton (2004). "Terephthalamide derivatives as mimetics of the helical region of Bak peptide target Bcl-xL protein." Bioorg Med Chem Lett **14**(6): 1375-9.

Yin, H. and A. D. Hamilton (2005a). "Strategies for targeting protein-protein interactions with synthetic agents." Angew Chem Int Ed Engl **44**(27): 4130-63.

Yin, H., G. I. Lee, K. A. Sedey, O. Kutzki, H. S. Park, B. P. Orner, J. T. Ernst, H. G. Wang, S. M. Sebti and A. D. Hamilton (2005b). "Terphenyl-Based Bak BH3 alpha-helical proteomimetics as low-molecular-weight antagonists of Bcl-xL." J Am Chem Soc **127**(29): 10191-6.

Yin, H., G. I. Lee, K. A. Sedey, J. M. Rodriguez, H. G. Wang, S. M. Sebti and A. D. Hamilton (2005c). "Terephthalamide derivatives as mimetics of helical peptides: disruption of the Bcl-x(L)/Bak interaction." J Am Chem Soc **127**(15): 5463-8.

Yin, X. M., K. Wang, A. Gross, Y. Zhao, S. Zinkel, B. Klocke, K. A. Roth and S. J. Korsmeyer (1999). "Bid-deficient mice are resistant to Fas-induced hepatocellular apoptosis." Nature **400**(6747): 886-91.

Youle, R. J. and A. Strasser (2008). "The BCL-2 protein family: opposing activities that mediate cell death." Nat Rev Mol Cell Biol **9**(1): 47-59.

Yu, C. and J. W. Taylor (1999). "Synthesis and study of peptides with semirigid i and i + 7 side-chain bridges designed for alpha-helix stabilization." Bioorg Med Chem **7**(1): 161-75.

Zamzami, N., S. A. Susin, P. Marchetti, T. Hirsch, I. Gomez-Monterrey, M. Castedo and G. Kroemer (1996). "Mitochondrial control of nuclear apoptosis." J Exp Med **183**(4): 1533-44.

Zapp, M. L. and M. R. Green (1989). "Sequence-specific RNA binding by the HIV-1 Rev protein." Nature **342**(6250): 714-6.

Zha, J., H. Harada, E. Yang, J. Jockel and S. J. Korsmeyer (1996). "Serine phosphorylation of death agonist BAD in response to survival factor results in binding to 14-3-3 not BCL-X(L)." Cell **87**(4): 619-28.

Zhang, Z., D. C. Burns, J. R. Kumita, O. S. Smart and G. A. Woolley (2003). "A water-soluble azobenzene cross-linker for photocontrol of peptide conformation." Bioconjug Chem **14**(4): 824-9.

Zhao, J., J. Zhou, M. Liu, H. Asanuma and M. Komiyama (2004). "Photoregulation of in vitro transcription/translation of GFP by tethering an azobenzene to T7 promoter." Nucleic Acids Symp Ser (48): 199-200.

Zhu, Q., S. Liang, L. Martin, S. Gasparini, A. Menez and C. Vita (2002). "Role of disulfide bonds in folding and activity of leiurotoxin I: just two disulfides suffice." Biochemistry **41**(38): 11488-94.

Ziegler, U. and P. Groscurth (2004). "Morphological features of cell death." News Physiol Sci **19**: 124-8.